

ADIABATIC CONNECTION AND UNIFORM
DENSITY SCALING: A BASIS FOR
IMPROVING DENSITY FUNCTIONAL
THEORY

BY RUDOLPH J. MAGYAR

A dissertation submitted to the
Graduate School—New Brunswick
Rutgers, The State University of New Jersey
in partial fulfillment of the requirements
for the degree of
Doctor of Philosophy
Graduate Program in Physics and Astronomy

Written under the direction of
Prof. Kieron Burke
and approved by

New Brunswick, New Jersey

October, 2003

ABSTRACT OF THE DISSERTATION

Adiabatic Connection and Uniform Density Scaling: a Basis for Improving Density Functional Theory

by Rudolph J. Magyar

Dissertation Director: Prof. Kieron Burke

Density Functional Theory (DFT) is an effective and popular approach to the quantum many-body problem. DFT is exact but, in practice, the exchange-correlation contribution to the total energy must be approximated. Because of the demand for higher accuracy in applications, the modeling and understanding of this exchange-correlation density functional is an important area of research and is the focus of this thesis. First, a DFT is developed for a one-dimensional contact interaction. Then, the focus returns to the Coulomb-interacting problem. Uniform density scaling relationships are generalized to spin-scaling relationships. The adiabatic connection is considered at both strong and weak interaction limits. In the strong limit, the strictly-correlated electron hypothesis is tested. In the weak limit, the accuracy of exact-exchange DFT as applied to large gap solids is examined.

Acknowledgements

I want to acknowledge all of those who supported me through the years. This list is long but hardly complete.

First of all, I would like to thank Kieron Burke. Without his guidance, I would never have learned what I know about DFT, and I would certainly never have come this far. The research group also deserves thanks for their encouragement and friendship. The members of the Burke group are Heiko Appel, Rene Gaudoin, Paul Hessler, Jacob Katriel, Neepa Maitra, Eunji Sim, Eugene Tsiper, Adam Wasserman, Jan Werschnik, Takeyce Whittingham, Federico Zahariev, and Fan Zhang. Special appreciation is due to those who helped read, proofread, and finalize the thesis. These are Adam, Takeyce, Rene, Neepa, Eugene, Andrzej Fleszar, Carrie Teresa, and especially January Teresa who must have the thesis memorized by now. I would like to thank my collaborators and friends in Berlin and Würzburg. They are E.K.U. (Hardy) Gross, Heiko, Jan, Ulf von Barth, Andrzej Fleszar, Nicole Helbig, Stephan Kurth, Nektarios Lathiot, Miguel Marques, and Angelica Zacarias.

I would like to express my sincerest appreciation and love to my friends and family as well. I thank Mike Schwartz and Jim Masterangelo for many entertaining nights at Doll's Place. I am grateful to my brothers, Pete and Andy, for exercising with me when I needed a break from my work. I thank my sister and parents for their support, and January, my fiancee and love, for being there through it all.

Table of Contents

Abstract	ii
Acknowledgements	iii
List of Tables	viii
List of Figures	xii
List of Abbreviations	xv
1. The Need for a Density-Based Electronic Structure Theory . .	1
1.1. The Importance of Electronic Structure Theory	1
1.2. An Assortment of Methods	3
1.3. The Advantages of a Density-Based Theory	4
1.4. The History of Density Functional Theory	6
1.5. Successes, Failures, and the Future	8
2. A Formal Introduction to Density Functional Theory	11
2.1. The Schrödinger Equation	11
2.2. Variational Principle	12
2.3. The Hohenberg-Kohn Theorem	14
2.4. Levy-Constrained Search Proof	15
2.5. Thomas-Fermi Theory	17
2.6. The Non-Interacting Kohn-Sham System	17
2.7. The Exchange Correlation Energy, Nature's Glue	19
2.8. Jacob's Ladder of Approximations	21

2.9. Exact Constraints on the Exchange-Correlation Functional	24
2.10. Cornerstones of a Density Functional Theory	26
3. A Simple Example: Density Functional Theory for a One-Dimensional Contact Interaction	29
3.1. One-Dimensional Contact-Interaction Models	29
3.2. Exact-Exchange Density Functional	31
3.3. Deltium: The One-Dimensional Uniform Fermi Gas	32
3.4. A Local-Density Correlation Functional	35
3.5. Diracium, the Contact-Interacting Analog of Helium	37
3.6. Exact-Exchange Treatment of Diracium	39
3.7. The Local Density Correlation Treatment of Diracium	40
3.8. The Exact Solution of Diracium	42
3.9. Comparison of the Diracium Results	44
3.10. Contact-Interacting Hooke's Atom	45
3.11. The Accuracy of Contact-Interacting Density Functional Theory .	47
4. Uniform Density and Spin-Density Scaling	49
4.1. Uniform Density Scaling	49
4.2. The Virial Theorem	50
4.3. The Generalization to Uniform Separate Spin Density Scaling . .	51
4.4. General Properties of Spin-Scaling	53
4.5. Spin-Scaling on the Uniform Gas	57
4.6. Calculations on Atoms	60
4.7. Spin-Scaling on Finite Systems	60
4.8. Constructing a Spin Adiabatic Connection	65
4.9. Remarks about Spin-Scaling	69

5. The Adiabatic Connection and Its Strongly Interacting Limit:	
Testing the Strictly Correlated Electron Hypothesis	71
5.1. Using the Adiabatic Connection to Study Functionals	71
5.2. Görling-Levy Perturbation Theory	74
5.3. The Strong Coupling Limit	75
5.4. The Strictly Correlated Electron Hypothesis	75
5.5. The Interaction Strength Interpolation, A Rung Five Functional .	76
5.6. Relationship Between Scaling and Coupling Constant	77
5.7. Solving Hooke’s Atom at Different Harmonic Well Strengths . . .	78
5.8. Testing the Simulated Scaling Method	78
5.9. Extrapolating to the Infinite Interaction Strength Limit	82
5.10. Simulating the Entire Adiabatic Connection Curve	83
5.11. Assessment of the Strictly Correlated Electron Hypothesis and the Interaction Strength Interpolation	87
6. The Adiabatic Connection and Its Weakly Interacting Limit: A	
Close Examination of Exact-Exchange Band Gaps	88
6.1. The Band Gap Problem in DFT	88
6.2. Introduction to Exact Exchange and Orbital Functionals	89
6.3. Previous Work with Exact Exchange	91
6.4. Bloch’s Theorem and Plane-Wave Methods	94
6.5. Pseudopotentials	96
6.6. The Implementation of Exact-Exchange	98
6.7. Exact Exchange on Finite Systems: Ne, Ar, Kr and Xe	99
6.8. Exact Exchange of Large Gap Extended Systems: Solid Ne, Ar, Kr and Xe	104
6.9. Revisiting the Band Gap Problem in DFT	107

Appendix A. Codes Used in this Thesis	114
A.1. Codes Specifically Written for this Thesis	114
A.2. Other Codes Used in this Thesis	116
References	117
Curriculum Vitae	132

List of Tables

2.1.	Components of the total energy for atoms. The results are from a combination of calculations and comparisons to experimental data [159, 142, 79, 145]. E_{tot} is the total ground-state energy of the system, T_s is the non-interacting kinetic energy contribution, V_{ext} is the contribution from the external potential, U_H is the Hartree contribution, E_x is the exchange contribution, and E_c is the correlation contribution.	20
2.2.	Typical errors for two different rungs of functionals as transcribed from John Perdew’s lecture notes from the DFT Summer School at Caramulo, Portugal, 2001. Atom. En. refers to atomization energies or the energy required to split a molecule to the individual atoms. Bonds refers to bond lengths. Structures refers to the most stable lattice structure. Energy barriers refer to the predicted energy of a transition state.	24
3.1.	Various components of the energy as separated via the virial theorem. $\langle \hat{T} \rangle$ is the kinetic energy contribution, $\langle \hat{V}_{ee} \rangle$ is the interaction contribution, and $\langle \hat{V}_{ext} \rangle$ is the external potential contribution. . .	45

3.2. Total energies for Diracium within various approximations with $\lambda = 1$. The exact results are from a numerical solution of the problem as outlined by Ref. [127], the second-order perturbation values are also given in the same reference. The EXX and the LDA results are from a self-consistent solution using the exact-exchange functional, Eq. (3.3), and the LDA functional, parameterization Eq. 3.20 respectively.	46
3.3. Critical Z 's for dissociation. LDA is according to the parameterization Eq. 3.20.	47
3.4. Total energies for the contact-interacting Hooke's Atom within various approximations, $\lambda = 1$. Exact is from a numerical solution of Eqs. 3.58 and 3.59. EXX is exact exchange. LDA is according to the parameterization Eq. 3.18.	47
4.1. He atom energies, both exactly and within several approximations. All energies in Hartrees; all functionals evaluated on self-consistent densities.	62
4.2. Li atom energies, both exactly and within several approximations. All energies in Hartrees, all functionals evaluated on self-consistent densities.	64
4.3. Spin adiabatic connection $\Delta U_{xc}(\lambda_{\uparrow})$ for He atom, both exactly and in several approximations.	66
5.1. Simulated scaling k and λ equivalences using the E_x scaling rule, Eq. (5.18), to determine λ	79
5.2. Higher derivatives of $U_C(\mu)$ with respect to μ for Hooke's atom ($k = 1/4$).	84
5.3. Higher derivatives of $U_C(\lambda)$ with respect to λ for Hooke's atom ($k = 1/4$).	84

5.4.	Accurate results for Hooke's atom with $k = 1/4$ evaluated on the exact densities.	85
5.5.	Interaction Strength Interpolation Results for Hooke's atom with $k = 1/4$. <i>Accurate</i> and <i>model</i> refer to the value of $U'_c(\mu = 0)$. The accurate value is from our simulation and the model is from Seidl's model [165].	85
6.1.	Neon atom energy levels (in eV). The KS orbital eigenvalues are from LDA, exact exchange (EXX) and exact exchange with LDA correlation (EXXc). Column QMC gives the eigenvalues obtained with the highly accurate Kohn-Sham potential of Ref. [198]. Column CI presents results of highly accurate Kohn-Sham calculation of Ref. [79].	99
6.2.	Argon atom energy levels (in eV). The KS orbital eigenvalues are from LDA, exact exchange (EXX) and exact exchange with LDA correlation Column CI presents results of highly accurate Kohn-Sham calculation of Ref. [79].	100
6.3.	Fundamental energy gaps $E_g = I - A$ and optical gaps from experiment and calculations in neutral atoms Ne, Ar, Kr and Xe. E_{og} expt. is the multiplet-averaged experimental transition energy from the ground state to p^5s^1 state. E_{og} KS is the calculated total-energy difference between the ground state and the excited atom in the (p^5s^1) configuration. $\Delta\epsilon_{KS}$ is the Kohn-Sham gap.	101
6.4.	Equilibrium cubic lattice spacing (in a.u.) from experiment and calculations.	108
6.5.	Ne-solid Kohn-Sham eigenvalues in eV from the LDA, EXX and EXX plus LDA correlation (EXXc) schemes at high-symmetry points. The presented eigenvalues are from the upper lying valence states and lowest conduction states.	109

6.6. Ar-solid Kohn-Sham eigenvalues in eV from the LDA, EXX and EXX plus LDA correlation (EXXc) schemes at high-symmetry points. The presented eigenvalues are from the upper lying valence states and lowest conduction states.	110
6.7. Kr-solid Kohn-Sham eigenvalues in eV from the LDA, EXX and EXX plus LDA correlation (EXXc) schemes at high-symmetry points. Spin-orbit splittings are included. The presented eigenvalues are from the upper lying valence states and lowest conduction states.	111
6.8. Xe-solid Kohn-Sham eigenvalues in eV from the LDA, EXX and EXX plus LDA correlation (EXXc) schemes at high-symmetry points. Spin-orbit splittings are included. The presented eigenvalues are from the upper lying valence states and lowest conduction states.	112
6.9. Calculated and measured energy gaps in noble-gas solids in eV. E_g^{LDA} , E_g^{EXX} and E_g^{EXXc} are Kohn-Sham gaps from the LDA, pure EXX and EXX plus LDA correlation schemes respectively. E_g^{Expt} is the experimental fundamental gap. Δ is the experimental optical gap.	112
6.10. Addition of the exchange-only derivative discontinuity to the KS gaps at the Γ point. LDA is the local density approximation result. EXX means exact-exchange and no correlation. Δ_x is the exchange contribution to the derivative discontinuity. HF is the all-electron Hartree-Fock orbital gap. ^a Ref.[201] ^b Ref.[202] ^c Ref.[203] ^d Ref.[202] ^e Ref.[202]	113

List of Figures

2.1.	Kohn-Sham Self-Consistent Cycle shown Schematically	20
2.2.	The adiabatic connection for Helium. The solid line is the exact result, the long dashed-line is from the LDA functional, and the short-dashed line is from the BLYP hybrid functional.	26
3.1.	Correlation energy per particle for Deltium, the one-dimensional uniform contact-interacting Fermi gas, $\lambda = 1$. The solid line is the exact result calculated from the Bethe-Ansatz integral equations. The long-dashed line is the simple LDA parameterization given by Eq. (3.18). The short-dashed line is the more accurate LDA parameterization given by Eq. (3.20).	37
3.2.	Correlation energy for Diracium, $\lambda = 1$, as obtained from $E_C \approx E_{exact} - E_{exx}$. The long-dashed line is second-order perturbation theory, the short-dashed line is LDA, and the solid line is exact. .	38
4.1.	Uniform Density Scaling of an exponential density, $n(r) = e^{-r}/4\pi$, by a factor $\gamma = 1/2$	49
4.2.	Spin-scaling of a uniform gas: exchange energy per particle, $\epsilon_x(n_{\uparrow\alpha}, n_{\downarrow})$, at $r_s = 2$ (dotted line) and 6 (solid line).	57
4.3.	Spin-scaling of a uniform gas: correlation energy per particle, $\epsilon_c(n_{\uparrow\alpha}, n_{\downarrow})$, at $r_s = 2$ (dotted line) and 6 (solid line).	58
4.4.	Spin-scaling of the He atom density using various approximate functionals for E_C : local spin density approximation (solid line), generalized gradient approximation (PBE, dashed line), BLYP (bars), self-interaction corrected LSD (short dashes).	61

4.5.	Up-spin scaling of the Li atom density using various approximate functionals for E_C : local spin density approximation (solid line), generalized gradient approximation (PBE, dashed line), BLYP (bars).	63
4.6.	Down-spin scaling of the Li atom density using various approximate functionals for E_C : local spin density approximation (solid line), generalized gradient approximation (PBE, dashed line), BLYP (bars).	64
4.7.	Single-spin adiabatic connection for He atom: local spin density approximation (solid line), generalized gradient approximation (PBE, dashed line), BLYP (bars), self-interaction corrected LSD (short dashes), <i>Exact</i> (fancy dashes).	67
5.1.	Simulated scaling of the density. We start with Hooke's atom at $k = 1/4$. Then, we solve at various other coupling constants and use simulated scaling to return us as closely as possible to the $k = 1/4$ density.	79
5.2.	PBE adiabatic connection curve for Hooke's atom ($k = 1/4$): $U_C(\mu = 1/\sqrt{\lambda})$. The solid line is generated using simulated scaling of the density and the dashed curve by exactly scaling the known functional. The exact PBE $U_C(\mu = 0)$ limit is shown (short dashes).	81
5.3.	The adiabatic connection curve for Hooke's atom ($k = 1/4$): $U_C(\mu)$. The solid line is the simulated curve. The SCE limit is shown as a dashed line.	82
5.4.	Simulated adiabatic connection curve for Hooke's atom ($k=1/4$): $U_C(\mu)$. The solid line is the simulated curve with the SCE $U_C(\mu = 0)$. The dashed curve is the ISI using exact inputs.	83

5.5. Adiabatic connection curve for Hooke's Atom using various functionals: The exact curve is the solid line, the PBE is the long dashed line, and the local density approximation (LDA) is the short dashed line.	86
6.1. Band structure of Ar along the L- Γ -X directions as calculated within EXX (solid lines) and LDA (dashed lines).	108

List of Abbreviations

LDA	local density approximation
GGA	generalized gradient approximation
SCE	strictly correlated electrons
BA	Bethe Ansatz
KS	Kohn-Sham
XC	exchange-correlation
X	exchange
C	correlation
ISI	interaction strength interpolation
DFT	density functional theory
HIV	human immune virus
PBE	Perdew-Burke-Ernzerhof GGA functional
EXX	exact exchange
EXXc	exact exchange with LDA correlation
SC	self-consistent
LSD	local spin-density
BLYP	Becke-Lee-Yang-Parr functional
QMC	quantum Monte Carlo
ADF	atomic density functional code
DF	density functional
GW	Green's functional - interaction vertex
CI	configuration interaction
HF	Hartree-Fock
Δ SCF	Δ self-consistent field

Chapter 1

The Need for a Density-Based Electronic Structure Theory

1.1 The Importance of Electronic Structure Theory

Electronic structure theory is the attempt to understand and accurately determine the properties of atoms, molecules, surfaces, and solids. The goal, chemical accuracy, would be invaluable in the custom design of materials, the simulation of chemical reactions, and the discovery of new pharmaceuticals.

Even though chemical accuracy has not yet been achieved, exciting results have already been obtained from electronic structure calculations. For example, density functional theory has been used to systematically search for the strongest possible combinations of metals without having to synthesize the combinations one-by-one in lab [1]. Searches like this save time and money while providing industry with potentially lucrative results. Another case in which density functional calculations have yielded useful results is in the Haber-Bosch process. This process is important in the production of ammonia. Specifically, the calculations predicted a new and improved catalyst for the reaction which was subsequently verified by experiment [2]. Yet another area where electronic structure calculations have been used is in simulations of how the enzymes in viruses interact. Results from these calculations on biological molecules are invaluable in understanding and fighting diseases like HIV [3, 4].

Two main objectives of computational physics are to give a better understanding of what is seen in experiments and to offer information about materials before

they are ever studied in the lab. For example, molecular and crystal structures depend on how the electronic ground-state energy varies when the positions of the atomic nuclei change[6]. By analyzing how the total energy changes, we can compute the forces acting on atoms. Results from a calculation like this could be used, for example, to determine how much strain can be applied to a metal rod before it breaks.

This thesis will deal with *ab initio* (Latin for “from the source”) or first principles methods. *Ab initio* calculations are based on the underlying rules of physics and do not require system-specific input based on experiments. These sorts of methods are the most technically demanding and expensive but promise to be most accurate. Since they are based on general rules of physics, these methods can be expected to reproduce nature when applied to unstudied systems.

Ab initio calculations are difficult. The trouble is that the electrons have been observed to obey complicated and nonintuitive quantum mechanical laws. According to quantum theory, the electrons can only be described probabilistically. This means that the absolute positions and velocities of the electrons cannot be known exactly; rather, the whole system must be described by a mathematical object – the wave-function. Experiments have shown that the wave-function satisfies the Schrödinger equation to a very good approximation. Unfortunately, solving this equation to find the wave-function is not generally feasible. One difficulty comes from the nature of the electrons. They are fundamentally identical. This has more than just philosophical implications. It means that all physical quantities must be left unchanged when two electrons switch places. For this to be true, the wave-function can only change at most by an overall sign. The other complication arises from terms in the Schrödinger equation that describe how the electrons interact and repel each other. This mutual repulsion makes the solution grow exceedingly complex as the number of electrons increases.

1.2 An Assortment of Methods

Only a few non-interacting quantum mechanical problems and precious fewer interacting problems have exact analytic solutions. Numerical methods offer the only possibility to find answers for more general situations. Computation alone is not enough. Careful understanding of the underlying physics is required to make computations feasible and reliable.

Several methods have been developed to deal with the electronic structure problem. It is insightful to briefly consider these so that the importance of a density-based theory becomes obvious.

Alternatives to *ab initio* methods are *empirical* methods such as force field methods. These methods solve problems by parameterization of similar well-studied problems [7]. Since these *empirical* methods are designed for certain classes of systems, they are not to be trusted when applied to general situations. These methods can be designed to work at various length scales but are not the best tool to explore new science reliably. *Ab initio* methods can be classified into two major subclasses.

The first subclass relies on finding increasingly better approximations to the wave-function. The simplest approximation is to assume that the many-particle wave-function is just a product of single-particle solutions. By enforcing the proper quantum mechanical law under particle exchange, we arrive at the Hartree-Fock (HF) approximation. For many systems, Hartree-Fock is reasonably accurate but since it involves bold assumptions about the form of the wave-function, it does not provide a complete theory for electronic structure [8, 9, 10]. A perturbation theory about the HF result is useful and provides improved results for finite systems [11]. Configuration interaction methods (CI) improve systematically upon this and can, in principle, give exact solutions [7]. However, exact CI is too

computationally expensive, especially for dozens or more electrons. Another approach is to vary parameters in a carefully chosen approximate wave-function[12]. The integrals involved in this scheme are complicated and often require Monte Carlo integration. This variational approach is also best for small systems where the number of parameters is small [13].

A second subclass of methods focuses on objects related to, but more manageable than, the wave-function. These methods may or may not offer a full description of the physics. An example is Green's function theory [14]. Like wave-function theory, Green's function theory can be exact. Its advantage is that the one- or even two-particle Green's function is a much simpler object than a many-electron wave-function and can be expanded schematically in Feynman diagrams. For large systems like solids, Green's function methods allow the descriptions of large numbers of particles in a compact form. The GW approximation to the self-energy is a practical implementation of Green's function theory and is useful for many applications [15, 16]. The G refers to the Green's function for the electrons, and W is the screened electron-electron interaction. Generally, GW results agree well with experiment; however, the calculations for many systems can only be performed on supercomputers. Yet simpler objects, like the density matrix [17], and even simpler, the density, form the bases for more manageable theories. Density functional theory is based on one of the simplest of these objects, the electronic density.

1.3 The Advantages of a Density-Based Theory

A grain of table salt has 3×10^{19} electrons, and many interesting molecules have hundreds, thousands, and even millions of electrons. For systems with this many electrons, the many-particle wave-function is prohibitively unwieldy and hard to find. To get an idea of the problem, imagine that we need to know values of the

wave-function at a few points in space. Let us record the wave-function at M points along each spatial direction. In three dimensions, an $M \times M \times M$ sized array would be large enough to store the sampled wave-function for a one-particle system. Adding another electron raises the array size by one power. For a system with N electrons, we would need M^{3N} entries in our array. For 10 electrons and only 10 sample points, we would need 10^{30} entries in our array! This array is simply too big for today's computers. Of course, in real calculations, there are more clever ways to describe the system than this, but the basic conclusion is the same. The wave-function is not a practical description for even a moderate number of electrons.

In order to examine larger systems more efficiently, it is enticing to consider objects that are easier to handle like the density and density matrix. For example, the density can be stored in an array with M^3 entries, and the density matrix would take up an array with M^6 entries. Notice that the density does not take up more memory as the number of electrons increases.

The efficiency of an electronic structure method is often characterized by the way a calculational effort grows with the number of electrons, N . Ideally, an electronic structure calculation for N electrons would be as complicated as a calculation for one electron times N . This is called order N and is for the most part not possible yet without a compromise in accuracy. DFT typically scales as N^3 but in some cases as N . Hartree Fock scales as N^3 . Full CI scales as $Exp(N)$, with approximate CI methods scaling as N^5 at best [7]. Since computer time and resources are limited, so is the size of calculations. The smaller the power of N , the larger the calculation that can be done. If we could use the density instead of the wave-function, we would greatly increase the size and scope of the problems we could answer exactly.

So, it would be ideal from a practical standpoint to have a complete description of the physics without having to calculate the awkward wave-function. The

trouble is whether this reduction is formally justified and whether it is in principle exact. Do we really lose information by not calculating the wave-function? Or could a complete theory be based on the density rather than the wave-function?

A common argument against this reduction is that the density seems to have less information than the wave-function. The wave-function, after all, has more arguments and represents explicitly all the electrons.

On the the other hand, there are reasons to believe a density-based theory might be rigorous. For small systems and systems varying slightly from the uniform limit we *can* find the potential from the density. For these systems at least, the reduction is exact. Why shouldn't we be able to find the potential from the density in general?

The answer is that we do have a complete density-based description of the physics because the density indeed contains all the same information as the wave-function! The information is just in a compact form.

Density functional theory is important for more than just its computational expediency; it is a conceptually new approach to quantum mechanics. The Kohn-Sham version of the theory, which we will discuss in more detail later, can be used to give a rigorous meaning to molecular orbitals and to clarify chemical notions of hardness and softness [18].

1.4 The History of Density Functional Theory

Investigations into a density-based theory of matter started about the same time as wave-function quantum mechanics. In 1927, Thomas and Fermi attempted a density-based description of atoms [19, 20]. At that time, there was no known formal justification for this method. For most practical applications, Thomas-Fermi theory was inadequate. Nevertheless, the idea of a density-based theory was appealing and work continued. For example, von Weizsäcker introduced the

first gradient density functional [21] in 1935.

The computer was developed in the forties and was a new tool for physics. If used properly, it could provide a quantitative theory of matter. Slater realized this and pushed for a density-based approximation to quantum theory that would be particularly compatible with computing larger systems. His $X\alpha$ approximation was found to be good but, like Thomas-Fermi theory, lacked a known formal justification [22].

Justification came in 1964 when Hohenberg and Kohn demonstrated that the density, as well as the potential, uniquely characterizes a ground-state electronic structure problem [23]. This observation suggested the introduction of a non-interacting Kohn-Sham counterpart with the same density as the interacting system [24]. The solutions for the non-interacting problem could be readily calculated and used to provide information about the interacting system.

According to Hohenberg and Kohn, the total ground-state energy is a functional of the density. In practice, the only part of the energy which must be approximated is the exchange-correlation energy. They suggested a simple approximation to this contribution, to use the local exchange-correlation energy from the uniform electron gas. The scheme became known as the local density approximation (LDA). At that time, simple approximations to the exchange-correlation energy of the uniform gas were known [25, 26, 27]. More accurate and essentially exact parameterizations have since been developed and are in common use today [31, 32, 33].

By the late seventies, DFT - mostly within the local density approximation - was widely applied to solids. Rough ideas about its accuracy were found [34, 35]. The LDA reproduced crystal structures well but underestimated band gaps. By the late seventies, people started to understand why LDA worked as well as it did and began trying to go beyond it by proposing gradient expansions [36, 37]. Today, several generalized gradient approximations are available [38, 39, 40, 41].

In 1979, Levy’s constrained search proof provided a more intuitive and constructive derivation of the Hohenberg-Kohn theorem [42, 43].

In 1988, a GGA was invented which was well-suited to chemical problems [38, 39]. Soon after, DFT methods were implemented into John Pople’s electronic structure code, Gaussian[44]. Since then, the number of DFT papers in quantum chemistry has increased exponentially [45]. DFT became even more popular in chemistry with the introduction of hybrid functionals which further increase accuracy [46, 47]. By 1998, DFT had become so ubiquitous, popular, and successful that the Noble prize in chemistry went to Walter Kohn “for his development of the density-functional theory” and John Pople “for his development of computational methods in quantum chemistry” [48].

Paralleling the development of ground-state theory, DFT has been extended to more general situations. Most notably, Runge and Gross generalized the theory to include time-dependent phenomena and excited states [49, 50]. In the nineties, DFT became a standard tool for excited-state as well as ground-state calculations [51]. Today, understanding and improving the accuracy of predictions for excited-states in DFT is an active area of research.

1.5 Successes, Failures, and the Future

Density functional theory provides ground-state structures, densities, energetics, and vibrational properties for interacting-electron systems. One of the greatest advantages of DFT is its generality; all elements are treated with the same functionals (excepting the inclusion of relativistic effects for heavier elements). Furthermore, the theory applies equally well to metallic, covalent, and ionic bonds. It even performs well for traditionally difficult cases like describing ozone. As a result of its generality, DFT is particularly suited to handle mixed systems like organometallic systems.

Because of the simplicity of its fundamental quantity, the density, DFT is highly efficient and can handle larger systems than other *ab initio* methods. The current practical limits are 100 atoms systems and 1000 atom clusters. Self-consistency typically takes about a dozen iterations for organic materials and semiconductors, but metals and transition metals often take more cycles to converge.

In solid-state physics, density functional theory has been exceptionally successful [5]. LDA gives lattice constants for simple crystals within 1% of the experimental values [6]. On average, crystal structures and the dispersion of the energy-bands are also well-described. DFT has also been used to study phase transitions in solids[52] and liquid metals[53, 54].

The introduction of more accurate functionals than the LDA has made DFT useful in atomic and molecular physics to study chemical reactions, the structure of biomolecules, and the nature of active sites on catalysts. Strong bonds in solids, in molecules, and at surfaces are typically within 0.02 Angstroms of the experimentally measured quantities. Bond angles and dihedral angles are typically calculated within a few percent of experiment. GGA binding energies are within 10 kJ/mol of experiment and are comparable to sophisticated CI approaches. Vibrational frequencies are 10-50 cm^{-1} [45].

DFT has even been used in biology and mineralogy [57, 58, 59, 60]. DFT is necessary for the *ab initio* study of large molecules when other *ab initio* methods are impractically slow. For example, DFT has helped explain the light sensitive mechanism in chlorophyll [55]. Another use for DFT is molecular dynamics where the forces on the nuclei are calculated classically in the electron's field as the simulation proceeds [56].

More exotic cases for DFT are super-conductivity [61], atoms in strong laser pulses [62], relativistic effects in heavy elements and nuclei [63], magnetic properties of alloys [64, 65], quantum fluid dynamics [66], and nuclear physics [67, 68].

Before density functional methods reach fruition, certain problems must be resolved. DFT fails to describe band gaps, hydrogen bonds, and van der Waals interactions. Currently, approximate functionals are not reliably accurate enough for thermo-chemistry. The understanding of scattering and excited states in DFT is still in its nascent stages [69]. These issues are more challenges than they are problems. DFT and its time-dependent extensions are exact and when sufficiently understood and approximated will describe all of the above. Exactly how implementable or practical the final approximations will be is unclear.

Nevertheless, density functional theory has a promising future in materials science, solid-state physics, and chemistry. This is because DFT can be used for a wide variety of ground-state problems for large and small systems with confidence. Several popular electronic structure codes are available and in wide use: Gaussian, Abinit, Octopus [44, 70, 71]. Currently, the accuracy of functionals continues to improve. Advances in pseudo-potential theory and order N techniques allow DFT to be applied accurately to even larger systems. DFT will be indispensable in future technological engineering tasks like the calculation of transport properties in molecular wires and the design of nano-machines.

Chapter 2

A Formal Introduction to Density Functional Theory

2.1 The Schrödinger Equation

The goal of the electronic structure problem is to understand the solutions of the Schrödinger equation,

$$\left(-\frac{\hbar^2}{2m_e} \sum_{i=1}^N \nabla_i^2 + \frac{1}{2} \sum_{\substack{i,j=1 \\ j \neq i}}^N \frac{e^2}{|\mathbf{r}_i - \mathbf{r}_j|} + \sum_{i=1}^N v_{ext}(\mathbf{r}_i) \right) \Psi(x_1 \dots x_N) = E \Psi(x_1 \dots x_N), \quad (2.1)$$

for different potentials, $v_{ext}(\mathbf{r})$, where $x_i = (\mathbf{r}_i, \sigma_i)$ represents a set of both position and spin values for the i -th electron, and N is the number of electrons. Sometimes the Schrödinger equation is written in operator form,

$$(\hat{T} + \hat{V}_{ee} + \hat{V}_{ext}) \Psi(x_1 \dots x_N) = E \Psi(x_1 \dots x_N), \quad (2.2)$$

where

$$\hat{T} = -\frac{\hbar^2}{2m_e} \sum_{i=1}^N \nabla_i^2 \quad (2.3)$$

is the kinetic energy operator,

$$\hat{V}_{ee} = \frac{1}{2} \sum_{i,j=1, j \neq i}^N \frac{e^2}{|\mathbf{r}_i - \mathbf{r}_j|} \quad (2.4)$$

is the electron-electron interaction, and

$$\hat{V}_{ext} = \sum_{i=1}^N v_{ext}(\mathbf{r}_i) \quad (2.5)$$

is the external potential. Typically, in solid-state physics and chemistry, the external potential is a Coulombic attraction to a set of nuclei,

$$v_{ext}(\mathbf{r}) = \sum_j \frac{Z_j e^2}{|\mathbf{r} - \mathbf{R}_j|}, \quad (2.6)$$

where \mathbf{R}_j and Z_j are the locations and charges of the nuclei. Sometimes, the external potential may have a different form as in realistic solid-state calculations. In this thesis, we use the Born-Oppenheimer approximation and fix the positions of the nuclei. This approximation is accurate because the typical mass of a nuclei is much larger than the mass of an electron.

Because the electrons are fermions, the wave-function, $\Psi(x_1 \dots x_N)$, is antisymmetric under particle interchange:

$$\Psi(x_1 \dots x_a \dots x_b \dots x_N) = -\Psi(x_1 \dots x_b \dots x_a \dots x_N). \quad (2.7)$$

This antisymmetry implies that no two fermions can occupy the same quantum state.

In principle, all of electronic physics within the fixed-nuclei approximation can be described accurately from Eqs. (2.1, 2.7, & 2.6). Unfortunately, as mentioned in Chapter 1, exact solutions in all but a few rare cases are unattainable.

In this thesis, we will be most concerned with a density-based theory. The total electron density is defined as

$$n(\mathbf{r}) = N \sum_{\sigma_1, \sigma_2 \dots \sigma_N} \int d\mathbf{r}_2 \dots d\mathbf{r}_N |\Psi(x, x_2 \dots x_N)|^2. \quad (2.8)$$

Henceforth, $e^2 = \hbar = m_e = 1$ and all energies will be in Hartrees and all lengths in Bohr radii, a_0 , unless explicitly stated. Recall that 1 Hartree = 27.2 eV = 628 kcal/mol and $a_0 = 52.9 \times 10^{-12} m = 0.529$ Angstroms.

2.2 Variational Principle

An important theoretical principle, upon which many calculations rely, is the variational principle. It tells us how to look for ground-state solutions. The exact

ground-state wave-function minimizes the expectation value of the Hamiltonian [72]:

$$E_{gs} = \min_{\Psi} \langle \Psi | \hat{H} | \Psi \rangle / \langle \Psi | \Psi \rangle. \quad (2.9)$$

A guessed normalized wave-function will always give a greater expectation value for the total energy unless of course the guess is exact! A rough derivation of the variational principle is as follows. Imagine we expand a trial solution in the complete basis of exact solutions for a chosen Hamiltonian:

$$|\Psi_{trial}\rangle = \sum_i c_i |\psi_i\rangle. \quad (2.10)$$

We require that the trial wave-function be normalized:

$$\langle \Psi_{trial} | \Psi_{trial} \rangle = \sum_i |c_i|^2 = 1. \quad (2.11)$$

Now, we write the energy expectation value using the trial wave-function,

$$E_{trial} = \langle \Psi_{trial} | \hat{H} | \Psi_{trial} \rangle = \sum_i |c_i|^2 E_i. \quad (2.12)$$

If the eigenvalues, E_i 's, are ordered then E_0 has the lowest value. We can only achieve the minimum if we have the maximum contribution of E_0 ; that is when $|c_0|^2 = 1$.

Two popular electronic structure methods, Hartree-Fock and configuration-interaction (CI), rely directly on this principle. Hartree-Fock theory is based on the minimization of Eq. (2.9) using one anti-symmetrized product of N single-particle orbitals or a Slater determinant [22]:

$$\Phi(x_1 \dots x_N) = \begin{vmatrix} \phi_1(x_1) & \dots & \phi_N(x_1) \\ \vdots & & \vdots \\ \phi_1(x_N) & \dots & \phi_N(x_N) \end{vmatrix}. \quad (2.13)$$

The latter, CI, involves minimization over a sum of different N -particle Slater determinants. The space of many-particle wave-functions is spanned by a set of

Slater determinants of orbitals from the complete set of single-particle orbitals. The exact wave-function can be expressed exactly this way. But since the number of Slater determinants can often be large, this scheme is only useful for small systems.

DFT relies on the variational principle, but in a different way as we will see in the next section.

2.3 The Hohenberg-Kohn Theorem

The traditional way to solve the ground-state electronic structure problem goes as follows. Start with an external potential and solve Eq. (2.1) to get the wave-function. Then, use the wave-function to find the electron density or other interesting properties. Schematically, this is as follows:

$$V_{ext} \rightarrow \Psi_{Many-body} \rightarrow n. \quad (2.14)$$

The problem is that the many-body wave-function is hard to get and difficult to handle for even small numbers of electrons.

Density functional theory starts with the observation that the wave-function and all physical properties derived from it are uniquely characterized by the ground-state density. The map between external potential and the electron density is one-to-one and unique up to an arbitrary constant shift in the potential:

$$n \leftrightarrow V_{ext}. \quad (2.15)$$

There are some caveats about systems with degenerate ground-states, and we will assume in what follows that the ground-state is non-degenerate. As seen before in Eq (2.14), the potential still determines the wave-function; but, since the potential is determined by the density, it follows that all derived quantities can be written as functionals of the density. In practice, writing everything in terms of the density might not be so simple to do, but theoretically it is possible.

The proof is by *reductio ab absurdum* [23]. Suppose that we have two different external potentials that each yield the same ground-state density. By different, we mean that the potentials differ by more than a constant. The two potentials will have different ground-state wave-functions. Now, we use the variational principle. If we use the ground-state wave-function for one of the potentials as a trial wave-function for the other, we find the inequality,

$$\langle \Psi_2 | \hat{T} + \hat{V}_{ee} + \hat{V}_{ext,1} | \Psi_2 \rangle > \langle \Psi_1 | \hat{T} + \hat{V}_{ee} + \hat{V}_{ext,1} | \Psi_1 \rangle. \quad (2.16)$$

Notice that this is an inequality. The equality can only be satisfied if both wave-functions are the same, and we had assumed this not to be true. The last term on both sides of Eq. (2.16) is equal since we assume that both wave-functions have the same density:

$$\langle \Psi_{1,2} | \hat{V}_{ext} | \Psi_{1,2} \rangle = \int d^3r n(\mathbf{r}) v_{ext}(\mathbf{r}). \quad (2.17)$$

If we cancel these terms in Eq. (2.16), we find

$$\langle \Psi_2 | \hat{T} + \hat{V}_{ee} | \Psi_2 \rangle > \langle \Psi_1 | \hat{T} + \hat{V}_{ee} | \Psi_1 \rangle. \quad (2.18)$$

Next, we repeat this but use the other wave-function as a trial wave-function for the first potential. We find

$$\langle \Psi_2 | \hat{T} + \hat{V}_{ee} | \Psi_2 \rangle < \langle \Psi_1 | \hat{T} + \hat{V}_{ee} | \Psi_1 \rangle. \quad (2.19)$$

Both 2.18 and 2.19 cannot be satisfied simultaneously. It can be expected that no two different potentials can yield the same density. One potential is uniquely related to one density, and conversely, the potential is uniquely determined by the density.

2.4 Levy-Constrained Search Proof

Another and perhaps more intuitive proof that the density uniquely characterizes a system comes from the Levy constrained search proof [42]. We rewrite the

variation principle, Eq. (2.9), for the total energy in two steps,

$$E[n] = \min_n \left[F[n] + \int d^3r v_{\text{ext}}(\mathbf{r}) n(\mathbf{r}) \right] \quad (2.20)$$

where the minimization is over all N -particle density-distributions. We have defined a new functional,

$$F[n] = \min_{\Psi \rightarrow n} \langle \Psi | \hat{T} + \hat{V}_{ee} | \Psi \rangle, \quad (2.21)$$

where the minimization is over all many-body wave-functions, Ψ , that yield the density, n . $F[n]$ does not depend on the form of the external potential. It is a universal functional of the density! That means that one well-chosen approximation for $F[n]$ should give accurate results for a large class of external potentials.

We can explicitly recover the potential from the density by minimizing Eq. (2.20) with the constraint that the density integrates up to a fixed number of electrons:

$$\delta \left\{ F[n] + \int d^3r n(\mathbf{r}) v_{\text{ext}}(\mathbf{r}) - \mu \int d^3r n(\mathbf{r}) \right\} = 0. \quad (2.22)$$

The result is

$$v_{\text{ext}}(\mathbf{r}) = \mu - \frac{\delta F[n]}{\delta n(\mathbf{r})}, \quad (2.23)$$

the external potential as a functional of the density.

Solving Eq. (2.22) would be equivalent to solving the many-particle Schrödinger equation if we have an accurate approximation for $F[n]$. Note that this, unlike Eq. (2.1), is an equation in one variable with only three components!

In DFT, the total energy is expressed as a functional of the density:

$$E[n] = T[n] + V_{\text{ee}}[n] + \int d^3r v_{\text{ext}}(\mathbf{r}) n(\mathbf{r}). \quad (2.24)$$

We split $F[n]$ into kinetic, $T[n]$, and interaction, $V_{\text{ee}}[n]$, parts.

2.5 Thomas-Fermi Theory

The first and simplest DFT was conceived in the early days of modern quantum mechanics. Thomas and Fermi wrote the total energy of an electron system as a pure functional of the density [19, 20],

$$E[n] = T_{TF}[n] + U_H[n] + \int d^3r n(\mathbf{r}) v_{\text{ext}}(\mathbf{r}) \quad (2.25)$$

with

$$T_{TF}[n] = \frac{3}{10}(2\pi^2)^{\frac{2}{3}} \int d^3r n^{\frac{5}{3}}(\mathbf{r}) \quad (2.26)$$

taken from the kinetic energy of a uniform non-interacting electron gas and with the next term being the classical Hartree term,

$$U_H[n] = \frac{1}{2} \int d^3r \int d^3r' \frac{n(\mathbf{r})n(\mathbf{r}')}{|\mathbf{r} - \mathbf{r}'|}. \quad (2.27)$$

Eq. (2.25) for the total energy can be minimized with respect to the density and solved for a variety of external potentials. For most applications, this approximation is not accurate enough because it fails to describe most quantum mechanical effects accurately. Most of this inaccuracy comes from the way the kinetic energy is treated as entirely local.

2.6 The Non-Interacting Kohn-Sham System

In practice, most DFT calculations rely on the analysis of a non-interacting counterpart to the interacting system [24]. The main idea is, instead of using the kinetic energy of a uniform electron gas, Eq (2.26), to use

$$T_s[n] = \min_{\phi_s \rightarrow n} \langle \phi_s | \hat{T} | \phi_s \rangle \quad (2.28)$$

where ϕ_s is a Slater determinant of single-particle orbitals, and the minimization is over all determinants that give the density n . This is the exact kinetic energy of a system of non-interacting electrons with a certain density.

The functional, $F[n]$, is the sum of this non-interacting kinetic part, the classical Hartree contribution, and $E_{\text{xc}}[n]$ which is everything left over. The total energy is

$$E[n] = T_{\text{s}}[n] + U_{\text{H}}[n] + E_{\text{xc}}[n] + \int d^3\mathbf{r} v_{\text{ext}}(\mathbf{r}) n(\mathbf{r}). \quad (2.29)$$

Sometimes, $E_{\text{xc}}[n]$ is split up into exchange and correlation parts, $E_{\text{x}}[n]$ and $E_{\text{c}}[n]$. Performing the Euler-Lagrange variation and constraining the particle number gives the Kohn-Sham equation,

$$v_{\text{KS}}(\mathbf{r}) = \mu - \frac{\delta T_{\text{s}}[n]}{\delta n(\mathbf{r})}. \quad (2.30)$$

Solving Eq. (2.30) is equivalent to solving

$$\left(-\frac{1}{2}\nabla^2 + v_{\text{KS}}([n]; \mathbf{r})\right) \phi_i(\mathbf{r}) = \epsilon_i \phi_i(\mathbf{r}). \quad (2.31)$$

For the Kohn-Sham (KS) orbitals in the local multiplicative KS potential,

$$v_{\text{KS}}(\mathbf{r}) = v_{\text{ext}}(\mathbf{r}) + v_{\text{H}}(\mathbf{r}) + v_{\text{xc}}(\mathbf{r}), \quad (2.32)$$

with $v_{\text{H}}(\mathbf{r}) = \delta U_{\text{H}}[n]/\delta n(\mathbf{r})$ and $v_{\text{xc}}(\mathbf{r}) = \delta E_{\text{xc}}[n]/\delta n(\mathbf{r})$. To get the density, we simply sum the contributions from the occupied KS orbitals,

$$n(\mathbf{r}) = \sum_i \theta(\mu - \epsilon_i) |\phi_i(\mathbf{r})|^2. \quad (2.33)$$

If the E_{xc} used in the calculation is exact, this density that comes out is also exact.

The Kohn-Sham equation, Eq. (2.31), must be solved using a self-consistent scheme. The scheme is as follows. An initial guess for the density is made and a KS potential is constructed from it. The resulting KS equation is solved for the KS orbitals, and the orbitals are then used to find a new density. The new density gives a new potential and we calculate again. This procedure is re-iterated until the density changes less than some chosen criteria. Figure 2.1 shows this schematically.

Analysis of this KS system can then be used to give information about the interacting system. For example, the total energy is related to the density and the KS eigenvalues through

$$E[n] = \sum_{occ.} \epsilon_{KS} + U_H[n] + E_{XC}[n] - \int d^3\mathbf{r} v_H(\mathbf{r}) n(\mathbf{r}) - \int d^3\mathbf{r} v_{XC}(\mathbf{r}) n(\mathbf{r}), \quad (2.34)$$

where the sum is over the eigenvalues for the occupied KS orbitals.

In this KS approach, a large portion of the total energy, the kinetic contribution, is treated exactly for a system of non-interacting electrons. It is important to note that the KS wave-function is not an approximation to the exact wave-function. In KS theory, only E_{XC} must be approximated, and this turns out to be amenable to local and semi-local approximations.

Is it true that for every interacting ground-state problem we can find this non-interacting counterpart? Two formal problems are the questions of N- and V-representability. A density is N-representable if it can be obtained from some N particle wave-function [73, 74]. A density is V-representable if it can be obtained from the ground-state wave-function for a local external potential. The former problem has been solved [42, 75, 76, 77], but the latter remains unsolved [42, 78].

The numerical problem of explicitly inverting the KS equation and finding the potential from the density, Eq. (2.30), has also been considered [79, 80, 81].

Incidentally, DFT is valid beyond fixed-nuclei approximation. A quantum mechanical description of the physics beyond the fixed-nuclei approximation is given by multi-component DFT [82].

2.7 The Exchange Correlation Energy, Nature's Glue

The exchange-correlation energy is sometimes referred to as *nature's glue* [83] because it is responsible for keeping much of matter together by counteracting some of the Coulomb repulsion. If nature only kept the classical interaction energy, the

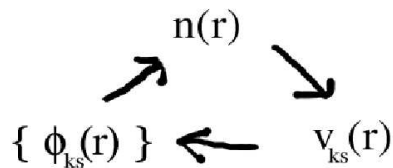


Figure 2.1: Kohn-Sham Self-Consistent Cycle shown Schematically

System	E_{tot}	T_s	V_{ext}	U_H	E_x	E_C
H	-0.500	0.500	-0.687	0.313	-0.313	0.000
He	-2.904	2.000	-2.867	2.049	-1.025	-0.042
Ne	-128.926	128.63	-311.15	66.086	-12.49	-0.390
Hooke's Atom, k=1/4	2.000	0.635	0.8881	1.0302	-0.515	-0.039

Table 2.1: Components of the total energy for atoms. The results are from a combination of calculations and comparisons to experimental data [159, 142, 79, 145]. E_{tot} is the total ground-state energy of the system, T_s is the non-interacting kinetic energy contribution, V_{ext} is the contribution from the external potential, U_H is the Hartree contribution, E_x is the exchange contribution, and E_C is the correlation contribution.

Hartree term, then chemical bonds would be weaker and longer. The exchange-correlation contribution reduces the interaction energy because it accounts for the tendency of electrons not to collide.

As mentioned earlier, the total energy is often expressed as a functional of the density, Eq. (2.24). To give a rough idea of the relative magnitudes of the various components of the energy, we present Table 2.1. The listed values are not all highly accurate and are shown just to give the reader an idea of the orders of magnitude of the energy contributions.

Because of the demand for ever-increasing accuracy in industry and the unmet demands of thermo-chemistry, finding more accurate approximations to this exchange-correlation energy is an important area of research.

2.8 Jacob's Ladder of Approximations

John Perdew has classified the ever-increasing detail, accuracy, and cost of density functionals according to a biblical analogy. Most popular functionals fall one way or another into this scheme. This is Jacob's ladder of approximations. Chemical accuracy is on top. [84]. Each rung preserves the formal, exact properties of the lower rungs:

1. The local density approximation (LDA)

The lowest rung of the ladder is LDA,

$$E_{\text{xc}}^{\text{LDA}}[n] = \int d^3r n(\mathbf{r}) \epsilon_{\text{xc}}(n(\mathbf{r})). \quad (2.35)$$

The idea is that at each point in a molecule or solid, an electron experiences the same effect from the surrounding electrons as if the electronic density were uniform and equal to the density where the affected electron is. The total interaction energy would then be an integral over all local contributions. The local energy per particle comes from the exact, known, and parameterized exchange-correlation energy of a uniform gas for the exchange correlation energy density at each point in space [24].

The LDA is correct for at least one physical system, the uniform gas, and satisfies many exact constraints [85, 86]. It is accurate for uniform and slowly varying densities and is useful in solid-state physics. Because of its simplicity, this functional is perhaps the most reliable.

A sketch of how the LDA is constructed starts with the exact ground-state energy of a uniform system. The exact ground-state energy of the three-dimensional uniform unpolarized Fermi gas, termed Jellium, in the high-density limit is a function of the electronic density [27]:

$$\lim_{r_s \rightarrow 0} \left(\frac{E}{N} \right) = \left[\frac{2.21}{r_s^2} - \frac{0.916}{r_s} + 0.0622 \ln r_s - 0.096 + \mathcal{O}(r_s) \right] \quad (2.36)$$

with

$$r_s = \left(\frac{3}{4\pi n} \right)^{\frac{1}{3}}. \quad (2.37)$$

The first term is the kinetic contribution. The next is the exchange contribution. And the remainder is the correlation contribution. The idea of the LDA is to take the exchange-correlation energy per particle from this uniform gas and to use this in the functional, Eq. (2.35).

The ground-state energy of Jellium is known through analytic forms for the high and low density limits and Monte Carlo calculations for intermediate densities [28]. Accurate parameterizations of the entire energy versus density curve have been constructed and are in use [40].

LDA tends to over-emphasize metallic character. In LDA, weak bonds like hydrogen bonds are over-estimated. Some successes and shortcomings of LDA are discussed in Ref. [29]. Numerically precise benchmark LDA results for atoms are available to test the precision of new codes [30].

2. The generalized gradient approximation (GGA)

A naïve gradient expansion about the local-density approximation is problematic [24, 23], but careful considerations lead to the generalized gradient approximations [37, 87, 41],

$$E_{\text{XC}}^{\text{GGA}}[n] = \int d^3r n(\mathbf{r}) \epsilon_{\text{XC}}(n(\mathbf{r}), \nabla n(\mathbf{r})). \quad (2.38)$$

GGA's preserve many of the exact features of LDA and provide results which are good for chemistry as well as solid-state physics. Table 2.2 shows how this higher rung functional outperforms the LDA in predicting many fundamental properties.

3. The meta-generalized gradient approximation (meta-GGA)

The next rung is the meta-GGA [88, 89],

$$E_{\text{XC}}^{\text{Meta-GGA}}[n] = \int d^3r n(\mathbf{r}) \epsilon_{\text{XC}}(n(\mathbf{r}), \nabla n(\mathbf{r}), \tau(\mathbf{r})), \quad (2.39)$$

which depends on the KS kinetic energy density,

$$\tau(\mathbf{r}) = \frac{1}{2} \sum_{\epsilon_i < \mu} |\nabla \phi_i(\mathbf{r})|^2. \quad (2.40)$$

The Meta-GGA is more accurate than the GGA for slowly varying or one-electron densities. Meta-GGA's are becoming implementable in quantum chemistry.

For the first two rungs, the functional derivative yielding the exchange-correlation potential,

$$v_{\text{xc}}(n; \mathbf{r}) = \frac{\delta E_{\text{xc}}[n]}{\delta n(\mathbf{r})}, \quad (2.41)$$

can be done analytically. It is less obvious how to take the functional derivatives with respect to τ . However, there are ways around this problem [90, 91].

4. Orbital functions of the occupied KS orbitals, Hyper-GGA's

Each step up Jacob's ladder brings more accuracy but also more computational cost. The next rung, orbital functionals of the first type,

$$E_{\text{xc}}^{\text{Orb.I}}[n] = E_{\text{xc}}^{\text{Orb.I}}[\phi_{KS}^{\text{Occ.}}\{n\}], \quad (2.42)$$

depends on the occupied KS orbitals [92]. The KS Orbitals are implicit functions of the density; consequently, $E_{\text{xc}}^{\text{Orb.I}}[n]$ is a density functional. Orbital functionals are considerably more expensive to implement self-consistently; however, the non-interacting kinetic energy is a functional of the occupied KS orbitals, and the approximate KS orbitals result from any self-consistent lower-rung calculation. Consequently, using this rung non-self-consistently in addition to a self-consistent lower rung calculation does not consume significantly more computer time and resources.

A side step from this rung is the idea of a hybrid functional [46, 93, 63],

$$E_{\text{xc}}^{\text{Hybrid}}[n] = (1 - b)E_{\text{xc}}^{\text{GGA}}[n] + bE_{\text{xc}}^{\text{Orb}}[\phi_{KS}]. \quad (2.43)$$

These are popular in chemistry for their accuracy and are appearing in solid-state physics [94]. The understanding of why they work is related to the adiabatic connection which we will discuss later [95].

5. Orbital functions of the unoccupied KS orbitals

The second-generation of orbital functionals,

$$E_{\text{xc}}^{\text{Orb.II}}[n] = E_{\text{xc}}^{\text{Orb.II}}[\phi_{\text{KS}}\{n\}], \quad (2.44)$$

includes the unoccupied non-interacting KS orbitals [96]. This rung can describe E_{xc} exactly in principle but is extremely difficult to implement since there are an infinite number of unoccupied orbitals. An example of a second-generation orbital functional is the Interaction Strength Interpolation (ISI) functional. This function will be discussed in more detail in Chapter 5.

There are other approaches outside the ladder of approximations. One example is self-interaction corrected DFT which ensures that DFT correctly describes one-electron systems and the long-range physics. Another approximation, weighted density approximation, uses the density only explicitly and approximates the pair correlation.

Rung	E_{x}	E_{c}	Atom.En.	Bonds	Structures	Energy Barriers
LDA	5%	0.5%	1.5 eV	1% short	Close Packing	100%
GGA	100%	5%	0.4 eV	1% long	Correct	30%

Table 2.2: Typical errors for two different rungs of functionals as transcribed from John Perdew’s lecture notes from the DFT Summer School at Caramulo, Portugal, 2001. Atom. En. refers to atomization energies or the energy required to split a molecule to the individual atoms. Bonds refers to bond lengths. Structures refers to the most stable lattice structure. Energy barriers refer to the predicted energy of a transition state.

2.9 Exact Constraints on the Exchange-Correlation Functional

The systematic way to climb Jacob’s Ladder and to improve approximations is by imposing exact constraints on approximate functionals. One of the most basic

exact constraints is that

$$E_{\text{xc}}[n] \leq 0. \quad (2.45)$$

The exchange-correlation energy is always negative. Other examples of exact constraints include the Lieb-Oxford bound [97], electron-hole properties [98, 99, 100], sum rules [87], satisfaction of the virial theorem [101], and proper behavior under uniform scaling laws [101]. A review of several known constraints and functionals that obey them is available [102].

An example of how exact constraints have been used to find better functionals is in the construction of generalized gradient approximations. Originally, gradient functionals were in the form of simple expansions about the uniform limit. When applied, it was discovered that gradient functionals were often less accurate than the local density approximation [103]. The trouble was that the approximation violated the exchange-hole sum-rule. Requiring that GGA obey this rule resulted in the generalized gradient approximation. The new approximation was accurate enough for even quantum chemistry.

Another useful construct is the adiabatic connection. Formally, we can express the unknown exchange-correlation functional as

$$E_{\text{xc}}[n] = \int_0^1 d\lambda \left(\langle \Psi_n^{\text{min},\lambda} | \hat{V}_{\text{ee}} | \Psi_n^{\text{min},\lambda} \rangle - U_H[n] \right) = \int_0^1 d\lambda U_{\text{xc}}(\lambda), \quad (2.46)$$

where $\Psi_n^{\text{min},\lambda}$ is the wave-function that minimizes $\langle \Psi | \hat{T}_s + \lambda \hat{V}_{\text{ee}} | \Psi \rangle$ and gives electron density, n , and $U_{\text{xc}}(\lambda)$ is exchange-correlation potential contribution.

Figure 2.2 shows the adiabatic connection curve for He. The area between the curve and the y-axis is the exchange-correlation energy. The weak interaction limit of the curve is the exchange contribution to this functional. Analysis for the shape of this curve has given insights into the accuracy of approximate functionals.

For example, notice that the LDA curve offers a poor description of both limits of the adiabatic curve. However, in actual calculations, we are interested

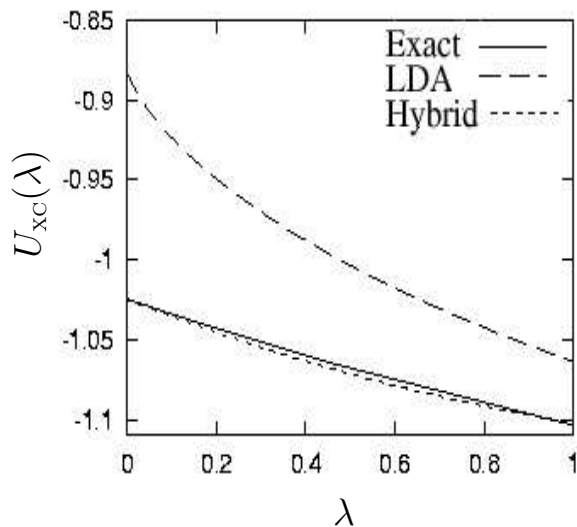


Figure 2.2: The adiabatic connection for Helium. The solid line is the exact result, the long dashed-line is from the LDA functional, and the short-dashed line is from the BLYP hybrid functional.

in the total energy. The coupling constant integral of the LDA curve is not a bad approximation to the integral over the exact curve. The accuracy of Hybrid functionals can be understood with this construct [104]. Hybrids can be thought of as approximate integrals over the curve. Since the exact small λ is exchange and standard approximations give a decent approximation to the $\lambda = 1$ limit, a suitable average of both gives a better approximation to the exchange-correlation energy.

2.10 Cornerstones of a Density Functional Theory

So far, we have seen the importance of density functional theory and the need to understand and approximate the exchange-correlation energy in accurate but practical ways. The remainder of this thesis will be dedicated to understanding the exchange-correlation energy functional at a fundamental level.

We will start by analyzing a delta-function interaction in Chapter 3. In developing a density functional theory for this interaction, we will show what kind of general considerations go into functional construction. In particular, we will see that a fairly accurate representation of the local density functional can be obtained by simply applying scaling arguments to a uniform system. We will explore the analogs of some Coulomb-interacting theorems to get an idea of what exact constraints are useful in functional construction. In particular, we will argue that a good parameterization to the delta-function LDA can be improved by ensuring that the high-density limit is properly satisfied.

In Chapter 4, we focus on the chemically interesting Coulomb-interacting problem. Uniform density scaling laws can be used to check and to improve approximations. Many of these scaling laws can be generalized to the case of spin DFT. Requiring that functionals obey many of these spin-scaling laws may enable more accurate treatment of magnetic systems.

Scaling is intimately tied with the adiabatic connection. Chapter 5 shows that analysis of the adiabatic connection can lead to more accurate functionals. In particular, we explore what happens when the electron-electron interaction becomes infinitely strong. We use a model system and a clever manipulation of scaling laws to test several hypotheses about this limit. This chapter ties in with the general theme of the thesis through the use of the adiabatic connection to create new functionals and to test theoretical models.

Another way to construct functionals from the adiabatic connection is to start with the small λ limit. Here, the integrand of Eq. (2.46) is known exactly. Taking this limit as a constant approximation to the integrand for all λ , we arrive at the exact exchange functional for the exchange-correlation energy. Considering DFT from this limit provides a systematic way to understand functional development in DFT. In section 2.9, analysis of this limit explains why hybrid functionals are so accurate. We have chosen to start from this limit to consider another fundamental

question in DFT: Should DFT describe the fundamental band gap for a solid?

Chapter 3

A Simple Example: Density Functional Theory for a One-Dimensional Contact Interaction

Three-dimensional electronic structure calculations are enormously complicated endeavors. It is helpful and insightful to focus on the underlying ideas of a density functional theory with as few complications as possible. To get an idea of what DFT is, how it works, and what considerations go into approximate functional development, we will introduce a one-dimensional analog of the Coulomb interaction. We will find a local-density functional for the exchange and correlation energies and explore some one-dimensional systems like the analog of helium and the Hooke's atom.

3.1 One-Dimensional Contact-Interaction Models

Density functional theory is typically applied to Coulomb-interacting fermions in three dimensions, but the Hohenberg-Kohn theorem holds for other interaction types and in other dimensions. We propose to consider the contact interaction in one spatial dimension,

$$v_{ee}(x_i - x_j) = \lambda \delta(x_i - x_j), \quad (3.1)$$

where x_i and x_j represent the spatial coordinates of the fermions, $\delta(x)$ is the Dirac delta function, and λ is the interaction strength. The Fermions have two spin-like states. The delta-function potential is a one-dimensional analog to the Coulomb one since it scales in a similar fashion. However, it differs in

that it is short-ranged. Note that although the interaction itself is short-ranged, the effective interaction need not be. This effective longer range comes from second-order effects. Note that DFT is a ground-state theory, and whether this one-dimensional system is a Luttinger and not a Fermi liquid is not important in what follows.

One-dimensional models are important for several reasons. Perhaps most obviously, they are useful in mathematical and statistical physics to illustrate problems and concepts that are sometimes hard to conceptualize in three dimensions.

Our motivation, however, is to use this one-dimensional model to understand density functional theory. Although the form will be different, many of the properties of the unknown exchange-correlation functional will still hold. Most of the general problems should persist as well. Solving these fundamental problems for contact-interaction DFT could lead to solutions of the similar problems in three-dimensional DFT. For example, this one-dimensional DFT could be used to examine the one-dimensional solids and transport through them. Or it could be used to study the analog of stretched H_2 . Contact-interacting models have already been used specifically in DFT to study scattering problems but without the inclusion of any correlation effects [69]. Furthermore, using DFT to study non-Coulombic interactions, like in the Hubbard model, is an exciting area of current research [105, 106].

It has been suggested that contact-interacting models should give a good representation of the physics of one-dimensional fermions in certain experimental contexts [107, 108, 109, 110]. Examples of such systems are semi-conductor quantum wires, conducting organic materials, and carbon nanotubes.

3.2 Exact-Exchange Density Functional

In this section, we will see that the Hartree-Fock theory is equivalent to exact-exchange DFT. Because of the anti-symmetry of the wave-function under particle interchange, particles with the same spin-labels will never be found at the same point in space and, consequently, will not experience the contact interaction between each other. Only opposite spins will interact directly.

The Hartree term depends only on the total electron density,

$$U_H[n] = \frac{1}{2} \int dx dx' n(x) (\lambda \delta(x - x')) n(x') = \frac{\lambda}{2} \int dx n(x)^2. \quad (3.2)$$

$n(x)$ is the total fermion density.

To first order in λ , there is an unphysical overcounting here because like spins should not interact via the delta-function. The exchange term must cancel these spurious like-spin interactions. A simple functional which would do this is

$$E_x[n_\uparrow, n_\downarrow] = -\frac{\lambda}{2} \int dx (n_\uparrow(x)^2 + n_\downarrow(x)^2) \quad (3.3)$$

where $n_\uparrow(x)$ corresponds to the local up-spin density, and $n_\downarrow(x)$ is the down-spin density. The total density is related to these via $n(x) = n_\uparrow(x) + n_\downarrow(x)$. Eq. (3.3) can be derived using the standard rules of many-body perturbation theory to first order in λ [111]. To simplify the notation, let

$$\zeta(x) = \frac{n_\uparrow(x) - n_\downarrow(x)}{n_\downarrow(x) + n_\uparrow(x)}. \quad (3.4)$$

Then, the exact-exchange functional is

$$E_x[n, \zeta] = -\frac{\lambda}{2} \int dx n(x)^2 (1 + \zeta(x)^2)/2. \quad (3.5)$$

For a one-electron system, $\zeta = 0$, and we have $E_x[n] = -U_H[n]$; exact-exchange is self-interaction free. This exact-exchange functional also satisfies the same equality as the three-dimensional Coulombic one for a spin-singlet two-electron system: $E_x[n] = -U_H[n]/2$.

3.3 Deltium: The One-Dimensional Uniform Fermi Gas

In order to obtain a local density correlation functional, we will consider the exact results for the one-dimensional unpolarized Fermi gas, termed Deltium. This Fermi gas will play the role of the uniform electron gas in Coulomb-interacting DFT. The Hamiltonian is [112, 113, 114, 115]

$$\hat{H} = -\frac{1}{2} \sum_i^N \frac{d^2}{dx_i^2} + \lambda \sum_{i<j} \delta(x_i - x_j), \quad (3.6)$$

where N is the number of electrons. We take N and the length, L , of the system to infinity while keeping the density, $n = N/L$, fixed. As noted in the previous section 3.2, the like spins will not be affected by the interaction; consequently, the polarized gas will resemble the non-interacting uniform polarized gas. Thus, we need only consider the unpolarized cases.

Let us review the non-interacting case, $\lambda = 0$, first. Then, we need to solve $\hat{H}\Psi(x_1\dots x_N) = E\Psi(x_1\dots x_N)$ with \hat{H} coming from Eq. (3.6). The many-body wave-function solution of Eq. (3.6) is a Slater determinant of N doubly-occupied plane-waves. The allowed momentum for the plane-waves are quantized by periodic boundary conditions. The total energy per particle of the non-interacting gas is purely kinetic,

$$t(n) = \frac{\pi^2}{24} n^2. \quad (3.7)$$

When interactions are present, the total energy per particle is

$$\epsilon(n) = t(n) + \epsilon_H(n) + \epsilon_x(n) + \epsilon_C(n), \quad (3.8)$$

where $\epsilon_H(n)$ is the Hartree energy per particle, $\epsilon_x(n)$ is the exchange energy per particle, and $\epsilon_C(n)$ is the correlation energy per particle.

Deltium with $\lambda \neq 0$ is exactly solvable via Bethe Ansatz methods [116, 117, 118, 119]. The technique is to guess a wave-function of the form,

$$\Psi(x_1, x_2, \dots, x_N) = \sum_P a_P e^{ik_{P_1}x_1 + \dots + ik_{P_N}x_N}, \quad (3.9)$$

where a_P is an amplitude that depends on the ordering, P , of momenta, k_i 's, for a particular Weyl chamber and spin-configuration. A Weyl chamber means an ordering of coordinates: $0 < x_1 < x_2 < \dots < x_N < L$. Particle interchange symmetries can be used to construct the wave-function in other Weyl chambers. The wave-function is continuous everywhere, but its derivative is discontinuous at the boundary between Weyl chambers:

$$\left[\frac{\partial \Psi(x_1, x_2, \dots, x_N)}{\partial x_i} - \frac{\partial \Psi(x_1, x_2, \dots, x_N)}{\partial x_{i+1}} \right]_{x_i=x_{i+1}} = \lambda \Psi(x_i). \quad (3.10)$$

In order to satisfy continuity and Eq. (3.10), the a_P and the k_i 's must be related via Yang-Baxter relationships [120]. For the uniform Fermi gas, the situation must be handled carefully because of the two spin-types. Nevertheless, with some careful book-keeping [120], the uniform unpolarized Fermi gas problem can be recast as a set of integral equations [121]:

$$\tau(y) = \frac{1}{2\pi} + \frac{2}{\pi} \int_{-\infty}^{\infty} d\Lambda \frac{\lambda \sigma(\Lambda)}{\lambda^2 + 4(y - \Lambda)^2} \quad (3.11)$$

and

$$\sigma(\Lambda) = \frac{1}{2\lambda} \int_{-k_{max}}^{k_{max}} dy \operatorname{sech}(\pi(y - \Lambda)/\lambda) \tau(y). \quad (3.12)$$

In the high-density limit, $k_{max} = \pi n/2$, and in the low-density limit, $k_{max} = \pi n$.

Equations (3.11) and (3.12) must be solved self-consistently for a chosen value of k_{max} to obtain the ground-state energy for the contact-interacting uniform Fermi gas. In order to do this, the integrals are transformed to the interval, $[-1, 1]$, and integrated using six-point quadrature rules. Once $\tau(y)$ is known, we can find the density and energy per particle. The density is

$$n = \int_{-k_{max}}^{k_{max}} dy \tau(y), \quad (3.13)$$

and the energy per particle is

$$\epsilon = \frac{1}{2n} \int_{-k_{max}}^{k_{max}} dy y^2 \tau(y). \quad (3.14)$$

The energy per particle for a wide range of densities could, in the spirit of the three-dimensional DFT, be parameterized in a way that would be useful for actual calculations.

We will consider both the high and low-density limits analytically and numerically. Since we are concerned with parameterizing a functional for correlation, we will subtract out the known kinetic, Hartree, and exchange contributions, and focus on the correlation part.

The forms in both limits come from a combination of dimensional analysis and examination of the exact Bethe Ansatz results. We find the coefficients, c_H and c_L , by fitting $\epsilon(n)$ to a fourth order polynomial in either n or $1/n$ depending on whether we want the low-density or high-density limits and by extracting the appropriate coefficients from the interpolations.

In the high-density limit, the correlation energy per particle approaches a constant:

$$\epsilon_c(n) = -c_H \lambda^2 + \dots \quad (3.15)$$

with $c_2^H = 0.042$. This result can probably be obtained from second-order perturbation theory on the non-interacting gas; however, we determined the constant from numerical analysis of the Bethe Ansatz results.

As we will see in Chapter 5, there is a relationship between scaling and coupling constant changes. Looking at a system with a high electron density is equivalent to considering a moderate-density system with a small interaction. In fact, in the high-density limit, the interaction energy is of the form of a perturbation in λ . The Hartree term is first order in λ and the correlation terms are second-order and higher.

In the low-density limit, the correlation energy per particle is

$$\epsilon_c(n) = -\frac{\lambda}{4}n + \frac{\pi^2}{8}n^2 - \frac{c_L}{\lambda}n^3 + \dots \quad (3.16)$$

with $c_2^L = 4.6$. Notice that the first term in Eq. (3.16) will exactly cancel the Hartree and exchange parts. By the converse argument, the low-density limit is the large λ limit. In this limit, the opposite-spin Fermions repel each other so strongly that the interaction mimics Fermi anti-symmetrization. Thus, the interaction energy per particle is kinetic-like. This means that the first term for the correlation energy must cancel the Hartree energy, and the next term in the correlation energy must be kinetic-like.

3.4 A Local-Density Correlation Functional

A simple parameterization of the correlation energy per particle is

$$\epsilon_C^{simple}(n) \approx -\frac{\lambda^2}{2\pi^2} \left(\frac{n}{n + \frac{2\lambda}{\pi^2}} \right). \quad (3.17)$$

This approximation gives the first two terms of the low-density limit correctly, and the next term approximately. The high-density limit is reproduced only approximately. For the parameterization, the first-order coefficients are $c_2^L = \pi^4/16 = 6.088$ in the low-density limit and $c_2^H = 1/2\pi^2 = 0.05$ in the high-density limit. Although these terms are not exactly described by the parameterization, the entire curve is well-described. The parameterization of ϵ_C as a maximum error of 19 % as $n \rightarrow \infty$.

Using Eq. (3.17), we can write an approximate correlation energy LDA functional for the unpolarized case,

$$E_C^{LDA,simple}[n] = \int dx n(x) \epsilon_{xC}^{unif.}(n(x)) \approx -\frac{\lambda^2}{2\pi^2} \int dx \frac{n^2(x)}{n(x) + \frac{2\lambda}{\pi^2}}. \quad (3.18)$$

Regions with more electron density will contribute more to the total energy. Therefore, it is important that the parameterization of the LDA reproduce the high-density limit correctly. We can do this in several ways. A simple solution is

to add a correction to the parameterization which dies down for smaller densities. The new parameterization of the LDA correlation energy per particle is then

$$\epsilon_c(n) \approx \frac{-\lambda^2}{2\pi^2} \left(\frac{n}{n + \frac{2\lambda}{\pi^2}} \right) \left(0.829 + (1 - 0.829)e^{-10n^2/\lambda^2} \right). \quad (3.19)$$

When $n \rightarrow \infty$, we find $\epsilon_c(n) = 0.829\epsilon_c^{simple}(n)$. The pre-factor, $c_H/c_H^2 = 0.829$, ensures that the high-density limit is satisfied. In the low-density limit, this reduces to Eq. (3.17) exponentially fast. The gaussian form and factor of 10 are chosen a bit arbitrarily to ensure that the connection between both limits is smooth. A better way of choosing this factor would be to fix it by matching an additional exact constraint in either the low or high-density limit. We leave further improvements on this parameterization for future work.

This approximation, Eq. (3.19), to the LDA is smooth and reproduces between 99-105% of the correlation energy per particle for all densities. This accuracy is sufficient to show that the one-dimensional LDA is an accurate and useful construct. This parameterization can be used in a local density correlation functional,

$$E_C^{LDA}[n] \approx -\frac{\lambda^2}{2\pi^2} \int_{-\infty}^{\infty} dx \frac{n^2(x)}{n(x) + \frac{2\lambda}{\pi^2}} \left(0.829 + (1 - 0.829)e^{-10n(x)^2/\lambda^2} \right). \quad (3.20)$$

Figure 3.1 compares the performance of these parameterizations to the exact numerical results for the uniform unpolarized gas.

In the fully-polarized case, there is no interaction contribution to the total energy, and the correlation energy functional is trivially

$$E_C^{LDA}[n] = 0. \quad (3.21)$$

We note here that the local density correlation potential is

$$\begin{aligned} v_c(n) = \frac{\delta E_C^{LDA}[n]}{\delta n} = & -\frac{\lambda^2}{2\pi^2} \frac{n^2 + \frac{2\lambda}{\pi^2}}{\left(n + \frac{2\lambda}{\pi^2}\right)^2} \left(0.829 + (1 - 0.829)e^{-10n^2/\lambda^2} \right) \\ & + 20n \frac{1}{2\pi^2} \left(\frac{n^2}{n + \frac{2\lambda}{\pi^2}} \right) (1 - 0.829) e^{-10n^2/\lambda^2}. \end{aligned} \quad (3.22)$$

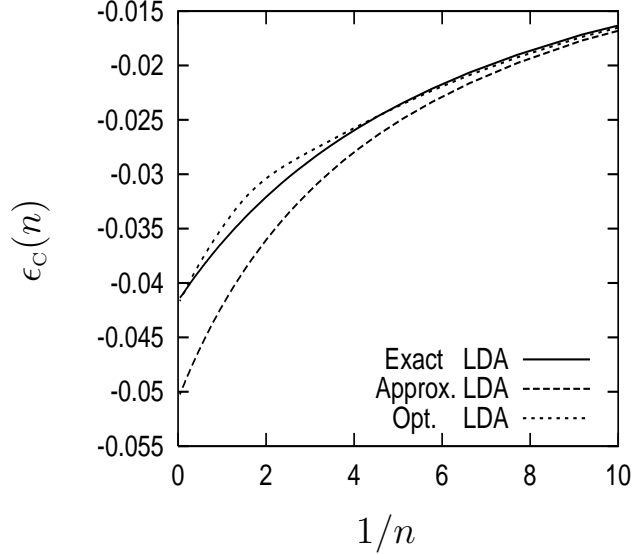


Figure 3.1: Correlation energy per particle for Deltium, the one-dimensional uniform contact-interacting Fermi gas, $\lambda = 1$. The solid line is the exact result calculated from the Bethe-Ansatz integral equations. The long-dashed line is the simple LDA parameterization given by Eq. (3.18). The short-dashed line is the more accurate LDA parameterization given by Eq. (3.20).

3.5 Diracium, the Contact-Interacting Analog of Helium

In order to assess the accuracy of the LDA to handle one-dimensional problems, we will start with perhaps the most difficult test case, a completely non-uniform system, Diracium. This is the one-dimensional analog of helium with traditional Coulomb terms replaced by delta-functions. The system is described by the Hamiltonian:

$$\hat{H} = -\frac{1}{2} \frac{d^2}{dx_1^2} - \frac{1}{2} \frac{d^2}{dx_2^2} - Z\delta(x_1) - Z\delta(x_2) + \lambda\delta(x_1 - x_2) \quad (3.23)$$

and the eigenvalue equation,

$$\hat{H}\Psi_{\sigma\sigma'}(x_1, x_2) = E\Psi_{\sigma\sigma'}(x_1, x_2), \quad (3.24)$$

where x_1 and x_2 are the positions of the electrons, σ and σ' are the spin-like labels of the electrons, Z is the magnitude of the external potential, and Ψ is

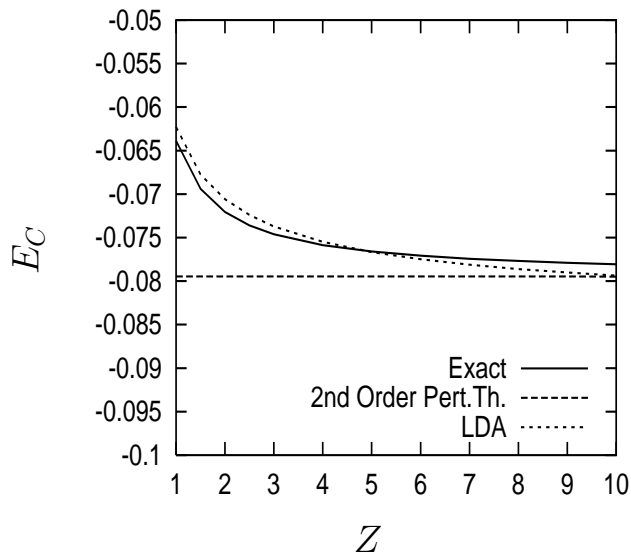


Figure 3.2: Correlation energy for Diracium, $\lambda = 1$, as obtained from $E_C \approx E_{exact} - E_{exx}$. The long-dashed line is second-order perturbation theory, the short-dashed line is LDA, and the solid line is exact.

an antisymmetric Fermi wave-function. A similar system, two delta-interacting fermions in a box, was the study of Ref. [122].

Diracium and the exact results obtainable from it are interesting since they offer the rare possibility of a model that can be exactly solved numerically right near the critical point of ionization. A vast amount of literature has developed around comparing ionization to phase transitions [123]. There is considerable interest in finding the critical exponents of ionization processes. So far, researchers have relied on using finite basis-size scaling techniques [124] and extrapolations from the infinite dimension limit [125, 126]. With this model, we propose to consider this limit exactly in future work.

For one particle, the delta-function admits only one bound state. If the fermions are polarized, only one fermion can be bound. In order to have a two-particle bound state, we must have opposite spins. By comparing the situation to an exactly solvable one, it can be shown that there is only one bound state for two particles in Eq. (3.24) [127].

We consider only the ground-state problem and leave the question of excited states for further work. First, we will solve the model analytically within the exact-exchange approximation. Then, we solve with the local density approximation to the correlation energy. Finally, we will present exact results.

3.6 Exact-Exchange Treatment of Diracium

In exact-exchange DFT, we write the total energy as a functional of the density,

$$E[n] = T_s[n] + U_H[n] + E_X[n] + \int_{-\infty}^{\infty} dx v_{\text{ext}}(x) n(x). \quad (3.25)$$

with $E_x[n] = E_x[n, \zeta = 0]$ given by Eq. (3.3). We minimize with respect to n , and constrain

$$\int_{-\infty}^{\infty} dx n(x) dx = 1 = P[n]. \quad (3.26)$$

The Euler-Lagrange equation is

$$\frac{\delta E}{\delta n} - \mu \frac{\delta P[x]}{\delta n} = 0, \quad (3.27)$$

and we find

$$\left(-\frac{1}{2} \frac{d^2}{dx^2} - Z\delta(x) + \frac{\lambda}{2} v_{KS}(x) \right) \phi_{KS}(x) = \epsilon_{EXX} \phi_{KS}(x) \quad (3.28)$$

defining $v_{KS}(x) = \delta U_H / \delta n(x) + \delta E_x / \delta n(x) = n(x)$. There is one doubly-occupied spatial KS orbital. The ground-state energy eigenvalue is

$$\epsilon_{EXX} = -\frac{1}{2} \left(Z - \frac{1}{2}\lambda \right)^2, \quad (3.29)$$

and the eigen-function is

$$\phi_{KS}(x) = \frac{1}{\sqrt{\lambda}} \left(Z - \frac{1}{2}\lambda \right) \text{csch} \left[\left(Z - \frac{1}{2}\lambda \right) |x| + \text{arccoth} \left(\frac{Z}{Z - \frac{1}{2}\lambda} \right) \right]. \quad (3.30)$$

The total EXX energy is given by Eq. (2.34),

$$E_{EXX} = \sum \epsilon_{EXX} + U_H[n] + E_X[n] - \frac{1}{2}\lambda \int_{-\infty}^{\infty} dx n^2(x). \quad (3.31)$$

The exact-exchange energy is thus

$$E_{EXX} = -Z^2 + \frac{Z\lambda}{2} - \frac{\lambda^2}{12} = -Z^2 \left(1 - \frac{1}{2} \left(\frac{\lambda}{Z} \right) + \frac{1}{12} \left(\frac{\lambda}{Z} \right)^2 \right). \quad (3.32)$$

It is interesting to note that Eq. (3.28) is related to the non-linear Schrödinger equation with a delta-function external potential. Incidentally, this solution of Eq. (3.28) was previously mentioned in astrophysics as a model for dense nuclear-matter in high magnetic fields [128]. It would be interesting to explore how density functional analysis of Diracium and Deltium could further that research.

3.7 The Local Density Correlation Treatment of Diracium

Now, we apply the local density approximation derived in Section 3.4. A rough approximation to the LDA correlation energy for Diracium can be gotten by plugging the exact-exchange density, twice the orbitals Eq (3.30) squared, into the simple LDA correlation functional, Eq. (3.33),

$$E_C^{LDA}(Z, \lambda) \approx -\frac{\lambda^2}{\pi^2} + \frac{2\lambda^4}{\pi^4} \frac{\beta}{Z - \lambda/2} \left[\arctan(\beta) - \arctan \left(\beta \frac{Z - \lambda/2}{Z} \right) \right] \quad (3.33)$$

with $\beta = \sqrt{\lambda^3/(\pi^2(Z - \lambda/2)^2 - 1)}$. Adding the LDA correlation to the EXX total energy generally improves the accuracy comparably to the self-consistent LDA.

DFT is a self-consistent theory, and a proper DFT treatment should take advantage of this. The KS equation for one orbital in the local density approximation is

$$-\frac{1}{2} \frac{d^2}{dx^2} \phi_{KS}(x) - Z\delta(x)\phi_{KS}(x) + \lambda|\phi_{KS}^2(x)|^2\phi_{KS}(x) + v_c(x)\phi_{KS}(x) = \epsilon_{KS}\phi_{KS}(x) \quad (3.34)$$

with $v_c(x)$ given by Eq. (3.22). We solved Eq. (3.34) numerically. The method was to guess the eigenvalue and then integrate the Schroedinger equation (3.34)

using the Numerov scheme [12]. The Numerov scheme solves differential equations of the form,

$$\frac{d^2}{dt^2}x(t) = f(t)x(t) \quad (3.35)$$

accurately by transforming to

$$w(t) = \left(1 - \frac{h^2}{12}f(t)\right)x(t) \quad (3.36)$$

where h is the uniform step in points sampled along the t axis. Then, we solve

$$w(h) + w(-h) - 2w(0) = h^2 f(0)x(0) + \mathcal{O}(h^6). \quad (3.37)$$

When using the Numerov scheme, we start from the known exponential asymptotic form of the orbital and integrate toward the origin. We check to see how well the trial solution satisfies the derivative discontinuity required by the delta-function external potential and use this information to guess a new eigenvalue. Then, we shoot again, and we repeat until the discontinuity is satisfied. With the valid wave-function, we create a density and start over. This is done until the density does not change appreciably between iterations and self-consistency is achieved.

In the low-density limit, Eq. (3.34) remains bound. We can see this by expanding the KS potential in the low-density limit:

$$-\frac{1}{2}\frac{d^2}{d^2x}\phi_{KS}(x) - Z\delta(x)\phi_{KS}(x) + \frac{3}{8}\pi^2\phi_{KS}(x) = -\epsilon_{KS}\phi_{KS}(x). \quad (3.38)$$

There is no explicit λ dependence in this equation. This is correct because the λ dependence is implicit in the limit taken above, and the LDA is kinetic-like in this limit. The solution to Eq. (3.38) is:

$$\phi_{KS}(x) = N\sqrt{\operatorname{csch}\left(2\sqrt{2\epsilon}(x+x_0)\right)} \quad (3.39)$$

with $N = (2\epsilon/\pi^2)^{\frac{1}{4}}$ and $x_0 = 1/(2\sqrt{2\epsilon}) \operatorname{arccoth}\left(Z/\sqrt{2\epsilon}\right)$. The KS eigenvalue is

$$\epsilon_{KS} = -\frac{1}{2}Z^2 \operatorname{sech}^2 \pi = -0.003721Z^2 \quad (3.40)$$

This approximation is an upper bound to the full LDA Hartree-Exchange correlation potential. Therefore, if the electron stays bound for all Z using this approximation, it would also stay bound for the full LDA potential. For small enough Z , the resulting density, n , is $\ll 2\lambda/\pi^2$, and this approximation will become reliable.

3.8 The Exact Solution of Diracium

The exact solution to Diracium is hard to come by. The simplest guess, a wave function which satisfies all the boundary conditions and satisfies the Schrödinger equation locally everywhere, just does not work. To see this try

$$\Psi(x_1, x_2) = N e^{-Z|x_1| - Z|x_2| + \frac{1}{2}\lambda|x_1 - x_2|}. \quad (3.41)$$

The normalization is

$$N = (2Z - \lambda) \sqrt{\frac{Z}{4Z - \lambda}}. \quad (3.42)$$

The reason it does not work is that it does not give the same eigenvalue globally. At best, this is a variational wave-function and predicts an approximate energy,

$$E = -(2Z - \lambda)^2 \left(\frac{Z}{4Z - \lambda} \right) \left[\frac{1}{2} + \frac{4Z^2 + \lambda^2}{4Z(2Z - \lambda)} \right]. \quad (3.43)$$

Rosenthal first found the exact solution [127] transforming the problem to momentum space and reducing the problem to the solution of a one-dimensional integral equation. Let us see how this works. First, rescaled the coordinates $x \rightarrow x/Z$. Then, the real-space wave-function is the Fourier transform of the momentum space one,

$$\psi(x_1, x_2) = \frac{1}{2\pi^2} \int_{-\infty}^{\infty} dk_1 dk_2 \left(\frac{F(k_1) + F(k_2) - \lambda' H(k_1 + k_2)}{k_1^2 + k_2^2 + p^2} \right) e^{-ik_1 x_1 - ik_2 x_2} \quad (3.44)$$

with $E = -Z^2 p^2/2$, $\lambda' = \lambda/Z$,

$$F(k) = \int_{-\infty}^{\infty} dx \psi(x, 0) e^{ikx}, \quad (3.45)$$

and

$$H(k) = \int_{-\infty}^{\infty} dx \psi(x, x) e^{ikx}. \quad (3.46)$$

$H(k)$ is related to $F(k)$ through

$$H(k) = \left(\frac{\sqrt{2p^2 + k^2}}{\sqrt{2p^2 + k^2} + \lambda'/\pi} \right) \frac{2}{\pi} \int_{-\infty}^{\infty} dk' \frac{F(k')}{(k' - k)^2 + k'^2 + p^2}. \quad (3.47)$$

We find $F(k)$ through the solution of the integral equation,

$$F(k)\phi(k) = \int_{-\infty}^{\infty} dx K(k, k')F(k') \quad (3.48)$$

with

$$\phi(k) = 1 - (k^2 + p^2)^{-\frac{1}{2}} \quad (3.49)$$

and

$$K(k, k') = \frac{1}{\pi} \left(\frac{1}{k^2 + k'^2 + p^2} \right) - \frac{2\lambda'}{\pi} \int_{-\infty}^{\infty} dk'' \left(\frac{1}{k^2 + (k - k'')^2 + p^2} \right) \left(\frac{1}{k'^2 + (k' - k'')^2 + p^2} \right) \left(\frac{(2p^2 + k''^2)^{\frac{1}{2}}}{(2p^2 + k''^2)^{\frac{1}{2}} + \lambda'} \right). \quad (3.50)$$

By exploiting the symmetries of the $F(k)$, the integral can be converted into one on the interval $k \in [0, \infty)$ with the integrand $K(k, k') + K(k, -k')$. Let $x = \frac{k}{k+1}$ and $dx = x^2/k^2 dk$, and use a Gauss-Legendre mesh with 20 points which is adequate for convergence. After discretizing space and replacing integration by a summation, we just need to solve a matrix equation,

$$\mu \mathbf{F} = \mathbf{K} \mathbf{F} \quad (3.51)$$

with $\mu = 1$. We guess p , solve the matrix problem, re-guess p , and repeat until $\mu = 1$.

Although the method converges quickly to the exact energy eigenvalue, it is not well-suited to give real-space wave-functions and densities. It is difficult to

obtain the real-space density from this scheme since the limited sampling of points in k -space makes the Fourier transforms inaccurate. It would be nice to extract the exact density because we could consider how the density changes just as the system becomes ionized. It may be possible to obtain the density by solving the two-dimensional Green's function problem with the exact p in an analogous way to scattering theory. This is currently under investigation.

Finally, we can use the virial theory to get the components of the energy T and $V_{ee} + V_{ext}$. The virial theorem tells that for Coulombic external potentials and interactions

$$\langle \hat{T} \rangle = -\frac{1}{2} \langle \hat{V}_{ee} \rangle - \frac{1}{2} \langle \hat{V}_{ext} \rangle. \quad (3.52)$$

The total energy is

$$E_{tot} = \langle \hat{T} \rangle + \langle \hat{V}_{ee} \rangle + \langle \hat{V}_{ext} \rangle. \quad (3.53)$$

Combine Eq. (3.52) and Eq. (3.53) to find $\langle \hat{T} \rangle = -E_{tot}$ and $\langle \hat{V}_{ee} \rangle$ and $\langle \hat{V}_{ext} \rangle$ can be evaluated by solving k space integrals:

$$\langle \hat{V}_{ee} \rangle = \lambda \int dk H(k)^2 \quad (3.54)$$

and

$$\langle \hat{V}_{ext} \rangle = -2Z \int dk F(k)^2. \quad (3.55)$$

Table 3.1 shows the various components of the energy as separated via the virial theorem.

3.9 Comparison of the Diracium Results

In Table 3.2, we see the results from a series of total-energy calculations for Diracium, $\lambda = 1$ and various Z . The LDA is greatly more accurate than the EXX functional and often more accurate than second-order perturbation theory. Second-order perturbation theory comes at a much larger computational cost since the second-order contribution requires calculation of the entire spectrum of

Z	$\langle \hat{T} \rangle$	$\langle \hat{V}_{ee} \rangle$	$\langle \hat{V}_{ext} \rangle$
0.377115	0.071112	0.002103	-0.144328
0.5	0.129282	0.108580	-0.367145
1	0.647210	1.237264	-2.531684
2	3.155390	3.507053	-9.817832
3	7.657948	5.580302	-20.896197
4	14.159193	7.611110	-35.929496
5	22.659929	9.627705	-54.947563
6	33.160416	11.637995	-77.958826
7	45.660761	13.644974	-104.966495
8	60.161018	15.650009	-135.972045
9	76.661217	17.653809	-170.976243
10	95.161376	19.656776	-209.97953
100	9950.16245	199.678509	-20100.0034

Table 3.1: Various components of the energy as separated via the virial theorem. $\langle \hat{T} \rangle$ is the kinetic energy contribution, $\langle \hat{V}_{ee} \rangle$ is the interaction contribution, and $\langle \hat{V}_{ext} \rangle$ is the external potential contribution.

excited states. Since LDA is non-perturbative, it is more accurate near Z_{crit} when the system becomes unstable and ionizes. Figure 3.2 shows the correlation energy within various approximations for Diracium.

In table 3.3, we see the critical ionization values within various approximations and the exact values. The total energy results refer to the Z at which the energy of the two-electron system and the one-electron system are equal:

$$E_{tot}(N = 2) = E_{tot}(N = 1) \quad (3.56)$$

with $E_{tot}(N = 1) = -Z^2/2$. The eigenvalue results are the Z when the highest occupied eigenvalue vanishes.

3.10 Contact-Interacting Hooke's Atom

Another test of this one-dimensional LDA is the contact-interacting Hooke's atom,

$$\hat{H} = -\frac{1}{2} \frac{d^2}{dx_1^2} - \frac{1}{2} \frac{d^2}{dx_2^2} + \frac{1}{2} \omega^2 x_1^2 + \frac{1}{2} \omega^2 x_2^2 + \lambda \delta(x_1 - x_2), \quad (3.57)$$

Z	Exact	LDA	EXX	2 Pert.
0.3	not bound	barely bound	not bound	-0.102793
0.377115	-0.711126	-0.022954	not bound	-0.116461
0.5	-0.129282	-0.117931	not bound	-0.162793
1	-0.647210	-0.642029	-0.583333	-0.662793
2	-3.155390	-3.152934	-3.083333	-3.162793
3	-7.657948	-7.656928	-7.583333	-7.662793
4	-14.159193	-14.15907	-14.08333	-14.162793
5	-22.659930	-22.660418	-22.58333	-22.662793
6	-33.160416	-33.161359	-33.08333	-33.162793
7	-45.660761	-45.662055	-45.58333	-45.662793
8	-60.161018	-60.162594	-60.08333	-60.162793
9	-76.661217	-76.663024	-76.58333	-76.662793
10	-95.161376	-95.162674	-95.08333	-95.162793
100	-9950.1625	-9950.16676	-9950.083	-9950.1628

Table 3.2: Total energies for Diracium within various approximations with $\lambda = 1$. The exact results are from a numerical solution of the problem as outlined by Ref. [127], the second-order perturbation values are also given in the same reference. The EXX and the LDA results are from a self-consistent solution using the exact-exchange functional, Eq. (3.3), and the LDA functional, parameterization Eq. 3.20 respectively.

where ω determines the strength of the harmonic well potential. This model has been used to model one-dimensional quantum dots [107] and has been considered in the context of time-dependent DFT [129]. The exact wave-function is given in terms of Whittaker functions and confluent hyper-geometric functions [107]. The total energy is

$$E = \frac{1}{2}\omega + \epsilon \quad (3.58)$$

with ϵ obtained from

$$\sqrt{2\omega} \Gamma\left(\frac{1}{4} - \frac{\epsilon}{2\omega}\right) / \Gamma\left(\frac{3}{4} - \frac{\epsilon}{2\omega}\right) = -\lambda. \quad (3.59)$$

Since the Hooke's atom stays bound for arbitrarily weak ω , we can test the LDA in the low-density limit.

The exact result for the total energy in this limit is

$$E = 2\omega. \quad (3.60)$$

Z_{crit}	Exact	LDA	EXX
Total Energy	0.38	0.67	0.77
Eigenvalue	0.38	0.0	0.5

Table 3.3: Critical Z 's for dissociation. LDA is according to the parameterization Eq. 3.20.

ω	Exact	EXX	LDA	E_C
0.001	0.00195	0.00800	0.00201	-0.00605
0.01	0.01851	0.03107	0.01883	-0.01256
0.1	0.16141	0.20959	0.16157	-0.04818
1	1.30675	1.37897	1.30353	-0.07222
10	11.15733	11.24020	11.14949	-0.08287
100	103.881057	103.967581	103.870274	-0.086524

Table 3.4: Total energies for the contact-interacting Hooke's Atom within various approximations, $\lambda = 1$. Exact is from a numerical solution of Eqs. 3.58 and 3.59. EXX is exact exchange. LDA is according to the parameterization Eq. 3.18.

In Table 3.4, we see that LDA greatly improves over the exact exchange formalism for all values of ω . The LDA reproduces the low-density, small ω , limit accurately. While the LDA overestimates the correlation in the high-density limit, it underestimates it in the low-density limit.

3.11 The Accuracy of Contact-Interacting Density Functional Theory

The one-dimensional local density approximation is accurate because:

- The exact treatment of exchange
- The freedom from self-interaction
- The local interaction term

In three dimensions these conditions might not always be met. It is interesting to point out that in this case, local DFT works well for strong local correlation.

In this chapter, we have examined a one-dimensional density functional theory of contact-interacting fermions. We noted that the exact-exchange functional is an explicit density functional. Then, we developed a local density functional for correlation. We have applied these functionals successfully to two simple models. In the future, we hope to use this model interaction to study problems in DFT in general. For example, we plan to use the LDA to examine ground-state symmetry problems in stretched H_2 and the interacting-electron solid (a generalized Kronig-Penney model) to investigate the band gap problem. We plan to use the excited state Bethe-Ansatz results to derive a local current density functional for this interaction. We hope to investigate the critical behavior of Diracium as the system ionizes. This is difficult to do for any three-dimensional system where exact results in the critical limit must be carefully extracted. This contact-interaction has already been used to analyze the scattering theory and in pedagogy, and we hope that this LDA will find fruitful applications there as well.

Chapter 4

Uniform Density and Spin-Density Scaling

In most applications, we are concerned with the Coulomb-interacting problem in three dimensions. In this chapter, we return to the study of Coulomb interacting density functional theory. We start by reviewing scaling and virial constraints on the exchange-correlation energy functional, and then, generalize these to the case of spin-density functional theory.

4.1 Uniform Density Scaling

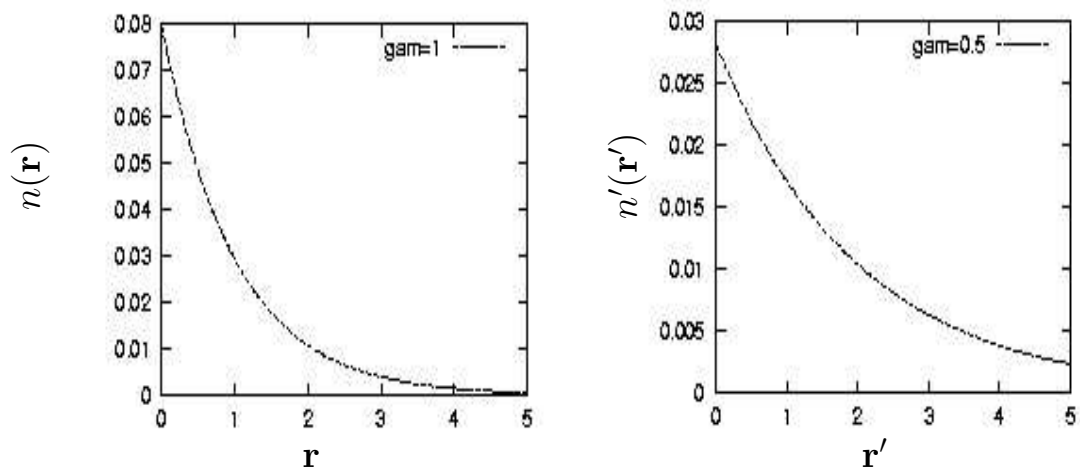


Figure 4.1: Uniform Density Scaling of an exponential density, $n(r) = e^{-r}/4\pi$, by a factor $\gamma = 1/2$.

Exact constraints limit the possible forms of approximations to E_{xc} and provide guidance for the construction of approximations [41]. For total-electron density functionals, Levy and Perdew [101] discovered a set of important scaling and

integral requirements that the exact functionals must satisfy. They introduced the concept of uniform coordinate density scaling. This scaling takes a density $n(\mathbf{r})$ into

$$n_\gamma(\mathbf{r}) = \gamma^3 n(\gamma\mathbf{r}), \quad 0 \leq \gamma < \infty \quad (4.1)$$

and is a natural way to explore the behavior of density functionals. Figure 4.1 illustrates the effect of scaling an exponentially decaying density. Integrating Eq. 4.1 over all space always yields the same number of electrons. Uniform density scaling is equivalent to changing all the length scales in the problem. Because of the Coulombic interaction term, the ground-state system is not invariant under this transformation. Many properties of the exact exchange-correlation functional have been found by studying its behavior under this scaling [98, 130, 131].

For example, the exchange energy changes as

$$E_x[n_\gamma] = \gamma E_x[n]. \quad (4.2)$$

All commonly-used approximations, such as the local density approximation (LDA), the generalized gradient approximation (GGA), and hybrids of GGA with exact exchange [46] satisfy this relation as it is imposed upon their construction. However, for correlation, only inequalities can be derived,

$$E_c[n_\gamma] > \gamma E_c[n] \quad (\gamma > 1), \quad (4.3)$$

which some approximations satisfy [40, 41] while others do not [39].

4.2 The Virial Theorem

Levy and Perdew further showed that translational invariance implies virial theorems relating potentials to energies. An example is

$$E_x[n] = - \int d^3r n(\mathbf{r}) \mathbf{r} \cdot \nabla v_x[n](\mathbf{r}) \quad (4.4)$$

with a more complicated corresponding relation for correlation. The virials have been used to construct energy densities directly from potentials [132]. Exact statements about exact functionals are nontrivial and extremely useful in the construction and analysis of approximate functionals. Functionals that violate these exact conditions are unlikely to give reliable and physical results when applied to wide ranges of materials.

4.3 The Generalization to Uniform Separate Spin Density Scaling

Modern density functional calculations do not employ *density* functionals but rather use *spin*-density functionals. The basic idea is to replace $E_{\text{xc}}[n]$ with $E_{\text{xc}}[n_{\uparrow}, n_{\downarrow}]$ so that the universal functional depends explicitly on both the up and down-spin electron densities. Formal justification for this scheme was first given by Barth and Hedin [133] and later by Rajagopal and Calloway [134] although some fundamental questions remain [135]. There are several compelling reasons for using spin-density functionals instead of total-electron density functionals. First, spin-density functionals can more accurately describe systems with odd numbers of electrons [136]. Spin-density functionals allow the treatment of electrons in collinear magnetic fields and yield magnetic response properties [137]. Accurate calculation of these properties would be far more difficult in total-density functional theory. The reason is that a local spin-density functional is a non-local total density functional. One cannot exaggerate how useful spin-density functional theory has been in accurately and efficiently calculating physical properties.

To help develop improved spin-density functionals, it would be of great interest to develop a formalism that probes the spin-dependence of functionals and yields exact conditions about their spin-dependence. Here, we investigate whether

scaling techniques developed for total-density functionals can be generalized to spin-density functional theory. Towards this end, we generalize uniform coordinate scaling of the density, Eq. (4.1), to separate scaling of spin-densities [138]:

$$\begin{aligned} n_{\uparrow\alpha}(\mathbf{r}) &= \alpha^3 n_{\uparrow}(\alpha\mathbf{r}), & 0 \leq \alpha < \infty \\ n_{\downarrow\beta}(\mathbf{r}) &= \beta^3 n_{\downarrow}(\beta\mathbf{r}), & 0 \leq \beta < \infty. \end{aligned} \quad (4.5)$$

According to this scheme, a spin-unpolarized system becomes spin-polarized for $\alpha \neq \beta$. There are many other ways we could have chosen to alter the spin densities. For example, we could require that the total density remain constant while the polarization changes. However, such a transformation would require introduction of ensembles because fractions of electrons would be changing spin. The present scheme is simply the logical extension of coordinate scaling to separate spin-densities.

A principal result of this work is that, under such a transformation, a spin-dependent virial theorem holds true. This theorem can be used to carefully check the convergence of spin-density functional calculations. It also provides a method for calculating the exact dependence of the correlation energy on spin-density for model systems for which accurate Kohn-Sham potentials have been found. Finally, it can be integrated over the scale factor α to give a new formal expression for the functional, E_{xc} .

Considerable progress has been made in density functional theory by writing E_{xc} as an integral over a coupling constant λ in what is called the adiabatic connection relationship [34, 35]. For example, the success of hybrid functionals such as B3LYP [46, 93] can be understood in terms of this adiabatic connection [104, 95]. The adiabatic connection is simply related to uniform coordinate scaling [139, 140]. By analogy, we relate spin-scaling to a spin-coupling constant integration, and we define a suitable generalization for this definition with a coupling constant for each spin-density.

We illustrate our formal results with several cases. For the uniform electron gas, we can perform this scaling exactly. We show how this transformation relates energies to changes in spin-polarization. In this case, considerable care must be taken to deal with the extended nature of the system. We also show the results of spin-scaling densities of small atoms using presently popular approximations. We close with a discussion of the fundamental difficulty underlying this spin-scaling approach.

We demonstrate all scaling relationships by scaling the up-spin densities. Results for scaling the down-spins are obtained in a similar fashion. Just swap the spin labels!

4.4 General Properties of Spin-Scaling

The first interesting property of the spin-scaling transformation, Eq. (4.5), is that it conserves the total number of electrons globally even though the scaled spin density might tend towards zero at any point. Even when $\alpha \rightarrow 0$, the up electrons do not vanish, but are merely spread over a very large volume. As α diminishes, the two spin-densities occupy the same coordinate space, but on two very distinct length scales. The scaled density presumably then has vanishingly small contribution to the correlation energy. For finite systems, we can consider this limit as the effective removal of one spin-density to infinitely far away. Assuming that interaction between opposite spins vanishes in this limit, we have a way of effectively removing one spin-density from the system. We will discuss what this means for extended systems later when we treat the uniform gas.

Another interesting property of the spin-scaling transformation is that a scaling of one spin density can always be written as a total density scaling plus an inverse spin-scaling of the other spin; that is

$$E_{\text{XC}}[n_{\uparrow\alpha}, n_{\downarrow}] = E_{\text{XC}}[\{ n_{\uparrow}, n_{\downarrow/\alpha} \}_{\alpha}] \quad (4.6)$$

where the parenthesis notation on the right indicates scaling the total density. Thus, without loss of generality, we need only scale one spin-density.

To understand what happens when a single spin-density is scaled, we first study exchange. Because the spin-up and down Kohn-Sham orbitals are independent, the exchange energy functional can be split into two parts, one for each spin [141]. The scaling relationships for total density functional theory generalize for each term independently. For an up-spin scaling, we find

$$\begin{aligned} E_x[n_{\uparrow\alpha}, n_{\downarrow}] &= \frac{1}{2}E_x[2n_{\uparrow\alpha}] + \frac{1}{2}E_x[2n_{\downarrow}] \\ &= \frac{\alpha}{2}E_x[2n_{\uparrow}] + \frac{1}{2}E_x[2n_{\downarrow}]. \end{aligned} \quad (4.7)$$

When $\alpha \rightarrow 0$, we are left with only the down contribution to exchange. Separate spin-scaling allows us to extract the contribution from each spin-density separately, e.g., $dE_x[n_{\uparrow\alpha}, n_{\downarrow}]/d\alpha$ at $\alpha = 1$ is the contribution to the exchange energy from the up-density. A plot of $E_x[n_{\uparrow\alpha}, n_{\downarrow}]$ versus α between 0 and 1 yields a straight line and is twice as negative at 1 as at 0.

Separate spin-scaling of the correlation energy is more complicated. Unlike $E_x[n_{\uparrow}, n_{\downarrow}]$, $E_C[n_{\uparrow}, n_{\downarrow}]$ cannot trivially be split into up and down parts. The Levy method of scaling the exact ground-state wave-function does not yield an inequality such as Eq. (4.3) because the spin-scaled wave-function is not a ground-state of another Coulomb-interacting Hamiltonian. Nor does it yield an equality as in the spin-scaled exchange case, Eq. (4.7), because the many-body wave-function is not simply the product of two single-spin wave-functions. In both cases, the two spins are coupled by a term $1/|\mathbf{r} - \alpha\mathbf{r}'|$.

To obtain an exact spin-scaling relationship for E_{XC} , we take a different route. Consider a change in the energy due to a small change in the up-spin density:

$$\delta E_{XC} = E_{XC}[n_{\uparrow} + \delta n_{\uparrow}, n_{\downarrow}] - E_{XC}[n_{\uparrow}, n_{\downarrow}]. \quad (4.8)$$

Use $v_{\text{XC}\uparrow}(\mathbf{r}) = \delta E_{\text{XC}}/\delta n_{\uparrow}(\mathbf{r})$ to rewrite δE_{XC} as

$$\delta E_{\text{XC}} = \int d^3r \delta n_{\uparrow}(\mathbf{r}) v_{\text{XC}\uparrow}[n_{\uparrow}, n_{\downarrow}](\mathbf{r}) \quad (4.9)$$

to first order in δn_{\uparrow} . Now, consider this change as coming from the following scaling of the density, $n_{\uparrow\alpha}(\mathbf{r}) = \alpha^3 n_{\uparrow}(\alpha\mathbf{r})$, where α is arbitrarily close to one. The change in the density is related to the derivative of this scaled density:

$$\left. \frac{dn_{\uparrow\alpha}(\mathbf{r})}{d\alpha} \right|_{\alpha=1} = 3n_{\uparrow}(\mathbf{r}) + \mathbf{r} \cdot \nabla n_{\uparrow}(\mathbf{r}). \quad (4.10)$$

Use Eqs. (4.9) and (4.10), and integrate by parts to find

$$\left. \frac{dE_{\text{XC}}[n_{\uparrow\alpha}, n_{\downarrow}]}{d\alpha} \right|_{\alpha=1} = - \int d^3r n_{\uparrow}(\mathbf{r}) \mathbf{r} \cdot \nabla v_{\text{XC}\uparrow}[n_{\uparrow}, n_{\downarrow}](\mathbf{r}). \quad (4.11)$$

Eq. (4.11) is an exact result showing how $dE_{\text{XC}}/d\alpha|_{\alpha=1}$ can be extracted from the spin-densities and potentials. For an initially unpolarized system, $n_{\uparrow} = n_{\downarrow} = n/2$, and $v_{\text{XC}\uparrow} = v_{\text{XC}\downarrow} = v_{\text{XC}}$. Thus, the right-hand-side of Eq. (4.11) becomes half the usual virial of the exchange-correlation potential. This virial is equal to $dE_{\text{XC}}[n_{\alpha}]/d\alpha|_{\alpha=1} = E_{\text{XC}} + T_{\text{C}}$ where T_{C} is the kinetic contribution to the correlation energy. Thus, for spin-unpolarized systems,

$$\left. \frac{dE_{\text{C}}[n_{\uparrow\alpha}, n_{\downarrow}]}{d\alpha} \right|_{\alpha=1} = \frac{1}{2} (E_{\text{C}} + T_{\text{C}}). \quad (4.12)$$

For initially polarized systems, there is no simple relation between the two types of scaling.

To generalize Eq. (4.11) to finite scalings, simply replace n_{\uparrow} on both sides by $n_{\uparrow\alpha}$, yielding:

$$\frac{dE_{\text{XC}}[n_{\uparrow\alpha}, n_{\downarrow}]}{d\alpha} = -\frac{1}{\alpha} \int d^3r n_{\uparrow\alpha}(r) \mathbf{r} \cdot \nabla v_{\text{XC}\uparrow}[n_{\uparrow\alpha}, n_{\downarrow}](\mathbf{r}). \quad (4.13)$$

We can then write the original spin-density functional as a scaling integral over this derivative:

$$E_{\text{XC}}[n_{\uparrow}, n_{\downarrow}] = \lim_{\alpha \rightarrow 0} E_{\text{C}}[n_{\uparrow\alpha}, n_{\downarrow}] + \int_0^1 d\alpha \frac{dE_{\text{XC}}[n_{\uparrow\alpha}, n_{\downarrow}]}{d\alpha}. \quad (4.14)$$

This is a new expression for the exchange-correlation energy as an integral over separately spin-scaled densities where the spin-scaled density is scaled to the low-density limit. With some physically reasonable assumptions, we expect

$$\lim_{\alpha \rightarrow 0} E_C[n_{\uparrow\alpha}, n_{\downarrow}] = E_C[0, n_{\downarrow}]. \quad (4.15)$$

For example, if the anti-parallel correlation hole vanishes as rapidly with scale factor as the parallel-spin correlation hole of the scaled density, this result would be true. Numerical results indicate that this is the case for the approximate functionals used in this paper. Nevertheless, we have not proven Eq. (4.15) here.

A symmetric formula can be written down by scaling the up and down-spins separately and averaging:

$$\begin{aligned} E_{\text{XC}}[n_{\uparrow}, n_{\downarrow}] &= \frac{1}{2} \lim_{\alpha \rightarrow 0} (E_{\text{XC}}[n_{\uparrow\alpha}, n_{\downarrow}] + E_{\text{XC}}[n_{\uparrow}, n_{\downarrow\alpha}]) \\ &+ \frac{1}{2} \int_0^1 d\alpha \int d^3r n_{\uparrow\alpha}(\mathbf{r}) \mathbf{r} \cdot \nabla v_{\text{XC}\uparrow}[n_{\uparrow\alpha}, n_{\downarrow}](\mathbf{r}) \\ &+ \frac{1}{2} \int_0^1 d\beta \int d^3r n_{\downarrow\beta}(\mathbf{r}) \mathbf{r} \cdot \nabla v_{\text{XC}\downarrow}[n_{\uparrow}, n_{\downarrow\beta}](\mathbf{r}). \end{aligned} \quad (4.16)$$

This result is the spin-density functional generalization of spin-decomposition, coordinate scaling, and the virial theorem. Each of these ideas yields separate results for pure exchange or uniform coordinate scaling, but all are combined here. Notice that the potentials depend on both spins, one scaled and the other unscaled. This reflects the difficulty in separating up and down-spin correlations.

The proof of Eq. (4.16) is true for exchange-correlation, but in taking the weakly-correlated limit. The result also holds true for exchange. In the exchange case, Eq. (4.16) reduces to Eq. (4.7) with equal contributions from the limit terms and the virial contributions. To obtain this result, recall how E_X scales (4.2). Since the energy contribution from each spin is separate and since the scaling law is linear, the limits in the first two terms of Eq. (4.16) are doable without any extra physical assumptions. The virial terms are a bit more difficult to handle as the exchange potentials change under scaling. In the end, the first

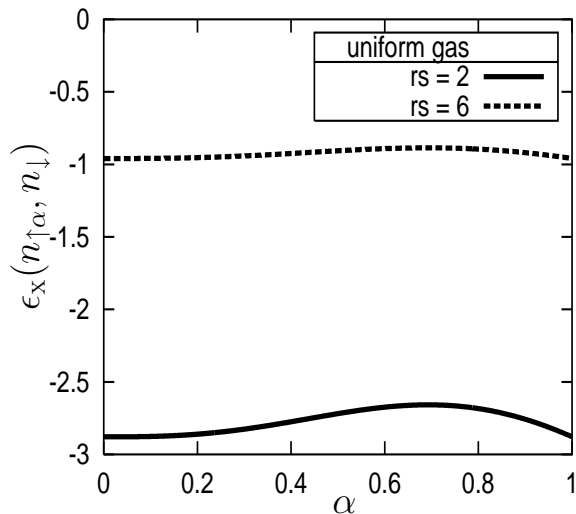


Figure 4.2: Spin-scaling of a uniform gas: exchange energy per particle, $\epsilon_x(n_{\uparrow\alpha}, n_{\downarrow})$, at $r_s = 2$ (dotted line) and 6 (solid line).

two terms contribute half the exchange energy while the virial terms contribute the other half.

4.5 Spin-Scaling on the Uniform Gas

To illustrate the effect of spin-scaling, we examine the uniform electron gas, a system for which we have essentially exact results. Great care must be taken to define quantities during separate spin-scaling of extended systems. Begin with a spin-unpolarized uniform electron gas of density n and Wigner-Seitz radius $r_s = (3/4\pi n)^{1/3}$. When one spin density is scaled, the system becomes spin-polarized, and relative spin-polarization is measured by

$$\zeta = \frac{n_{\uparrow} - n_{\downarrow}}{n_{\uparrow} + n_{\downarrow}}. \quad (4.17)$$

We assume that for a spin-polarized uniform system, the exchange-correlation energy per electron, $\epsilon_{xc}^{\text{unif}}(r_s, \zeta)$, is known exactly. We use the correlation energy

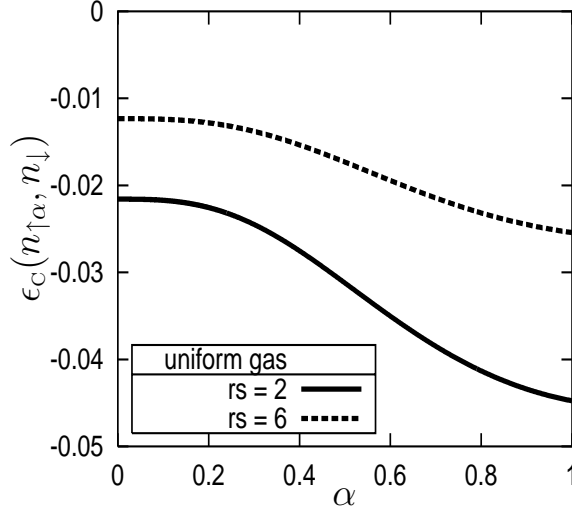


Figure 4.3: Spin-scaling of a uniform gas: correlation energy per particle, $\epsilon_C(n_{\uparrow\alpha}, n_{\downarrow})$, at $r_s = 2$ (dotted line) and 6 (solid line).

parameterization of Perdew and Wang [40] to make our figures.

To perform separate spin-scaling of this system, we focus on a region deep in the interior of any finite but large sample. A simple example is a jellium sphere of radius $R \gg r_s$. The correlation energy density deep in the interior will tend to that of the truly translationally invariant uniform gas as $R \rightarrow \infty$. At $\alpha = 1$, we have an unpolarized system with $n_{\uparrow} = n_{\downarrow} = n/2$. The up-spin-scaling, $n_{\uparrow} = \alpha^3 n/2$, changes both the total density and the spin-polarization. Deep in the interior

$$r_s(\alpha) = r_s \left(\frac{2}{1 + \alpha^3} \right)^{1/3} \quad (4.18)$$

where r_s is the Seitz radius of the original unpolarized gas, and

$$\zeta(\alpha) = \frac{\alpha^3 - 1}{\alpha^3 + 1}. \quad (4.19)$$

The energy density here is then

$$e_{\text{XC}}(\alpha) = e_{\text{XC}}^{\text{unif}}(n_{\uparrow\alpha}, n_{\downarrow}) = e_{\text{XC}}^{\text{unif}}(r_s(\alpha), \zeta(\alpha)), \quad (4.20)$$

and the energy per particle is

$$\epsilon_{\text{xc}}(\alpha) = e_{\text{xc}}(\alpha)/n(\alpha) \quad (4.21)$$

where $n(\alpha)$ is the interior density.

To illustrate the effects of this spin-scaling, consider the simple exchange case. Deep in the interior, we have a uniform gas of density $n_{\uparrow\alpha}$ and n_{\downarrow} , and the energy densities of these two are given by Eq. (4.7), since the integrals provide simple volume factors. The Slater factor of $n^{4/3}$ in the exchange density of the uniform gas produces a factor of $(1 + \alpha^4)$. When transforming to the energy per electron, there is another factor of $(1 + \alpha^3)$ due to the density out front. Thus, the exchange energy per electron is

$$\epsilon_{\text{x}}(\alpha) = \left(\frac{1 + \alpha^4}{1 + \alpha^3} \right) \epsilon_{\text{x}}^{\text{unpol.}}(n). \quad (4.22)$$

This variation is shown in Fig. (4.2). This result may appear to disagree with Eq. (4.7), but it is valid deep in the interior only. To recover the total exchange energy, one must include those electrons in a shell between R and R/α with the full polarized uniform density $\alpha^3 n/2$. The exchange energy integral includes this contribution, and then agrees with Eq. (4.7).

Near $\alpha = 1$, Eq. (4.22) yields $(1 + \alpha) \epsilon_{\text{x}}^{\text{unpol.}}/2$ in agreement with a naive application of Eq. (4.7). This is because, in the construction of the energy from the energy per electron, the factor of the density accounts for changes in the number electrons to first order. So, the derivative at $\alpha = 1$ remains a good measure of the contribution to the total exchange energy from one spin-density. On the other hand, as $\alpha \rightarrow 0$, the exchange energy per electron in the interior returns to that of the original unpolarized case. This reflects the fact that exchange applies to each spin separately so that the exchange per electron of the down-spin density is independent of the presence of the up-spin density.

Figure 4.3 shows the uniform electron gas correlation energy per particle scaled from unpolarized ($\alpha = 1$) to fully-polarized limits ($\alpha = 0$). Again, the curves

become flat as $\alpha \rightarrow 0$ because for small α , there is very little contribution from the up-spins. Now, however, there is a dramatic reduction from $\alpha = 1$ to $\alpha = 0$ because of the difference in correlation between unpolarized and fully-polarized gases. Note that the correlation changes tend to cancel the exchange variations.

4.6 Calculations on Atoms

In these calculations, the atomic density functional (ADF) code generates ground-state atomic densities. It finds the orbitals on a real-space log mesh using the Numerov method to integrate the Schrödinger equation and the shooting method to hone in on the Kohn-Sham eigenvalues. The calculation is, like the one in the last chapter, looped over until self-consistency is achieved. All angular orbital parts are averaged over. The code includes exact-exchange; however, we do not use this feature.

The following results are obtained by solving the KS equation within various approximations to get a ground-state density. The density was then scaled and splined to a larger mesh when necessary, and plugged into various functionals.

4.7 Spin-Scaling on Finite Systems

Next, we examine the behavior of finite systems under separate spin-scaling. We choose the He and Li atoms to demonstrate the effects on the simplest non-trivial unpolarized and spin-polarized cases. For each system, we solve the Kohn-Sham equations using a specific density functional approximation. The resulting self-consistent densities are then spin-scaled and the approximate energies evaluated on the scaled densities using that same functional. Since these are approximate functionals, neither the densities nor the energies are exact. We are unaware of any system, aside from the uniform gas, for which exact spin-scaled

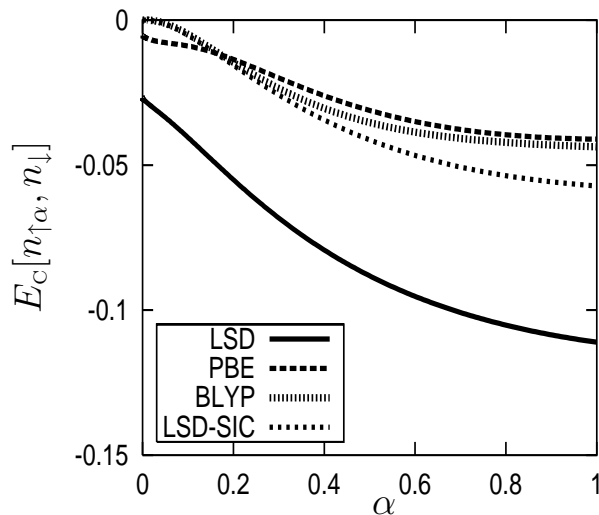


Figure 4.4: Spin-scaling of the He atom density using various approximate functionals for E_C : local spin density approximation (solid line), generalized gradient approximation (PBE, dashed line), BLYP (bars), self-interaction corrected LSD (short dashes).

plots are easily obtainable. For now, we must compare plots generated from approximate functionals. Even the simple atomic calculations presented here were rather demanding since, especially for very small spin-scaling parameters, integrals containing densities on two extremely distinct length scales are needed.

The He atom (Fig. 4.4) is spin unpolarized at $\alpha = 1$. Scaling either spin density gives the same results. The LSD curve gives far too much correlation and does not vanish as $\alpha \rightarrow 0$. We expect that in the fully-scaled limit, as we have argued in section 4.4, the correlation energy should vanish. This is because the two electrons are now on very different length scales and so should not interact with each other. The residual value at $\alpha \rightarrow 0$ reflects the self-interaction error in LSD for the remaining (unscaled) one-electron density. The PBE curve is on the right scale but also has a residual self-interaction error as $\alpha \rightarrow 0$. The BLYP functional [38, 39] is popular in quantum chemistry and gets both limits correct. However, the functional’s lack of self-interaction error is because the correlation energy vanishes for *any* fully-polarized system. This vanishing is incorrect for

Approx.	E_x	E_C	$E_C[n_\uparrow, 0]$	$dE_C/d\alpha$
LSD	-0.862	-0.111	-0.027	-0.022
PBE	-1.005	-0.041	-0.005	-0.002
SIC	-1.031	-0.058	0.000	-0.011
BLYP	-1.018	-0.044	0.000	-0.005
exact	-1.026	-0.042	0.000	-0.003

Table 4.1: He atom energies, both exactly and within several approximations. All energies in Hartrees; all functionals evaluated on self-consistent densities.

any atom other than H or He. Finally, the LSD-SIC curve [32] is probably the most accurate in shape (if not quantitatively) since this functional handles the self-interaction error appropriately. We further observe that the curves appear quite different from those of the uniform gas. The atomic curves are much flatter near $\alpha \rightarrow 1$ and have appreciable slope near $\alpha \rightarrow 0$. This is because these energies are integrated over the entire system, including the contribution from the entire spin-scaled density, whereas the energy densities in the uniform gas case were only those in the interior.

Quantitative results are listed in Table 4.1. The exact He values, including the derivative at $\alpha = 1$, using Eq. (4.12), were taken from Ref. [142, 144]. Note that PBE yields the most accurate value for this derivative. The BLYP correlation energy is too flat as a function of scale parameter. BLYP produces too small a value for T_C leading to a lack of cancellation with E_C and a subsequent overestimate of the derivative at $\alpha = 1$. LSD-SIC has a similar problem. The LSD value, while far too large, is about 8% of the LSD correlation energy, close to the same fraction for PBE, and not far from exact. However, the important point here is that results from separate spin-scaling are a new tool for examining the accuracy of the treatment of spin-dependence in approximate spin-density functionals.

The Li atom (Figs.4.5 and 4.6) is the smallest non-trivial odd-electron atom. We choose the up-spin density to have occupation $1s2s$. As the up-spin is scaled

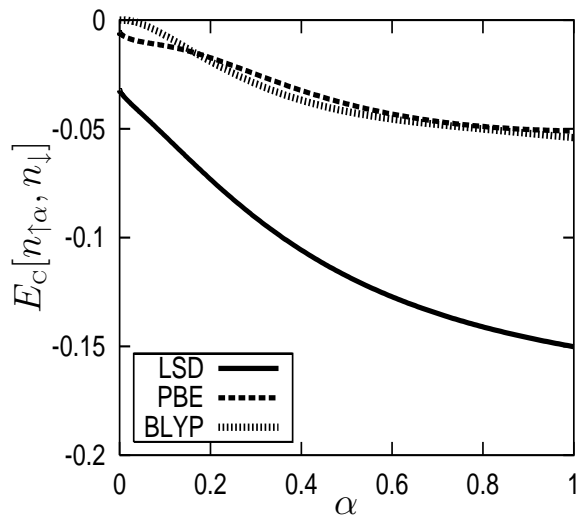


Figure 4.5: Up-spin scaling of the Li atom density using various approximate functionals for E_C : local spin density approximation (solid line), generalized gradient approximation (PBE, dashed line), BLYP (bars).

away, as in Fig. 4.5, we find a curve very similar to that of He, Fig. 4.4. The primary difference is the greater correlation energy for $\alpha = 1$.

On the other hand, scaling away the down-density gives a very different picture, Fig. 4.6. The most dramatic changes in the correlation energy now occur at small α . Near $\alpha \rightarrow 1$, the system energy is quite insensitive to spin-scaling, especially in GGA. This is exactly opposite to what we have seen for the uniform gas. It is an open question whether this would be observed with the exact functional. For up-spin scaling, we expect the correlation energy to vanish as $\alpha \rightarrow 0$. But for down-spin scaling one expects a finite correlation energy in the limit $\beta \rightarrow 0$. The two spin-up electrons remain and are still correlated. In this case, the BLYP functional errs noticeably since it predicts no correlation energy for the remaining two electrons.

Quantitative results for Li are given in Table 4.2. The exact result for E_X is the E_X of a self-consistent OEP calculation. Using the highly accurate energy prediction from [145], we deduce the exact $E_C = E_T - E_{T,OEP}$. The other exact results are not extractable from the literature here, but could be calculated from

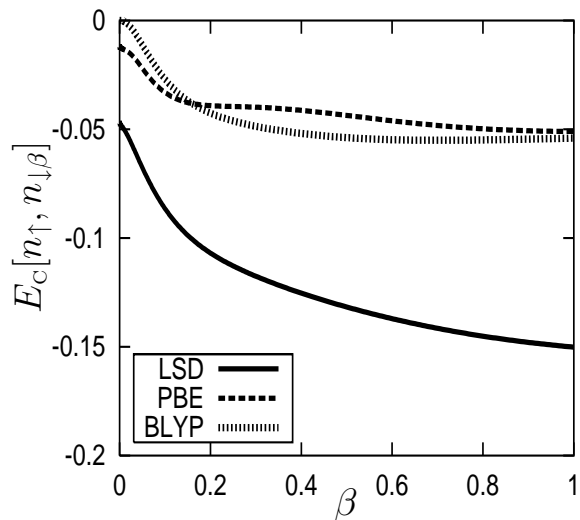


Figure 4.6: Down-spin scaling of the Li atom density using various approximate functionals for E_C : local spin density approximation (solid line), generalized gradient approximation (PBE, dashed line), BLYP (bars).

Approx.	E_x	E_C	$E_C[n_\uparrow, 0]$	$dE_C/d\alpha$	$E_C[0, n_\downarrow]$	$dE_C/d\beta$
LSD	-1.514	-0.150	-0.047	-0.037	-0.032	-0.019
PBE	-1.751	-0.051	-0.012	-0.004	-0.005	-0.001
BLYP	-1.771	-0.054	-0.054	-0.020	0.000	-0.005
exact	-1.781	-0.046	-	-	0.000	-

Table 4.2: Li atom energies, both exactly and within several approximations. All energies in Hartrees, all functionals evaluated on self-consistent densities.

known exact potentials and densities [79]. Even in this simple case, an SIC calculation is difficult. For the up-spin density, one would need to find the $1s$ and $2s$ orbitals for each value of α that yield the spin-scaled densities.

4.8 Constructing a Spin Adiabatic Connection

Here, we define an analog of the adiabatic connection within the spin-scaling formalism. Traditionally, we think of λ as a parameter in the Hamiltonian, but this way of thinking becomes prohibitively complicated in spin-density functional theory. We would have to define three coupling constants: λ_{\uparrow} , λ_{\downarrow} , and $\lambda_{\uparrow\downarrow}$. Even if we did that, it would be non-trivial to relate changes in these coupling constants to changes in the electron density. Instead, we *define* a relationship between spin-scaling and a spin-dependent *coupling parameter*. For total-density scaling, the relationship between scaling and evaluating a functional at a different coupling constant is [101, 139]

$$E_{\text{xc}}^{\lambda}[n] = \lambda^2 E_{\text{xc}}[n_{1/\lambda}]. \quad (4.23)$$

The adiabatic connection formula is

$$E_{\text{xc}} = \int_0^1 d\lambda \frac{dE_{\text{xc}}^{\lambda}}{d\lambda} = \int_0^1 d\lambda U_{\text{xc}}(\lambda). \quad (4.24)$$

By virtue of the Hellmann-Feynman theorem, $U_{\text{xc}}(\lambda)$ can be identified as the potential contribution to exchange-correlation at coupling constant λ . The integrand $U_{\text{xc}}(\lambda)$ can be plotted both exactly and within density functional approximations, and its behavior lends insight into deficiencies of functionals [146]. For separate spin-scaling, we apply the same ideas but now to

$$\Delta E_{\text{xc}}[n_{\uparrow}, n_{\downarrow}] = E_{\text{xc}}[n_{\uparrow}, n_{\downarrow}] - E_{\text{xc}}[0, n_{\downarrow}], \quad (4.25)$$

the exchange-correlation energy difference between the physical system and the system with one spin-density removed while keeping the remaining spin-density

	LSD	PBE	SIC	BLYP	exact
$\Delta U_{\text{xc}}(0)$	-0.43	-0.50	-0.53	-0.51	-0.51
$\Delta U_{\text{xc}}(1)$	-0.58	-0.57	-0.62	-0.59	-0.60
ΔE_{xc}	-0.54	-0.54	-0.57	-0.55	-0.56

Table 4.3: Spin adiabatic connection $\Delta U_{\text{xc}}(\lambda_{\uparrow})$ for He atom, both exactly and in several approximations.

fixed. For polarized systems, this quantity depends on which spin-density is removed. We define

$$\Delta E_{\text{xc}}^{\lambda_{\uparrow}} = \lambda_{\uparrow}^2 \Delta E_{\text{xc}}[n_{1/\lambda_{\uparrow}}, n_{\downarrow}] \quad (4.26)$$

and

$$\Delta U_{\text{xc}}(\lambda_{\uparrow}) = d\Delta E_{\text{xc}}^{\lambda_{\uparrow}}/d\lambda_{\uparrow}, \quad (4.27)$$

so that

$$\Delta E_{\text{xc}} = \int_0^1 d\lambda_{\uparrow} \Delta U_{\text{xc}}(\lambda_{\uparrow}). \quad (4.28)$$

This produces a spin-dependent decomposition of the exchange-correlation energy, related to separate spin-scaling rather than total-density scaling, with the integral now including the high-density limit. As $\lambda_{\uparrow} \rightarrow 0$, exchange dominates, and $U_{\text{xc}}(\lambda_{\uparrow}) \rightarrow U_{\text{x}}(\lambda_{\uparrow})$ which is just $E_{\text{x}}[2n_{\uparrow}]/2$ according to the simple results for exchange in Sec. 4.4. Furthermore, in the absence of correlation, $U_{\text{xc}}(\lambda_{\uparrow})$ is independent of λ_{\uparrow} . This is not true if one uses Eq. (4.23).

This spin adiabatic connection formula should prove useful for the improvement of present-day functionals in the same way that the adiabatic connection formula has been useful for improving total-density functionals. For example, it might be possible to perform Görling-Levy perturbation theory [147] in this parameter (λ_{\uparrow}) or to extract a correlation contribution to kinetic energy [148]. We show the spin adiabatic connection for the He atom in Fig. 4.7. In generating each adiabatic connection plot, we now take the scaled spin-density to the high-density limit. The area under each curve is precisely ΔE_{xc} for a particular

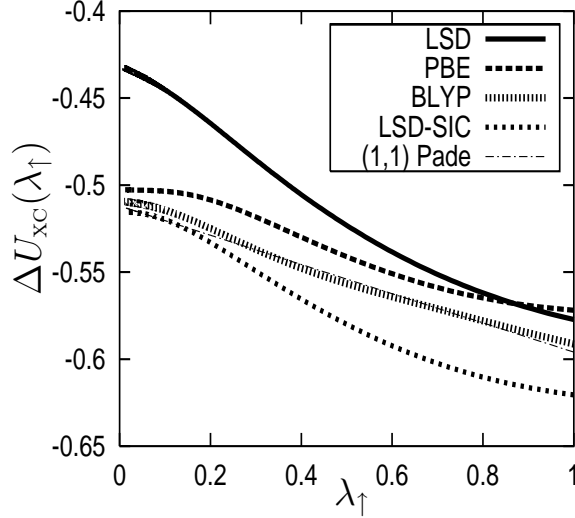


Figure 4.7: Single-spin adiabatic connection for He atom: local spin density approximation (solid line), generalized gradient approximation (PBE, dashed line), BLYP (bars), self-interaction corrected LSD (short dashes), *Exact* (fancy dashes).

approximation. To get $E_{\text{xc}}[n_{\uparrow}, n_{\downarrow}]$, we must add the contribution from the unscaled spin, $E_{\text{xc}}[0, n_{\downarrow}]$. The spin adiabatic connection curve looks quite similar to the regular adiabatic connection curve: for the He atom, $\Delta U_{\text{xc}}(\lambda_{\uparrow})$ becomes more negative with λ everywhere and is close to linear. This suggests that the spin correlation effects are weak for this system, just as the correlation effects are.

To better understand how popular approximations perform, we would like to compare with the exact curve. In principle, this requires a sophisticated wavefunction calculation designed to reproduce the spin-scaled densities at every point in the adiabatic connection curve. Here, we use a simple interpolation that should be highly accurate. Analytic formulae give exact limits for $\Delta U_{\text{xc}}(\lambda_{\uparrow})$. At the small λ_{\uparrow} limit, exchange dominates, and we are left with the exchange contribution from the scaled spin to the total energy:

$$\Delta U_{\text{xc}}(\lambda_{\uparrow} = 0) = \frac{1}{2} E_{\text{x}}[n]. \quad (4.29)$$

At the other end,

$$\Delta U_{\text{xc}}(\lambda_{\uparrow} = 1) = 2E_{\text{xc}}[n_{\uparrow}, n_{\downarrow}] - 2E_{\text{xc}}[0, n_{\downarrow}]$$

$$-dE_{\text{xc}}[n_{\uparrow\alpha}, n_{\downarrow}]/d\alpha|_{\alpha=1}. \quad (4.30)$$

For a spin-unpolarized two-electron system like the He atom, this becomes

$$\begin{aligned} \Delta U_{\text{xc}}(\lambda_{\uparrow} = 1) &= E_{\text{x}}/2 + 2E_{\text{c}} - (E_{\text{c}} + T_{\text{c}})/2 \\ &\quad (2 \text{ electrons, unpol.}). \end{aligned} \quad (4.31)$$

For He at $\lambda_{\uparrow} = 1$, $\Delta U_{\text{xc}}(\lambda_{\uparrow}) = -0.60$. To approximate the exact curve, we use a (1,1) pade. The values $\Delta U_{\text{xc}}(0)$, $\Delta U_{\text{xc}}(1)$, and ΔE_{xc} fix the three unknown parameters. This pade turns out to be nearly a straight line.

Table 4.3 shows the exact limits and the limits given by several popular functionals. BLYP reproduces both limits most accurately and is mostly linear. This should come as no surprise as BLYP yields good energies and accounts for He's self-interaction error (if a bit serendipitously). However, we do not expect such good results from BLYP when using it on Li. For Li, as we have seen in section 4.7, BLYP predicts no correlation energy when only one electron is scaled away. BLYP will fail noticeably and uncontrollably in this case. The LSD functional dramatically underestimates the single-spin exchange energy and, therefore, gets the small λ_{\uparrow} limit quite wrong. This reflects the usual error for LDA exchange. However, notice how well LSD performs at $\lambda_{\uparrow} = 1$. The value here is only a 3% overestimate of the exact value, much better than the 9% overestimate for the exchange-correlation energy. Furthermore, the LSD derivative as $\lambda_{\uparrow} \rightarrow 1$ is almost exact. PBE and LDA-SIC are qualitatively similar, the greater error in LSD-SIC being due to the errors in LSD. Both show a flattening of the curve as $\lambda_{\uparrow} \rightarrow 0$, much more than BLYP. Our *exact* curve is too crudely constructed to indicate which behavior is more accurate.

Ideally, we would compare approximations to the exact adiabatic plot for this and other systems such as the Li atom. The plots are not easy to generate. But even so, analysis of the exact limits is sufficient to garner a deeper understanding of how functionals treat and mistreat spin-densities.

4.9 Remarks about Spin-Scaling

Both scaling and the adiabatic decomposition formula have proven extremely useful in studying and constructing total-density functionals. We have suggested the possibility of scaling spin-densities separately, derived a new virial theorem, given new exact results for the He atom, and pointed out the difficulties of deducing exact theorems from this decomposition. While exact calculations are difficult to perform and exact results appear difficult to prove within this approach, any results would be very useful and likely to improve spin-density functional theory's treatment of magnetic properties.

We close with a significant challenge to developing separate spin-scaling. In the total-density scaling of Eq. (4.1), the density is both squeezed (or spread) and is also translated. The squeezing is independent of the choice of origin, but the translation is not. This origin-dependence should not affect the exchange-correlation energy because space is translationally invariant. However, when an individual spin-density is scaled, the remaining spin-density remains fixed in space. This means the resulting density depends on the choice of origin for the separate spin-scaling. So while $E_C[n_{\uparrow\alpha}, n_{\downarrow}]$ is a spin-density functional of $n_{\uparrow\alpha}$ and n_{\downarrow} , it is *not* a pure spin-density functional of the original spin-densities because of this origin dependence. Most likely, a method of transforming away this origin dependence, as found for virial energy densities in [149], will be needed to make this spin-scaling technique more physical and useful. For atoms, we made the obvious choice of origin at the center of the nucleus. Origin dependence will become acute in applications to molecules and even worse for solids. On the other hand, the non-uniform coordinate scaling of Görling and Levy [150] suffers from the same difficulties for non-spherical densities but has still produced useful limits for approximate density functionals [151].

However, it is important to stress that the spin-virial relationship is unaffected by this challenge. For α arbitrarily close to 1, the spin-scaled energies are independent of the choice of origin, and these difficulties are irrelevant. The spin-virial relationship is an exact constraint and gives us a useful measure of how the correlation energy is affected by small changes in the spin-densities. It also leads to a natural decomposition of energy changes due to separate spin-densities. It should be useful in determining whether calculations are self-consistent for each spin-density separately. This might be useful, for example, in systems where it is important to calculate small differences between spin-densities.

Chapter 5

The Adiabatic Connection and Its Strongly Interacting Limit: Testing the Strictly Correlated Electron Hypothesis

In this chapter, we will use another tool, the adiabatic connection, to analyze the unknown exchange-correlation energy functional. The adiabatic connection curve will be accurately calculated beyond the physical interaction strength using a simulated scaling method. This is done for the Hooke's atom, two interacting electrons in a harmonic well potential. Extrapolation of the accurate curve to the infinite coupling limit agrees well with the strictly correlated electron (SCE) hypothesis. The interaction strength interpolation is shown to be a good, but not perfect, fit to the adiabatic curve.

5.1 Using the Adiabatic Connection to Study Functionals

A formal and general expression for the exchange-correlation energy is according to the adiabatic connection [34],

$$E_{\text{xc}}[n] = \int_0^1 d\lambda U_{\text{xc}}[n](\lambda), \quad (5.1)$$

where $U_{\text{xc}}[n](\lambda)$ is the exchange-correlation potential energy of a density, n , at coupling constant, λ (see Eq. (5.3)). Analysis of the integrand, $U_{\text{xc}}[n](\lambda)$, leads to many rigorous relationships that the exact exchange-correlation energy satisfies and approximate functionals should satisfy. For example, Görling and Levy obtained a perturbation series expression for the exchange-correlation energy

[147] by expanding about the weak interaction limit. Another fruitful result is the understanding of why hybrid functionals like PBE0 [152] and B3LYP [93] perform so well [146, 95, 104].

Because the exchange-correlation energy is the area under the adiabatic connection curve between $\lambda = 0$ to 1, most interest in $U_{\text{xc}}(\lambda)$ has been confined to this domain. However, there is no fundamental reason to restrict study to this domain. In fact, certain exact properties of the adiabatic connection curve outside this domain have been used to better approximate the curve between $\lambda = 0$ and $\lambda = 1$ [153]. One example is the consideration of the strong interaction limit, $\lambda \rightarrow \infty$. A model for this strongly interacting limit is the strictly correlated electron (SCE) hypothesis [153] which states that, because of the strong Coulomb repulsion, the individual electrons distribute themselves as far apart as possible but are constrained to yield a given density. Finding one electron uniquely pins the others into position. Among other predictions, this SCE model says that U_{xc} can also be expanded about the strong interaction strength limit ($\lambda \rightarrow \infty$). Information from this infinite limit, combined with the Görling-Levy expansion about $\lambda = 0$, leads to the suggestion of the interaction strength interpolation (ISI) for the entire curve. Exchange-correlation energies from the ISI are considerably more accurate than those using only the first two terms in the perturbation series [154].

Another reason to consider large coupling strengths is that approximate exchange-correlation energy functionals for this limit might be more accurate [155]. It has long been known that standard approximate density functionals, such as the local density approximation (LDA) or the PBE generalized gradient approximation (GGA), are better for exchange-correlation together than they are for exchange alone. This is due to a cancellation of errors between approximations to the exchange and correlation energy [104, 156]. If this cancellation between exchange and correlation grows with larger coupling constants, approximate density

functionals in this regime will be more accurate.

This chapter is a detailed study of some of these suggestions. We employ a simulated scaling procedure [157], originally developed for the range $\lambda = 0$ to 1, and extend the simulated adiabatic connection curve to larger coupling constants [158]. At some point along the adiabatic connection curve, the simulated scaling method is expected to break down. Nevertheless, the curve can be extrapolated from there to the infinite coupling limit. This analysis yields interesting new information about the strong interaction limit.

We work with Hooke’s atom because it remains bound no matter how strongly the electrons interact. Hooke’s atom is the unpolarized two-electron system described by the Hamiltonian [159] ,

$$\hat{H} = -\frac{1}{2} (\nabla_1^2 + \nabla_2^2) + \frac{k}{2} (\mathbf{r}_1^2 + \mathbf{r}_2^2) + \frac{1}{|\mathbf{r}_1 - \mathbf{r}_2|}, \quad (5.2)$$

where k is the harmonic force constant, \mathbf{r}_1 and \mathbf{r}_2 are the position operators for each electron, and ∇_1^2 and ∇_2^2 are the Laplacian operators for each. This is not just an exactly solvable model with Coulomb interactions but also an important *physical system*. For example, many authors have used this system to model quantum dots [160, 161].

Although we could have performed calculations for the Hooke’s atom at various harmonic well strengths, we will focus on $k = 1/4$. For this spring constant, the Hooke’s atom happens to admit an analytic solution [162]. Furthermore, for this k value, the correlation energy is comparable to that of the Helium atom.

The simulated curves indicate that the SCE predictions for $U_{\text{xc}}(\infty)$ are correct. Next, assuming the validity of the SCE hypothesis, we generate a highly accurate simulation of the entire curve. This allows us to calculate higher derivatives of $U_{\text{xc}}(\lambda)$ around key points: $\lambda = 0$, 1, and ∞ . This information should be useful for the testing and improvement of existing functionals. We also compare the interaction strength interpolation (ISI) with the accurate simulated result.

5.2 Görling-Levy Perturbation Theory

The integrand of Eq. (5.1) is

$$U_{\text{xc}}[n](\lambda) = \langle \Psi_n^{\text{min},\lambda} | \hat{V}_{\text{ee}} | \Psi_n^{\text{min},\lambda} \rangle - U_H[n], \quad (5.3)$$

where $U_H[n]$ is the Hartree energy, \hat{V}_{ee} is the electron-electron Coulomb interaction, and $\Psi_n^{\text{min},\lambda}$ is the wave-function that minimizes $\langle \Psi_n^{\text{min},\lambda} | \hat{T} + \lambda \hat{V}_{\text{ee}} | \Psi_n^{\text{min},\lambda} \rangle$ and yields the density $n(\mathbf{r})$. The functional, $U_{\text{xc}}[n](\lambda)$, as a function of λ makes up the adiabatic connection curve. At $\lambda = 0$, Eq. 5.3 is just E_x , the exchange energy evaluated at a given density. Later, for convenience, we will subtract this contribution and write $U_c(\lambda) = U_{\text{xc}}(\lambda) - E_x$.

At small λ , one may write the Görling-Levy series for U_{xc} [163, 164]:

$$U_{\text{xc}}[n](\lambda) = E_x[n] + 2E_c^{\text{GL2}}[n]\lambda + \mathcal{O}(\lambda^2), \quad \lambda \rightarrow 0 \quad (5.4)$$

where E_x is the exchange energy, and $E_c^{\text{GL2}}[n]$ is the second order contribution to the correlation energy. The exchange-energy functional for a polarized system is

$$E_x[n] = -\frac{1}{2} \sum_{kk'\sigma}^{\text{occ}} \int \int \frac{\phi_{k\sigma}^*(r) \phi_{k\sigma}(r') \phi_{k'\sigma}(r') \phi_{k'\sigma}^*(r)}{|r - r'|}, \quad (5.5)$$

and Görling-Levy correlation term is

$$E_c^{\text{GL2}}[n] = -\sum_{\nu=1}^{\infty} \frac{|\langle \Phi_{KS} | \hat{V}_{\text{ee}} - \hat{V}_{\text{H}} - \hat{V}_{\text{x}} | \Phi_{KS}^{\nu} \rangle|^2}{E_{KS}^{\nu} - E_{KS}}, \quad (5.6)$$

where Φ_{KS}^{ν} is the ν th excited state of the KS Hamiltonian as described by a KS Slater-determinant of orbitals [163, 147]. The operators are defined as follows: $\hat{V}_{\text{ee}} = 1/|\hat{\mathbf{r}} - \hat{\mathbf{r}}'|$, $\hat{V}_{\text{H}} = v_{\text{H}}(\hat{\mathbf{r}})$, and $\hat{V}_{\text{x}} = v_{\text{x}}(\hat{\mathbf{r}})$. To get the exchange-correlation energy from Eq. (5.4), we need to integrate from $\lambda = 0$ to 1. Unfortunately, there is no guarantee that the series will converge and that the higher order terms are negligible [154].

5.3 The Strong Coupling Limit

Further exact properties of U_{xc} might be useful to help understand the adiabatic curve and to use this information to construct a new functional. An interesting limit is when $\lambda \rightarrow \infty$. This leads us to the second theoretical point, the strong coupling limit. This limit corresponds to strongly interacting electrons which still yield the physical density. In this limit, the integrand is finite [98]. We can expand $U_{\text{xc}}(\lambda)$ about the infinite limit:

$$U_{\text{xc}}[n](\lambda) = U_{\text{xc}}[n](\infty) + U'_{\text{xc}}[n](\infty)/\sqrt{\lambda} + \mathcal{O}(1/\lambda), \quad \lambda \rightarrow \infty \quad (5.7)$$

where $U_{\text{xc}}[n](\infty)$ and $U'_{\text{xc}}[n](\infty)$ are the zeroth and first terms in the expansion.

5.4 The Strictly Correlated Electron Hypothesis

It has been suggested that the electrons behave in a strictly correlated manner at this limit [153]. The electrons still produce a given density distribution, but finding one electron determines the position of all the others. Information about this limit can be incorporated into an interpolation formula which reproduces both limits exactly and can be integrated analytically.

For spherically symmetric two-electron systems in three dimensions, the SCE model admits an exact solution for $U_{\text{xc}}(\infty)$ and provides one of two contributions to $U'_{\text{xc}}(\infty)$ [165]. One question asked in this chapter is how large the missing contribution to $U'_{\text{xc}}(\infty)$ is. We will calculate the SCE limit and part of the first correction term for the Hooke's atom $k = 1/4$ according to the expressions given by Seidl in Ref. [165].

According to the Seidl hypothesis, the electrons behave in a strictly correlated manner at this limit. By strict correlation, we mean that determination of the position of one electron constrains the position of all the other electrons so that knowledge of one electron position determines all the electrons positions.

However, it must be stressed that the electrons still yield the physical density distribution.

For spherically symmetric two-electron systems in three dimensions, the SCE model admits an exact solution for $U_{\text{xc}}(\infty)$.

$$U_{\text{xc}}^{\text{SCE}}[n](\infty) = V_{\text{ee}}^{\text{SCE}}[n](\infty) - U_{\text{H}}[n] \quad (5.8)$$

The Hartree piece, $U_{\text{H}}[n]$, can be calculated exactly with the equation (2.27). This leaves the $V_{\text{ee}}^{\text{SCE}}[n]$ to be evaluated. If the electron positions are strict functions of one another, we may write the V_{ee} term as

$$V_{\text{ee}}^{\text{SCE}}[n](\infty) = 2\pi \int_0^\infty dr \frac{r^2 n(r)}{r + f(r)}. \quad (5.9)$$

We have replaced $|\mathbf{r} - \mathbf{r}'|$ with $r + f(r)$ since we know that the electrons must be on opposite sides of the nucleus. Then,

$$U_{\text{xc}}^{\text{SCE}}(\infty) = 2\pi \int_0^\infty dr \frac{r^2 n(r)}{r + f(r)} - U_{\text{H}}[n]. \quad (5.10)$$

We only need to find $f(r)$, the position of a second electron given the position of the first at r . This amounts to solving the differential equation,

$$f'(r) = \frac{r^2 n(r)}{f(r)^2 n(f(r))} \quad (5.11)$$

with the starting condition $4\pi \int_0^{r_0} dr r^2 n(r) = 1$ at $f(r_0) = r_0$. Given set of density values and the r points they are defined on, we solve this equation numerically using a sixth order Runge-Kutta scheme.

If one assumes that the electrons oscillate about this SCE electron limit in quantum harmonic oscillator potential, we can obtain an expression for $U'_{\text{xc}}(\infty)$.

5.5 The Interaction Strength Interpolation, A Rung Five Functional

The combined information from the first two terms of the Görling-Levy series and the strong interaction limit can be used to create a rung five functional. This is

a rung five because the exact-exchange depends on the occupied orbitals and the second order correlation term depends on the unoccupied orbitals. This is the Interaction Strength Interpolation (ISI) models Eq. (5.3) [154] :

$$U_{\text{xc}}(\lambda)[n] = U_{\text{xc}}(\infty) - X/(\sqrt{1 + Y\lambda} + Z) \quad (5.12)$$

with $x = -2E_{\text{C}}^{\text{GL2}}[n]$, $y = U'_{\text{xc}}(\infty)$, $z = E_{\text{x}}[n] - U_{\text{xc}}(\infty)$, $X = xy^2/z^2$, $Y = x^2y^2/z^4$, and $Z = xy^2/z^3 - 1$. The functional (5.12) can be integrated using Eq. (5.1) to obtain E_{xc} . Eq. (5.12) satisfies the known limits of the adiabatic connection but is not size consistent.

5.6 Relationship Between Scaling and Coupling Constant

The relationship between the coupling constant and scale factor is important for the procedure we used to simulate the adiabatic connection curve. A density, $n(\mathbf{r})$, is scaled according to Eq. (4.1). The exchange-correlation energy at a coupling constant, λ , and density, $n(\mathbf{r})$, is simply related to the exchange-correlation energy at a scaled density [140, 101]:

$$E_{\text{xc}}^{\lambda}[n] = \lambda^2 E_{\text{xc}}[n_{1/\lambda}]. \quad (5.13)$$

The integrand in Eq. (5.1) is $U_{\text{xc}}(\lambda) = dE_{\text{xc}}^{\lambda}/d\lambda$. Under both coupling constant and scaling transformations, we can sometimes show how parts of the exact energy transform. For example,

$$E_{\text{x}}^{\lambda}[n] = \lambda E_{\text{x}}[n] \text{ or } E_{\text{x}}[n_{\gamma}] = \gamma E_{\text{x}}[n]. \quad (5.14)$$

We use this observation later to identify scale factors between two scaled densities.

5.7 Solving Hooke's Atom at Different Harmonic Well Strengths

Hooke's atom is described by the Hamiltonian, Eq. (5.2). It is separable in $\mathbf{u} = \mathbf{r}_2 - \mathbf{r}_1$ and $\mathbf{R} = \frac{1}{2}(\mathbf{r}_1 + \mathbf{r}_2)$. One part is a harmonic oscillator with a mass of two and eigenvalue, $E_R = \frac{3}{2}\sqrt{k}$. The other term is

$$\left(-\nabla_{\mathbf{u}}^2 + \frac{1}{2}k\mathbf{u}^2 + \frac{1}{|\mathbf{u}|}\right)\phi(\mathbf{u}) = E_u\phi(\mathbf{u}).$$

For the ground state, there is no angular momentum contribution. At $k = \frac{1}{4}$, the solution is

$$\phi(u) = C\left(1 + \frac{u}{2}\right)e^{-\frac{u^2}{8}}, \quad (5.15)$$

and the spherically-symmetric exact ground-state density is

$$n(r) = \frac{\pi\sqrt{2\pi}}{4\pi^{\frac{5}{2}}(5\sqrt{\pi} + 8)r} e^{-\frac{1}{2}r^2} \left[7r + r^3 + \frac{8}{\sqrt{2\pi}}re^{-\frac{1}{2}r^2} + 4(1 + r^2)\text{erf}\left(-\frac{1}{2}r^2\right)\right] \quad (5.16)$$

with the energy $E_{tot} = 2$ or $E_u = \frac{5}{4}$ plus $E_R = \frac{3}{4}$. For a list of other interesting solutions and results from Hooke's atom, see Ref. [143].

For arbitrary k , the solution can not be expressed in terms of elementary functions, but can nevertheless be calculated numerically. The exact results for Hooke's atom are readily compared to functional approximations by taking the numerically exact densities as input into approximate functionals.

5.8 Testing the Simulated Scaling Method

In order to generate highly accurate adiabatic connection plots, we use the procedure developed by Frydel, Terilla, and Burke [157]. To find the adiabatic connection curve, we need $E_{xc}^\lambda[n]$ for a set of λ 's. For Hooke's atom, we know the exact densities and the exact E_{xc} at different k values. Instead of changing λ , which is difficult, we use Eq. (5.13). A small change in the strength of external

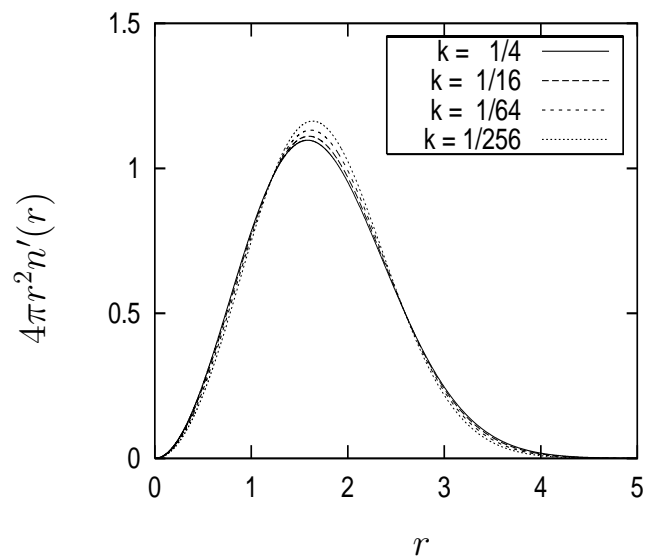


Figure 5.1: Simulated scaling of the density. We start with Hooke’s atom at $k = 1/4$. Then, we solve at various other coupling constants and use simulated scaling to return us as closely as possible to the $k = 1/4$ density.

potential yields another density, qualitatively similar to the original density but on a different scale. If we can solve the system exactly at this different external potential strength, we have an approximation to the exchange-correlation energy for a scaled density. When the densities do not qualitatively change shape much, this scheme is highly accurate. To find $U_{\text{xc}}(\lambda)$, we differentiate Eq. (5.13) with this highly accurate approximation to the exact $E_{\text{xc}}[n_{1/\lambda}]$. Including a first order correction term increases the accuracy of this method:

$$E_{\text{c}}[n_{\gamma}] \approx E_{\text{c}}[n'] + \int d^3r v_{\text{c}}[n'](\mathbf{r}) (n_{\gamma}(\mathbf{r}) - n'(\mathbf{r}))$$

Table 5.1: Simulated scaling k and λ equivalences using the E_{x} scaling rule, Eq. (5.18), to determine λ .

k	λ	k	λ
1/4	1.000	1/4	1.000
1/16	1.460	1	0.689
1/64	2.151	4	0.478
1/256	3.197	16	0.334

$$+ \mathcal{O}(\delta n)^2, \quad (5.17)$$

where $v_c(\mathbf{r}) = \delta E_C[n]/\delta n(\mathbf{r})$ is the correlation contribution to the Kohn-Sham potential. This method gives highly accurate energies for Hooke's atom ($k = 1/4$) and for Helium when λ varies from 0 to 1. The error at $\lambda = 0$ is 0.3 mHartrees, and the estimated error for λ close to one is less than 1 mHartree [157].

For each simulated scaling, we must assign an appropriate scale factor, but which properly scaled density does the approximately scaled density mimic? The original paper discusses several possibilities. They all require knowing how a chosen component of the energy changes with uniform density scaling. We use the E_x method:

$$\lambda = 1/\gamma = E_x[n]/E_x[n']. \quad (5.18)$$

Since we use E_x to assign λ , the $U_x(\infty)$ contribution to $U_{xc}(\infty)$ necessarily scales properly for all values of λ , and so we show only $U_c(\lambda)$.

In this paper, we examine the adiabatic connection curve at large interaction strengths. This method only works for $\lambda > 1$ for systems that remain bound as the external potential is weakened. Even with this restriction, the method must ultimately fail as $\lambda \rightarrow \infty$. Specifically for Hooke's atom, Cioslowski showed that at a certain critical strength for the external potential, $k_c = 0.0016$ ($\lambda_c = 4.138$), the density changes shape qualitatively [166]. Beyond this value, the simulated scaling might no longer be a good approximation to exact-scaling. On the other hand, the method fails for He almost immediately as the two-electron ion unbinds at nuclear charge, $Z = 0.9$.

To test this procedure and to develop a rule for its reliability, we apply the procedure in a case where we already know the correct answer, namely with an approximate functional. A generalized gradient approximation (GGA) mimics the complexity of the true functional better than, say, the local density approximation. Because of its first principle derivation and reliability, we use PBE here [41]. Since we have the analytic form for the PBE functional, we can scale the

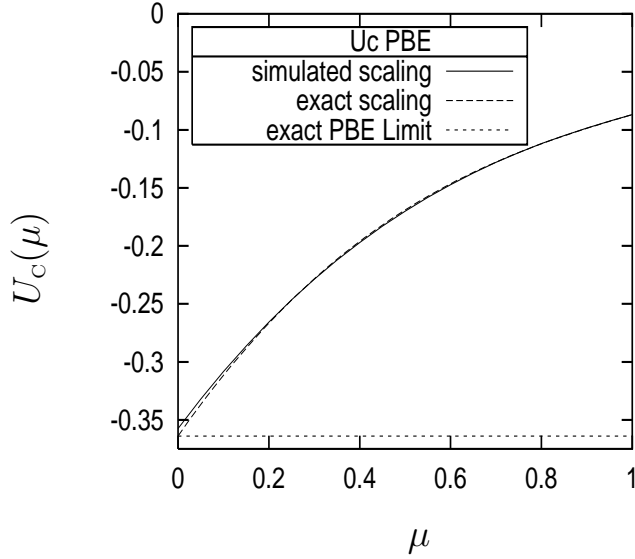


Figure 5.2: PBE adiabatic connection curve for Hooke’s atom ($k = 1/4$): $U_c(\mu = 1/\sqrt{\lambda})$. The solid line is generated using simulated scaling of the density and the dashed curve by exactly scaling the known functional. The exact PBE $U_c(\mu = 0)$ limit is shown (short dashes).

input density to generate the entire adiabatic curve, Fig. 5.2. The curve is shown as a function of $\mu = 1/\sqrt{\lambda}$ so that the region $\lambda \in 1, \infty$ can appear on a finite-sized plot.

PBE results for certain key λ values are listed in Table 5.4. An explicit expression [155] for the PBE functional as $\mu \rightarrow 0$ is

$$U_{xc}^{PBE}(\infty)[n] = \int d^3r n(r) \epsilon_x(n) \left(F_x^{PBE}(s) + \frac{0.964}{1 + y + y^2} \right) \quad (5.19)$$

where $y = 0.2263 s^2$, s is the reduced gradient, $\epsilon_x(n)$ is the exchange energy per particle of the uniform gas, and $F_x^{PBE}(s)$ is an exchange enhancement factor [41].

We need a criterion for how far along the adiabatic connection we can trust the simulated density scaling to mimic the exactly-scaled density. Our criterion is to terminate the simulations at $\mu = \mu_c = 1/\sqrt{\lambda_c} = 0.4916$ where the density

qualitatively changes shape [166]. Even at this point, the first order correction in Eq. (5.17) still improves upon the zeroth order simulation. This is a highly conservative estimate; it is likely that the curves are accurate to smaller μ 's.

To get a prediction for $U_c(\mu = 0)$, we must extrapolate the simulation to $\mu = 0$. This is done by fitting the simulated data to an n^{th} order polynomial and extrapolating this polynomial to $\mu = 0$. The third order polynomial connecting four sample points best reproduces the known $U_c^{\text{PBE}}(\infty)$. In Fig. 5.2, we show the exactly-scaled PBE functional and the polynomial interpolation. We see that the simulated curve is almost on top of the exact curve. However, they do differ slightly in the $U_c(\mu = 0)$ values. For the simulated curve, $U_c(\mu = 0) = -0.357$, and the scaled result is -0.363 from Eq. (5.19), a 6 mHartree error.

5.9 Extrapolating to the Infinite Interaction Strength Limit

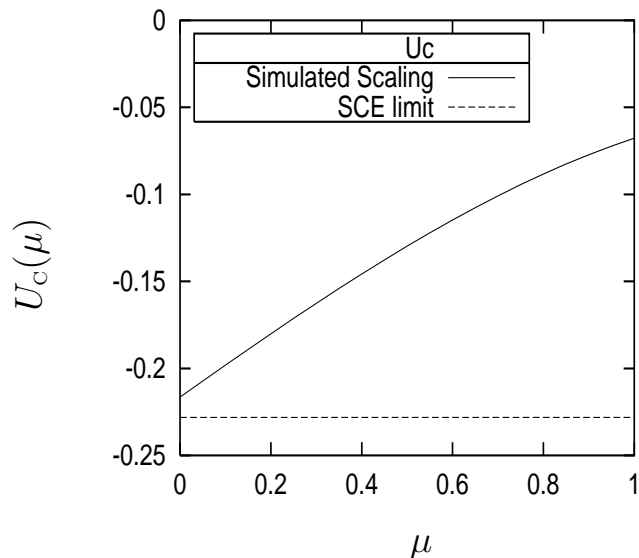


Figure 5.3: The adiabatic connection curve for Hooke's atom ($k = 1/4$): $U_c(\mu)$. The solid line is the simulated curve. The SCE limit is shown as a dashed line.

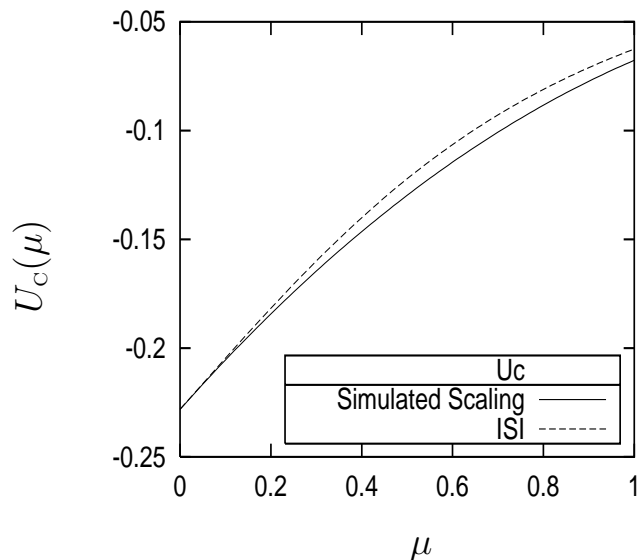


Figure 5.4: Simulated adiabatic connection curve for Hooke’s atom ($k=1/4$): $U_c(\mu)$. The solid line is the simulated curve with the SCE $U_c(\mu = 0)$. The dashed curve is the ISI using exact inputs.

The simulated adiabatic connection curve for Hooke’s atom $k = 1/4$ in Fig. (5.3) approaches the SCE $U_c(\mu = 0)$ limit. As in section 5.8 for the PBE functional, we reproduce the entire curve by fitting the simulated points to a third order polynomial. Since the simulated scaling method is only reliable between $\mu = 1/2$ and 1, we must extrapolate the curve over the domain $\mu = 0$ to $1/2$ by a polynomial. The extrapolated prediction for $U_c(\mu = 0)$, -0.206 , is 22 mHartrees from the strictly correlated electron prediction, -0.228 . We do not expect as good agreement as in section 5.8 because the true E_c functional is more complicated than a GGA, and we regard the result as consistent with the SCE hypothesis.

5.10 Simulating the Entire Adiabatic Connection Curve

In section 5.9, we used an extrapolation scheme to complete the adiabatic curve. Here, we combine the simulated part with the SCE electron limit to produce a highly accurate adiabatic connection curve for all coupling strengths. From this

curve, we calculate the first terms in Taylor expansions about both $\lambda = 0$ and 1, and $\mu = 0$ and 1. Using these new results, we assess the accuracy of the Interaction Strength Interpolation (ISI) with accurate inputs.

Table 5.2: Higher derivatives of $U_c(\mu)$ with respect to μ for Hooke’s atom ($k = 1/4$).

μ	$U_c(\mu)$	$U'_c(\mu)$	$U''_c(\mu)$
0	-0.228	0.235	-0.156
1	-0.068	0.088	0.221

Table 5.3: Higher derivatives of $U_c(\lambda)$ with respect to λ for Hooke’s atom ($k = 1/4$).

λ	$U_c(\lambda)$	$U'_c(\lambda)$	$U''_c(\lambda)$	$U^{(3)}_c(\lambda)$	$U^{(4)}_c(\lambda)$
0	0.0000	-0.101	0.095	-0.107	0.124
1	-0.0677	-0.044	0.032	-0.032	0.039

The $\mu < 1$ simulated adiabatic connection curve is shown in Fig. 5.4. The curve was generated by fitting the simulated data points from $\mu = 0.5$ to 1 and including the SCE $U_c(\mu = 0)$ in the point set. We used a third order polynomial, the order that best reproduced the adiabatic curve for the PBE functional in section 5.8. This curve should be an excellent approximation to the exact curve. From the plot, we see that the derivative $dU_c(\mu)/d\mu$ is positive everywhere along the adiabatic curve. This implies that $dU_c(\lambda)/d\lambda$ is negative, and the adiabatic curve is convex. All calculated $U_c(\lambda)$ curves for $0 \leq \lambda \leq 1$ have $dU_c(\lambda)/d\lambda < 0$, but the inequality has never been generally proven. Our result extends this observation to $\lambda \geq 1$ for this system.

Derivatives of $U_c(\mu)$ are obtained from the coefficients in the polynomial extrapolation. Two higher derivatives of $U_c(\mu)$ with respect to μ are shown in table 5.2. Seidl’s model for $U'_c(\mu = 0) = 0.281$ [165] does not agree with the accurate

Table 5.4: Accurate results for Hooke’s atom with $k = 1/4$ evaluated on the exact densities.

	E_x	$2E_C^{GL2}$	E_C	$U_C(\mu = 1)$	$U_C(\mu = 0)$	$U'_C(\mu = 0)$
PBE	-0.493	-0.168	-0.051	-0.087	-0.363	0.561
Exact	-0.515	-0.101	-0.039	-0.068	-0.228	0.235

Table 5.5: Interaction Strength Interpolation Results for Hooke’s atom with $k = 1/4$. *Accurate* and *model* refer to the value of $U'_C(\mu = 0)$. The accurate value is from our simulation and the model is from Seidl’s model [165].

Method	$U'_C(\mu = 0)$	$U_C(\lambda = 1)$	Error	E_C	Error
ISI (accurate)	0.235	-0.063	8 %	-0.036	6 %
ISI (model)	0.281	-0.060	11 %	-0.035	9 %

$U'_C(\mu = 0)$. This indicates that the missing contributions to the SCE $U'_C(\mu = 0)$ mentioned by Seidl are, at least for this system, not negligible.

Several higher derivatives of $U_C(\lambda)$ with respect to λ are listed in table 5.3. Here, we need not restrict ourselves to a third order polynomial interpolation because we have a dense sampling of data points over the range $\lambda = 0$ to 4. The higher derivatives reported in terms of λ are expected to be highly accurate.

The interaction strength interpolation (ISI), as originally formulated [154], is an interpolation scheme for the entire adiabatic connection curve. It used exact values at $\lambda = 0$ and carefully chosen GGA values at $\mu = 0$. We now ask how well the ISI with accurate inputs compares to the simulated curve. The answer tells us how good the choice of curve in the ISI is. For the inputs to the ISI, we use the exact E_x and E_C^{GL2} which are derivable from the simulated curves in Ref. [157] and are given in Table 5.4. For $U_{xc}(\infty)$, we use the SCE prediction which, judging from the results in section 5.9, we believe to be exact. For $U'_C(\mu = 0)$, we input two different values: the accurate simulated value and Seidl’s prediction. The results are shown in table 5.5. The ISI interpolation does not perform exceptionally well with accurate inputs as already noticed in [167]. For example, the magnitude of

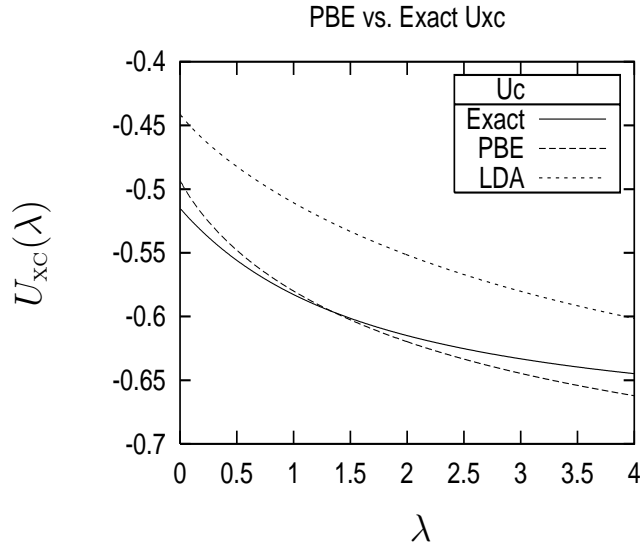


Figure 5.5: Adiabatic connection curve for Hooke’s Atom using various functionals: The exact curve is the solid line, the PBE is the long dashed line, and the local density approximation (LDA) is the short dashed line.

$U_{xc}(1)$ is underestimated by 5 mHartrees. Perhaps, this is a result of the way the $U'_c(\mu = 0)$ limit is included in the interpolation equation. For this system, incorporating the accurate value for $U'_c(\mu = 0)$ in the ISI does *not* greatly improve its accuracy.

In Fig. 5.5, we see how the PBE and LDA adiabatic connection curves compare to the accurate curve. The PBE curve clearly crosses the accurate curve. Because its exact limit, $\lim_{\mu \rightarrow 0} U_{xc}^{LDA}(\mu) = 1.964E_x^{LDA}$, is below the SCE prediction, the LDA curve must also cross the accurate one at some larger interaction strength. Since both curves cross the exact curve at some $\lambda > 1$, the cancellation of errors between exchange and correlation in E_{xc}^λ will eventually grow smaller beyond some critical interaction strength and become an addition of errors. It has been argued that because the exchange correlation on-top hole grows more local as the interaction strength increases [104, 168], local functionals for E_{xc}^λ would work better as λ increases. This is certainly true for our system in the range,

$0 \leq \lambda \leq 1$; however, the adiabatic plots indicate that as λ grows, the energy depends on the density in an increasingly nonlocal way. The accuracy of the on-top hole is less relevant to the total energies in the strongly interacting region of the adiabatic connection curve. This is related to a self-correlation error as noted in [155]. Both LDA and GGA functionals rely on the LDA treatment of the uniform gas, and the LDA cannot properly reproduce the Wigner crystallization limit due to this strong self-correlation error [169]. Meta-GGAs are self-correlation free and behave better in this limit [88].

5.11 Assessment of the Strictly Correlated Electron Hypothesis and the Interaction Strength Interpolation

In this work, we have extended the method of Ref. [157] to simulate the adiabatic connection curve to interaction strengths greater than the physical value for a simple model system. In doing so, we kept in mind that the method must fail at some μ_c as $\mu \rightarrow 0$ ($\mu = 1/\sqrt{\lambda}$) and performed an extrapolation to the strong interaction limit. This simulated curve agreed with the SCE hypothesis. To generate a highly accurate curve for $\mu = 0$ to 1, we included the SCE $U_c(\mu = 0)$ in the set of points and interpolated. Using this accurate adiabatic curve, we found higher derivatives at key coupling constants: $\lambda = 0$, 1, and ∞ . Finally, we compared some popular approximate functionals to the accurate curve.

Chapter 6

The Adiabatic Connection and Its Weakly Interacting Limit: A Close Examination of Exact-Exchange Band Gaps

Now, we turn our attention to the other end of the adiabatic connection, the small λ limit. In this limit, the first order contribution to the exact exchange-correlation functional is the exact-exchange functional. This is a non-local orbital functional and satisfies different constraints than the local density approximation. We will use exact-exchange to investigate the problem of how well density functionals predict band gaps in solids. This is related to what physical meaning, if any, the Kohn-Sham orbitals have.

6.1 The Band Gap Problem in DFT

In solid-state physics, the local density approximation (LDA) correctly describes ground-state properties like the density and equilibrium lattice structures. A notable exception to this success is the failure to describe energy gaps. The fundamental energy gap, E_g , is defined as the difference between the ionization potential, I_p , and electron affinity, A . The ionization potential and the affinity are defined as total energy differences between the $N - 1$ and N electron systems and the N and $N + 1$ electron systems respectively. Thus, the fundamental gap can be found from ground-state energies of systems with different numbers of electrons:

$$E_g = I - A = E[N + 1] + E[N - 1] - 2E[N], \quad (6.1)$$

where $E[N + 1]$, $E[N]$, and $E[N - 1]$ are the ground-state energies of the systems with $N + 1$, N , and $N - 1$ electrons respectively. For example, if the N electron ground-state is a neutral atom, then the $N + 1$ system is a negative ion, and the $N - 1$ system is a positive ion. Since the fundamental gap is a ground-state property, it should be well-described by ground-state DFT.

It has been shown that the fundamental gap can be re-expressed in the following form[170, 171]:

$$E_g = E_g^{KS} + \Delta_{xc}, \quad (6.2)$$

where Δ_{xc} is called the derivative discontinuity, and

$$E_g^{KS} = \epsilon_{N+1}(N) - \epsilon_N(N), \quad (6.3)$$

is called the Kohn-Sham orbital gap or just KS gap. The notation $\epsilon_L(M)$ is the eigenvalue for the L^{th} KS orbital in the M electron system. In ensemble density functional theory, the constraint on integer number of electrons is relaxed, and the discontinuity is defined as [172]

$$\Delta_{xc} = \lim_{\omega \rightarrow 0} \left\{ \frac{\delta E_{xc}[n]}{\delta n} \Big|_{N+\omega} - \frac{\delta E_{xc}[n]}{\delta n} \Big|_{N-\omega} \right\}_N. \quad (6.4)$$

In exact KS theory, the ionization potential, I_p , is equal to the eigenvalue of the highest occupied KS orbital eigenvalue. This means that the ionization potential can be found from the N electron system. For approximate functionals, the relationship between the ionization potential and the highest occupied orbital eigenvalue is not known.

6.2 Introduction to Exact Exchange and Orbital Functionals

Exact exchange (EXX) in DFT is the Fock exchange integral evaluated on the KS orbitals, $\phi_k(r)$'s [176]:

$$E_x[n] = -\frac{1}{2} \sum_{kk'\sigma} \int d^3r d^3r' \frac{\phi_{k,\sigma}^*(\mathbf{r})\phi_{k,\sigma}(\mathbf{r}')\phi_{k',\sigma}(\mathbf{r})\phi_{k',\sigma}^*(\mathbf{r}')}{|\mathbf{r} - \mathbf{r}'|}. \quad (6.5)$$

The sum is over all occupied KS orbitals. These orbitals minimize $T_S[n]$ for a given density, $n(\mathbf{r})$, and are, therefore, implicit functionals of the electron density. Since T_S and E_x depend on the orbitals, they are both implicit functionals of the density.

The exact-exchange scheme and the Hartree-Fock differ because the Hartree-Fock and KS orbitals are not the same. In the Hartree-Fock scheme these orbitals obey an equation with the semi-local potential while in the KS scheme they are determined by the KS equations with a local-multiplicative potential.

One of the most difficult aspects of performing EXX calculations is determining the local-multiplicative potential, $v_x[n](\mathbf{r}) = \delta E_x[n]/\delta n(\mathbf{r})$. The potential can be obtained by the chain-rule differentiation:

$$v_x(\mathbf{r}) = \frac{\delta E_x[n]}{\delta n(\mathbf{r})} = \sum_{k,occ} \int d^3r'' d^3r' \left[\frac{\delta E_x[n]}{\delta \phi_k(\mathbf{r}')} \frac{\delta \phi_k(\mathbf{r}')}{\delta v_{KS}(\mathbf{r}'')} + c.c. \right] \frac{\delta v_{KS}(\mathbf{r}'')}{\delta n(\mathbf{r})}. \quad (6.6)$$

Optimized effective potential (OEP) and optimized potential method (OPM) refer to the numerical scheme to take the functional derivative and are often used to label exact-exchange calculations. The solution of Eq. (6.6) usually involves solving a complicated integral equation. Because of this, exact exchange calculations are much slower and more difficult than the LDA calculations. Self-consistent exact-exchange calculations are much more complicated than LDA ones, and the EXX calculations can be as slow as GW calculations.

The exact-exchange functional solves several known problems with local and semi-local functionals. Namely, atomic EXX potentials have the correct asymptotic behavior, $v(\mathbf{r}) \sim -1/|r|$, and are self-interaction free. Loosely, self-interaction-free means that the functional will give the correct results for one-electron atoms!

It is inconsistent to add local correlation to an orbital functional for exchange. The reason is that local correlation violates several exact constraints on E_{XC} that E_x satisfies! Nevertheless, real systems do have correlation, and so, in our

calculations, we sometimes include correlation in a crude way by adding the local density contribution to the orbital exchange.

Another advantage of exact-exchange DFT is that the exchange-discontinuity can be calculated exactly:

$$\Delta_x = \langle c | \hat{V}_{nl} - \hat{V}_x | c \rangle - \langle v | \hat{V}_{nl} - \hat{V}_x | v \rangle \quad (6.7)$$

where $|c\rangle$ and $|v\rangle$ are the lowest conduction and the highest valence orbitals [173, 174]. In the systems that we will consider and at the Γ point in the Brillouin zone, \hat{V}_{nl} is the non-local Fock operator and \hat{V}_x is the local multiplicative KS exchange-potential operator.

6.3 Previous Work with Exact Exchange

For over two decades, the exact-exchange functional has been successfully applied to atoms and molecules [175, 176]. Only recently has it been applied to semiconductors, insulators and metals [177, 178, 179, 173, 180, 182, 183].

A surprising result of the EXX calculations for sp-semiconductors is that the KS energy gaps are very close to the experimental fundamental gaps with an error of about 1-3%. This contrasts typical LDA results in which the gaps are always too small. In the EXX case, a larger gap than in LDA is to be expected because the EXX potential is self-interaction free and, thus, binds more strongly than LDA potential. For example, the EXX-KS eigenvalues in atoms are greater in magnitude than their LDA counterparts. Since the occupied valence orbitals generally have a greater self-interaction contribution than the more de-localized unoccupied orbitals, the EXX-KS gap should widen compared to that of the LDA.

It is curious that exact-exchange calculations should predict sp-semiconductor band gaps well. For one, Hartree-Fock calculations do poorly at predicting band gaps. More importantly, it is unknown whether the KS band structure should give the exact band gaps or not [170, 171]. The prevailing belief is that the *exact*

KS gaps are smaller than the true gaps for solids [35]. As there are no exact KS potentials for solids available, this belief is yet unverified. It is not known how large the discontinuity Δ_{xc} , Eq. (6.4), of the *exact* exchange-correlation density-functional is. A KS potential has been derived from GW calculations and has been used to test this idea [184]. It was found that the presumably accurate KS potential for silicon gave fundamental gaps much smaller than the experimental ones.

The EXX functional is the only density functional so far predicting band gaps close to experiment. This success has some important practical consequences. One of them is the possibility of using the KS eigenvalue spectrum as a first, approximate description of excitations and as a fast tool to interpret experiments. Another, perhaps more important, use for EXX results is as a better starting point for more accurate calculations of excitations via the time-dependent density functional theory.

In this chapter, we assess the performance of exact-exchange for materials very different from sp-semiconductors, namely, the noble-gas crystals. These systems have previously been studied using LDA [185]. Solid Ne, Ar, Kr and Xe are special systems since they are composed of almost independent atoms. The individual tightly bound close-shell atoms bind very weakly with one another. In fact, the shape of the charge density for isolated atoms and for solids is rather similar and we might expect the energetics to be similar as well. Because the electron charge is localized around the atom and is far from uniform, these systems are a difficult case for LDA. Indeed, as will be seen in Table 6.4, the LDA description of the equilibrium structural properties for these solids is much less satisfactory than usual. These solids are large-gap insulators with experimental fundamental gaps ranging between 21.4 eV for neon and 9.8 eV for xenon. They also have large exciton binding energies on the order of several eV.

Since the solids are a loosely-bound ensemble of atoms, a comparison between

various electronic properties in the solid phase and in isolated atoms is meaningful and interesting. We will investigate both cases, solid and gas, with LDA and EXX. As will be seen later, in the atomic case EXX resembles highly accurate Kohn-Sham results when available. LDA correlation mixed with exact-exchange deteriorates the quality of results except in the cases when total-energy differences are involved. Then, an account of the correlation seems to be necessary.

Our results show that EXX, with and without LDA correlation, widens the LDA-KS gaps of noble-gas solids by about 1.3-3.4 eV. The KS gaps are not as close to the experimental gaps as reported for sp-semiconductors. When considered along with previous observations that the EXX-KS gaps for diamond[173] and MgO[177] are smaller than the experimental gaps, our results suggest that EXX does not generally reproduce the fundamental gap.

For atoms, the exact KS gaps between the highest occupied orbital and unoccupied orbitals, it has been suggested, might be better approximations to the *excitonic* or *optical* gaps than to the quasi-particle or fundamental gaps[186]. The latter is defined by generalization of Eq. (6.1) to higher excited states, and the former is the gap between the ground and excited-states of the N -electron system. Some calculations using *almost exact* Kohn-Sham atomic potentials seem to support this idea[187], but it is not always clear that KS orbital eigenvalue differences should approximate the optical gaps. This is investigated in detail in Ref. [188].

Our EXX results for noble-gas atoms (Section 6.7) show that in this case the KS eigenvalue differences are closer to the optical gap than the fundamental gap.

For the semiconductors, the exciton binding energy is very small (on the order of meV), and the optical and fundamental gaps are not sufficiently resolved to be able to identify which gap the KS one is closest to. Until more accurate correlation-energy functionals are known, little more can be said about the KS gaps in semiconductors.

For noble-gas solids, the optical and quasi-particle gaps differ by several eV, and the electronic structure for the solids is similar to that of the isolated atoms. The calculations could shed light on the situation. What we have found is that the EXX KS-gaps for noble-gas solids are, unlike the case of semiconductors, significantly smaller than the quasi-particle gaps. They are also smaller than the experimental optical gaps by about 20 % of the experimental value. A fundamental question remains then: would *exact* correlation approximately align the KS and optical gaps for noble-gas solids, or does correlation in the solid phase have a qualitatively different character and role than it does for finite, atomic systems?

6.4 Bloch's Theorem and Plane-Wave Methods

In our calculations, we use a plane-wave basis. There are several advantages to working in a plane-wave basis set. The basis vectors are orthogonal and complete, the kinetic energy operator is diagonal. Most importantly for our purposes, the basis set can be systematically improved. Ref. [189] gives a good review of the details of the plane-wave and pseudopotential method.

Bloch's theorem [190] tells us that for a periodic potential, we can write each single-particle non-interacting orbital as a product of a plane-wave and a periodic function,

$$\Psi_{n,\mathbf{k}}(\mathbf{r}) = e^{i\mathbf{k}\cdot\mathbf{r}} u_{n,\mathbf{k}}(\mathbf{r}), \quad (6.8)$$

where \mathbf{k} is a vector which labels the orbital. $u_{n,\mathbf{k}}(\mathbf{r})$ is periodic in \mathbf{R} , a vector spanning the side of one unit cell:

$$u_{n,\mathbf{k}}(\mathbf{r} + \mathbf{R}) = u_{n,\mathbf{k}}(\mathbf{r}). \quad (6.9)$$

The periodic function can be expressed in terms of reciprocal lattice vectors, \mathbf{G} 's,

$$u_{n,\mathbf{k}}(\mathbf{r}) = \sum_{\mathbf{G}} c_{n,\mathbf{k}}(\mathbf{G}) e^{i\mathbf{G}\cdot\mathbf{r}}. \quad (6.10)$$

The set of G 's is defined as the vectors which satisfy $\mathbf{G} \cdot \mathbf{R} = 2\pi n$ where n is an integer. The \mathbf{k} 's are defined only up to the addition of a reciprocal lattice vector, \mathbf{G} . A continuous distribution of \mathbf{k} 's with no doubling is called the Brillouin zone. The shape of the Brillouin zone reflects the geometry of the crystal.

In the calculations, sums over the Brillouin zone must be done to obtain the density and other quantities. For example, a typical sum would be

$$\int_{BZ} d^3k f(\mathbf{k}) \approx \frac{(2\pi)^3}{\text{Vol}} \sum w_i f(\mathbf{k}_i) \quad (6.11)$$

where Vol is the volume of the sample. It is too expensive to calculate a dense sampling of \mathbf{k} points. Fortunately, it can be shown that an accurate approximation to this sort of integral is possible with a sparse sampling of carefully selected \mathbf{k} points. In particular, we sample points of low symmetry in the irreducible wedge of the Brillouin zone and use symmetry to obtain a larger set of terms. In our calculations, the special k points minimize the error in the discretization according to a scheme by H. J. Monkhorst and J. D. Pack [191].

We can expand the Bloch function in terms of reciprocal lattice vectors,

$$\phi_{\mathbf{k},n}^{KS}(\mathbf{r}) = \frac{1}{\sqrt{V}} \sum_{\mathbf{G}} C_{\mathbf{k},n}(\mathbf{G}) e^{i(\mathbf{k}+\mathbf{G})\cdot\mathbf{r}}. \quad (6.12)$$

The Fourier transform of the potential is

$$v(\mathbf{G}) = \frac{1}{8\pi^3} \int d^3r v(\mathbf{r}) e^{-i\mathbf{G}\cdot\mathbf{r}}. \quad (6.13)$$

In order to get the KS potential, the density is calculated in real space according to

$$n(\mathbf{r}) \approx \sum_{\mathbf{k},occ} |\phi_{\mathbf{k}}|^2(\mathbf{r}). \quad (6.14)$$

The potential is calculated in one real-space cell, and then, Fourier-transformed to reciprocal space.

In reciprocal space, the Kohn-Sham equation is

$$\left[\sum_{\mathbf{G}'} \frac{1}{2} |\mathbf{k} + \mathbf{G}'|^2 \delta_{\mathbf{G},\mathbf{G}'} + v_{KS}(\mathbf{G} - \mathbf{G}') \right] c_n(\mathbf{k} + \mathbf{G}') = \epsilon_n c_n(\mathbf{k} + \mathbf{G}). \quad (6.15)$$

This is one matrix problem in G for each k value sampled. The equation can be diagonalized using standard Lapack routines. We impose a cut-off so that the matrix is finite in size and can be diagonalized in a finite time,

$$\frac{1}{2}|\mathbf{G} + \mathbf{k}|^2 \leq E_{cut}. \quad (6.16)$$

In our calculations, we use semi-local pseudopotentials so that $v_{KS}(\mathbf{G} - \mathbf{G}')$ is replaced with the semi-local version, $v_{KS}(\mathbf{G}, \mathbf{G}')$.

6.5 Pseudopotentials

Valence electrons ¹ occupy the highest energy occupied orbitals and are chemically active. The rest of the electrons are core electrons. We can greatly reduce the size of a calculation by replacing the core electrons with an effective potential. In *frozen-core approximation*, we imagine that the core electrons are unaffected by changes in the valence. The effective potentials replace the Coulomb potentials centered on the nuclei.

Even with this simplification, calculations on real solids are demanding. One of the reasons is that the valence orbitals must be orthogonal to the core orbitals. For example, orbital oscillations near the nucleus would mean that the cut-off for a plane-wave basis would be large. The need for a large basis set can be alleviated by carefully choosing the effective potential. A pseudopotential gives orbitals that are equal to the exact ones beyond some radius. Below that radius, the pseudo-orbitals are chosen to be free of unwanted nodes and oscillations.

In most modern calculations, *ab initio* pseudopotentials are popular. The pseudopotentials are typically constructed from purely first principles. First, an atomic code finds the KS orbitals for a given atomic charge, Z . The orbitals are matched to pseudo-orbitals beyond a critical radius, and the pseudopotential is found by inverting the pseudo-Schrödinger equation with these orbitals.

¹By electrons, we mean non-interacting electrons or Kohn-Sham orbital occupancies.

Ensuring that the pseudo-orbitals are smooth requires that the pseudopotentials depend on the angular momentum eigenvalues, l :

$$\hat{V}_{pseudo}(r) = \sum_{l,m} V_l(r) |l, m\rangle \langle l, m|. \quad (6.17)$$

Thus, smooth pseudopotentials are semi-local. In principle, a fully local pseudopotential is possible but the potential would not be smooth [192].

Kohn-Sham DFT is strictly only valid for local multiplicative external potentials, but pseudopotentials are often semi-local. The validity of the formalism comes into question. The DFT pseudopotential method is often justified by its success. In generalized KS theory, there is no problem with the semi-local potential [193, 73].

While there is no compelling theoretical reason to abandon semi-local pseudopotentials, there is a practical one. Semi-local pseudopotentials are inconvenient for plane-wave calculations. The Kleinman-Bylander scheme transforms a semi-local pseudopotential to an effectively local one [194].

The pseudo potential should represent the effective core potential that one non-interacting electron in the valence would experience. The construction, thus far, gives us an effective pseudopotential from the core and the other valence electrons. We need to remove the valence-valence interactions to get the ionic pseudopotential. This can be done as follows:

$$v_l^{pseudo}(\mathbf{r}) = v_l(\mathbf{r}) - v_H[n_v](\mathbf{r}) - v_{xc}[n_v + n_c](\mathbf{r}). \quad (6.18)$$

We remove all the Hartree interaction of the valence and all of the exchange-correlation. For the exact-exchange, this unscreening is not as simple to do since $v_x(\mathbf{r})$ is not known explicitly as a functional of the density. The result is that an alternative screening procedure is needed [195].

In our calculations, we use an EXX compatible Troullier-Martins type pseudopotential calculated from the Moukara et al. code [195].

6.6 The Implementation of Exact-Exchange

The exact-exchange potential can be computed analytically in a basis set by requiring that a linear change in the potential cause a linear change in the charge density. This is formally shown in Ref. [173, 182]. In a plane-wave basis, the Fourier transformed exchange potential is

$$v_x(\mathbf{G}) = \sum_{\mathbf{G}' \neq 0} [F(\mathbf{G}') - F^*(\mathbf{G}')] \tilde{\chi}_0^{-1}(\mathbf{G}, \mathbf{G}'), \quad (6.19)$$

where $\tilde{\chi}_0$ is the inverse of the momentum space response function, $\tilde{\chi}_0(\mathbf{G}, \mathbf{G}')$. The $\mathbf{G} = \mathbf{G}'$ component is removed to ensure that only charge conserving variations are allowed.

$$\tilde{\chi}_0(\mathbf{G}, \mathbf{G}') = \frac{4}{Vol.} \sum_{c\nu\mathbf{k}} \frac{\langle \nu\mathbf{k} | e^{-i\mathbf{G}\cdot\mathbf{r}} | c\mathbf{k} \rangle \langle c\mathbf{k} | e^{i\mathbf{G}'\cdot\mathbf{r}} | \nu\mathbf{k} \rangle}{\epsilon_{\nu\mathbf{k}} - \epsilon_{c\mathbf{k}}}, \quad \mathbf{G} \neq \mathbf{G}', \quad (6.20)$$

and

$$F(\mathbf{G}) = \frac{2}{Vol.} \sum_{\nu c\mathbf{k}} \frac{\langle \nu\mathbf{k} | \hat{v}_x^{NL} | c\mathbf{k} \rangle \langle c\mathbf{k} | e^{-i\mathbf{G}\cdot\mathbf{r}} | \nu\mathbf{k} \rangle}{\epsilon_{\nu\mathbf{k}} - \epsilon_{c\mathbf{k}}}, \quad (6.21)$$

where in a basis,

$$v_x^{NL}(\mathbf{k}, \mathbf{G}, \mathbf{G}') = -\frac{4\pi e^2}{Vol.} \sum_{\nu\mathbf{q}\mathbf{G}_i} \frac{C_{\nu\mathbf{q}}(\mathbf{G} + \mathbf{G}_i) C_{\nu\mathbf{q}}^*(\mathbf{G}' + \mathbf{G}_i)}{|\mathbf{q} - \mathbf{k} + \mathbf{G}_i|^2} \quad (6.22)$$

with $C_{\nu\mathbf{k}}(\mathbf{G}) = \langle \mathbf{k} + \mathbf{G} | \nu\mathbf{k} \rangle$. The label ν refers to valence orbitals, and c refers to conduction orbitals. We sum over all conduction orbitals, \mathbf{G} 's, and \mathbf{G}' 's in our basis.

In our actual calculations for each approximate E_{xc} (LDA, EXX and EXXc), we generated a pseudopotential using the same functional [196, 197, 182]. For solid krypton and xenon, we performed a relativistic calculation and account for the spin-orbit interaction perturbatively.

The cut-off energy for the plane-wave basis was typically 50 – 120 Hartree and determined by convergence. Convergence means that the plane wave cut-off is large enough so that increasing the cut-off no longer changes the band

Ne	LDA	EXX	EXXc	QMC	CI	Expt.
1s	-824.34	-838.30	-840.38	-838.18	-838.30	
2s	-35.97	-46.73	-48.40	-44.93	-45.01	
2p	-13.54	-23.14	-24.76	-21.61	-21.69	-21.56
3s	-0.07	-5.23	-5.77	-4.97		-4.9
3p		-3.11	-3.40	-3.00		-2.94
4s		-1.95	-2.03	-1.90		-1.89
3d		-1.57	-1.63	-1.55		-1.53

Table 6.1: Neon atom energy levels (in eV). The KS orbital eigenvalues are from LDA, exact exchange (EXX) and exact exchange with LDA correlation (EXXc). Column QMC gives the eigenvalues obtained with the highly accurate Kohn-Sham potential of Ref. [198]. Column CI presents results of highly accurate Kohn-Sham calculation of Ref. [79].

gaps by more than ≈ 0.1 eV. The k-summations consist of 2 mean value points in the irreducible part of the Brillouin zone. We perform all calculations at the experimental lattice constants: Ne($8.435 a_0$), Ar($9.94 a_0$), Kr($10.66 a_0$), and Xe($11.59 a_0$). The noble-gas solids have an FCC structure.

6.7 Exact Exchange on Finite Systems: Ne, Ar, Kr and Xe

It is interesting and instructive to start our investigation by analyzing the properties of the isolated atoms where the density-functional calculations are more advanced and can be used to test various approximations. Atomic DFT is more advanced in this context in two senses. First, highly accurate KS potentials are available for a few light atoms like Ne[198, 199] and Ar[199]. Second, for a finite system, it is computationally feasible to calculate the fundamental gap, Eq.(6.1), from the total-energy differences. In this section, we will present several results for the noble-gas atoms and draw some conclusions about the validity of certain approximations.

Ar	LDA	EXX	EXXc	CI	Expt.
1s	-3095.39	-3112.99	-3115.42	-3113.82	
2s	-293.61	-303.27	-305.13	-302.59	
2p	-229.67	-237.46	-239.36	-236.85	
3s	-24.02	-29.90	-31.37	-28.79	
3p	-10.40	-16.07	-17.48	-14.88	-15.76
4s	-0.26	-4.37	-4.94		-4.08
4p		-2.77	-3.09		-2.66
3d		-1.86	-2.29		-1.83

Table 6.2: Argon atom energy levels (in eV). The KS orbital eigenvalues are from LDA, exact exchange (EXX) and exact exchange with LDA correlation Column CI presents results of highly accurate Kohn-Sham calculation of Ref. [79].

In Tables 6.1 and 6.2, the KS eigenvalues for Ne and Ar are presented. The results are for LDA, pure exact-exchange (EXX), exact-exchange plus LDA correlation (EXXc) and highly accurate, almost exact KS potentials. The column denoted QMC in Table 6.1 shows the orbital eigenvalues calculated by Umrigar and Gonze[198] from a Quantum Monte Carlo ground-state density for the Ne atom. The column denoted CI in Tables 6.1 and 6.2 shows Morrison and Zhao’s results [79] from highly accurate configuration interaction densities. The column called *Expt.* contains the negatives of the experimental first ionization-potentials. The column also contains the experimental binding energies of a few excited states. The binding energies of unoccupied states are the experimental optical gaps between the ground state and a relevant excited state minus the ionization potential. The reported optical gaps are a weighted average of singlet and triplet optical gaps. In tables 6.1 and 6.2, we report only the experimental binding energy for the highest occupied state. This is because the eigenvalue of the highest occupied state has a physical meaning; it is the negative of the ionization potential. For the unoccupied states, it has been suggested that the KS eigenvalues approximate the experimental binding energies of the excited atom

		Ne	Ar	Kr	Xe
Expt:	E_g	21.56	15.76	14.00	12.13
Expt:	E_{og}	16.63	11.57	9.94	8.35
LDA:	I-A	22.66	16.17	14.44	12.73
	$\Delta\epsilon_{KS}$	13.47	10.14	8.76	7.50
	E_{og}	17.74	11.96	10.32	8.87
EXX:	I-A	19.83	14.77	13.22	11.66
	$\Delta\epsilon_{KS}$	17.91	11.70	9.81	8.12
	E_{og}	15.16	10.96	9.58	8.32
EXXc:	I-A	21.31	16.03	14.61	12.79
	$\Delta\epsilon_{KS}$	18.99	12.54	10.58	8.82
	E_{og}	16.08	11.72	10.28	8.97

Table 6.3: Fundamental energy gaps E_g =I-A and optical gaps from experiment and calculations in neutral atoms Ne, Ar, Kr and Xe. E_{og} expt. is the multiplet-averaged experimental transition energy from the ground state to p^5s^1 state. E_{og} KS is the calculated total-energy difference between the ground state and the excited atom in the (p^5s^1) configuration. $\Delta\epsilon_{KS}$ is the Kohn-Sham gap.

well [186, 187]. This idea has been explicitly verified for helium[186], beryllium [186] and neon atoms[187] and some plausible arguments have been put forward to explain why [186].

The LDA eigenvalues are smaller in magnitude than their EXX and EXXc counterparts. This is mostly due to the large self-interaction error inherent in LDA. Another consequence of the self-interaction error is that LDA typically has only one unoccupied orbital. The EXX eigenvalues for Ne and Ar are deeper than the exact ones. This means that the EXX scheme binds Ne and Ar too strongly. Exact correlation would correct this over-binding. Adding LDA correlation to EXX deepens the eigenvalues even more. For example, the EXX uppermost occupied eigenvalues are roughly 1.5, 0.3 eV deeper than the exact KS eigenvalues for Ne and Ar respectively. In the EXXc scheme, the difference grows to 3.2 and 1.7 eV respectively. For occupied states, the expected behavior of *exact* correlation in DFT is similar to the role of correlation in the many-body Green's

functions approach. There, correlation shifts the eigenvalues, or poles of the one-particle Green's functions, in the opposite direction as Hartree-Fock. Thus, the binding energies of occupied orbitals are far too strong within Hartree-Fock. The EXX KS occupied orbitals are more bound than the exact KS orbitals, but the effect is much smaller than in Hartree-Fock.

The analogy between Hartree-Fock and exact-exchange breaks down for unoccupied states. In this case, EXX results in deeper unoccupied orbitals than experiment finds and adding LDA correlation makes them even deeper. On the other hand, Hartree-Fock theory hardly binds at all. This striking difference between EXX and Hartree-Fock is because Hartree-Fock has an exponentially decaying potential for the unoccupied orbitals. In contrast, the EXX potential has a Coulombic tail for all orbitals. The Hartree-Fock potential is self-interaction free only for occupied orbitals, whereas the KS potential (exact and EXX) is self-interaction free for all orbitals.

For the heavier atoms Kr and Xe, we performed a full relativistic OEP calculation since relativistic effects should be important. In these cases, we have neither the exact KS potentials nor eigenvalues with which to compare the results. However, a comparison with the experimental first ionization-potential shows that, when spin-orbit interaction is neglected, the exact exchange calculation slightly overbinds the uppermost occupied level. Here again, LDA correlation added to exact-exchange lowers the eigenvalues. For lighter atoms, adding LDA correlation to exact-exchange results degrades one-electron properties.

For finite systems, it is possible to relate certain excitations with total-energy differences. This is the case with the first ionization potential, $I = E[N - 1] - E[N]$, electron affinity, $A = E[N] - E[N + 1]$, and the energy gap E_g , Eq.(6.1). The electron affinity, A , defined by a total energy difference, is zero within LDA for most atoms. This is because LDA does not bind the corresponding $N + 1$ electron system. In the case of noble-gas atoms, however, the experimental affinity does

vanish, and the LDA result is adventitiously correct. Since the affinity vanishes, the gap must equal the ionization energy. Using Eq. (6.1) and LDA for the atomic gap is problematic because LDA usually does not bind the $N + 1$ system needed to find the affinity. On the other hand, because the LDA discontinuity disappears and the orbital eigenvalues are well defined, Eq. (6.2) gives a prediction for the gap. The discontinuity disappears because the LDA potential depends continuously on the density. The same problem plagues EXX which does not bind the $N + 1$ system as far as our calculations suggest. EXXc gives a small, but finite, value for the affinity. Table 6.3 shows the atomic energy gaps, E_g , the experimental ones and then those calculated from total-energy differences within LDA, EXX and EXXc schemes.

The energy gaps are compared to the KS eigenvalue differences $\Delta\epsilon_{KS}$. In addition, the (triplet-singlet averaged) first optical-gap and the *total-energy optical gap*, $E_{og} = E[N]^* - E[N]$ are presented. Here, $E[N]$ is the total ground-state energy and $E[N]^*$ is the total energy of an excited state in which there is a hole in the uppermost p-shell and an electron in the next s-shell. We calculate both using the same ground-state energy functionals.

First, we note that the KS gap rather poorly approximates the experimental fundamental gap. The average deviation over the four elements between the KS and true gaps is 5.9, 4.0, 3.1 eV for LDA, EXX and EXXc schemes. As shown by the data, LDA KS gaps deviate the most from experiment. When expressed in percents, LDA, EXX, and EXXc KS gaps account for 63 %, 75 % and 80 % of the experimental fundamental gaps respectively. This is not surprising since there is no reason that the KS gap should be close to the fundamental gap. For Ne (Table 6.1), the highly accurate KS energy gap amounts to 77 % of the experimental one. For Ar (Table 6.2), we estimate the exact KS gap to be about 68 % of the experimental one. The situation changes when we compare KS energy gaps to experimental optical gaps. It turns out that LDA, EXX and EXXc

schemes reproduce the atomic optical gaps with 13 %, 3 % and 9 % respectively. The highly accurate KS gap of Ne amounts to 99.9 % of the optical gap. In particular, the good agreement of the EXX scheme with experiment is to be noted. An interesting question is whether similar trends take place in the solid phase. We might expect the answer to be yes if the solid is composed of an array of weakly interacting atoms.

The experimental fundamental gap of noble-gas atoms agrees fairly well with the calculated total-energy differences (Eq. 6.1). For all four elements, the different functionals reproduce the experimental atomic gaps, on average, to 4 %, 6 % and 3 % accuracy respectively. A total-energy calculation for the *optical gaps* agrees by about 5 %, 5 % and 4 % with experiment for LDA, EXX and EXXc schemes respectively. In the total-energy difference calculations, accounting for correlation seems to be important since the best total-energy difference results come from the EXXc scheme, the worst with the exact-exchange only.

6.8 Exact Exchange of Large Gap Extended Systems: Solid Ne, Ar, Kr and Xe

In this section, we will consider the results for solid Ne, Ar, Kr and Xe.

In Table 6.4, the experimental and calculated equilibrium lattice constants are presented. The calculations were performed in the fixed nuclei approximation with no accounting for the zero point motion of the nuclei. As already noted, column VIII solids resemble loosely-bound isolated atoms. For such systems, the total energy only weakly depends on the inter-atomic distances. Thus, the energy-volume curve is very flat and the system hardly binds. In the absence of stronger inter-atomic interactions, the theoretical determination of equilibrium properties is subject to a large uncertainty. The usual convergence criteria for total-energy determination may be insufficient, and computational details, like pseudopotential

construction, can matter. To ensure reliability, we have double-checked the LDA results using independent, publicly available LDA codes [70, 200].

As shown in Table 6.4, the structural equilibrium properties of column VIII solids are very poorly described by all three functionals. For example, the error in the lattice constant for neon is more than 13 %. This discrepancy is unusually large; for most solids, LDA gives a lattice-constant within about 1-2%. For Ar, Kr and Xe, the LDA discrepancy is about 5% not as drastic as for Ne. However, the disagreement is still much larger than usual. In contrast to LDA which underestimates the lattice spacing, EXX overestimates it for Ar, Kr and Xe. Except when applied to neon, the combined scheme, exact-exchange plus LDA correlation (EXXc), is the closest to experiment. This result is similar to what was seen in section 6.7 for atomic calculations of total energy differences for which some accounting for correlation is important. None of these schemes reproduce the long-range van der Waals effects. These effects are responsible for the binding of noble-gas solids, and so it is not surprising that the calculated structural properties differ so much from experiment.

Figure 6.1 shows the band structure along the L- Γ -X directions for Ar. The solid line represents the EXX band structure, and the dashed line corresponds to the LDA one. In Tables 6.5, 6.6, 6.7, and 6.8, the KS eigenvalues at high symmetry points Γ , X and L are presented. In Table 6.9, the KS energy gaps are compared with the experimental fundamental energy gaps and with the optical gaps for solid Ne, Ar, Kr and Xe. It is important to keep in mind that for this special class of atoms, the description of the LDA, EXX and EXXc electronic structure might be expected to be less accurate in the solid phase than for atoms because in addition to only approximating at best short range correlation, the functionals do not account for the long range van der Waals effects.

It is interesting to consider how well LDA, EXX and EXXc describe the electronic structure of noble-gas solids. In LDA, the KS gaps are, on average, 55%

of the experimental gaps. This is a typical result for solids, and slightly less accurate than for the atomic LDA limit. For noble-gas solids EXX and EXXc reproduce about 68% of the fundamental gap, whereas in the atomic limit the KS gap ranged on average to 74% and 79% of the experimental fundamental gaps for EXX and EXXc respectively. That the EXX and EXXc KS gaps in noble-gas solids are not reproduced as accurately as for the semiconductors is noteworthy. However, the atomic results suggested that the EXX-KS gaps should not be expected to approximate the fundamental gaps as well as the optical gaps. Since the noble-gas solids have a large exciton binding energy, the optical gap is appreciably smaller than the fundamental gap. What we observe in Table 6.9 is that the EXX and EXXc KS gaps are still pronouncedly smaller than optical gaps in the solids. The calculations reproduce only about 80%-81% of the experimental optical gaps. This is worse than in the atomic limit. It is not clear if this disagreement is because solids require more accurate treatment of correlation than atoms. Or perhaps, the KS gaps in solids need not be close to optical gaps at all. The column noble-gas solids are good materials to investigate what, if any, physical meaning the KS gaps have; however, a definitive answer seems to require the use of more accurate correlation functionals. In section 6.7, exact-exchange with LDA correlation gave less accurate one-particle properties for isolated atoms. For solids, the accuracy of KS-EXXc gaps is slightly better than with pure EXX. This improvement could be an artifact of overbinding in the valence bands.

While the valence bands show a limited dispersion (See Fig. 6.1 for argon), conduction bands exhibit a rather pronounced dispersion. This is consistent with the observation that the Brillouin zone average of the valence band width, or the energy distance between occupied s and p bands, is very close to the energy gap between s and p valence orbitals in isolated atoms. This is not the case with the energy gaps between occupied and empty bands for corresponding orbitals in atoms. The solid gaps are appreciably smaller than in atoms.

Another remarkable result is that the LDA valence-band width is smaller than the EXX width for neon. For argon, both widths are comparable. For krypton and xenon, the EXX width is smaller. We recall that previous EXX calculations have shown for sp-semiconductors that EXX leads to narrower total valence-band widths than LDA. Only for diamond was the opposite observed.

We conclude by showing the effect of adding the exact-exchange contribution to the exact derivative discontinuity, Eq. (6.7), in Table 6.10. Notice that adding the exact-exchange discontinuities to the DFT exact-exchange gap returns us to the Hartree-Fock results.

6.9 Revisiting the Band Gap Problem in DFT

In this chapter, we have applied exact-exchange Ne, Ar, Kr and Xe. It was previously shown for isolated noble-gas atoms that the accurate Kohn-Sham energy gap is an excellent approximation to the optical gap but not to the fundamental (quasi-particle) gap. The EXX KS gaps for these atoms are also in very good agreement (3 % on average) with experimental optical gaps. We asked whether the same holds true for the solid phase. In contrast to previous results for sp-semiconductors, the EXX KS gaps in noble-gas solids are appreciably smaller than the experimental fundamental gaps, and they are 20% smaller than the experimental optical gaps. It is not clear whether this result refutes the observations for atoms or whether a more accurate correlation functional is necessary. Row X solids are bound by van der Waals effects. Because the functionals applied in this chapter do not properly describe effects, the structural properties of the solids are poorly described. The solids are bound, but the inaccuracy of the equilibrium lattice constant is unusually large.

	Ne	Ar	Kr	Xe
$a_{Expt.}$	8.44	9.94	10.66	11.59
a_{LDA}	7.29	9.35	10.13	11.14
a_{EXX}	7.23	10.13	11.07	12.66
a_{EXXc}	7.06	9.80	10.77	12.06

Table 6.4: Equilibrium cubic lattice spacing (in a.u.) from experiment and calculations.

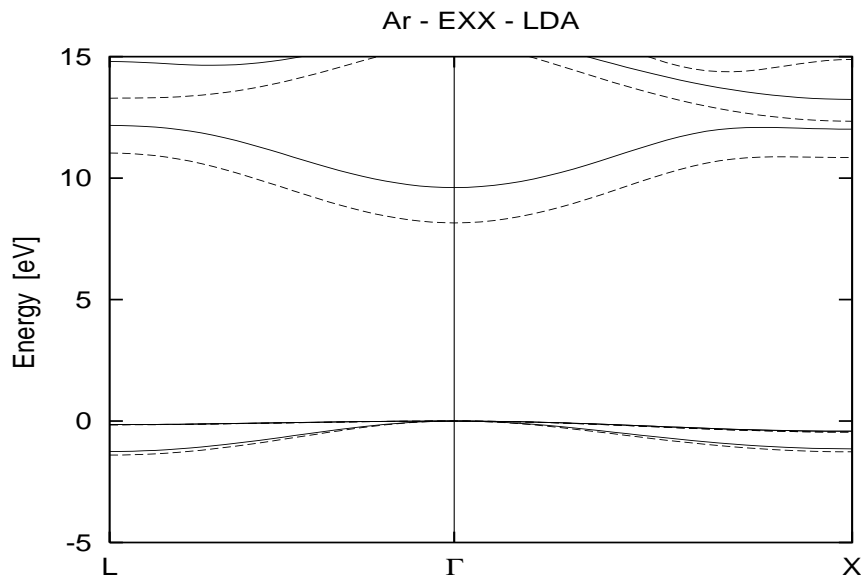


Figure 6.1: Band structure of Ar along the L- Γ -X directions as calculated within EXX (solid lines) and LDA (dashed lines).

Ne	LDA	EXX	EXXc
Γ	-22.98	-24.04	-24.22
	0.00	0.00	0.00
	11.32	14.15	14.76
	29.26	31.71	32.28
X	-22.87	-23.96	-24.14
	-0.62	-0.56	-0.53
	-0.20	-0.22	-0.21
	18.21	21.24	21.91
	19.00	21.79	22.38
L	-22.90	-23.98	-24.16
	-0.69	-0.58	-0.55
	-0.07	-0.06	-0.06
	17.06	19.84	20.42
	17.21	20.05	20.68

Table 6.5: Ne-solid Kohn-Sham eigenvalues in eV from the LDA, EXX and EXX plus LDA correlation (EXXc) schemes at high-symmetry points. The presented eigenvalues are from the upper lying valence states and lowest conduction states.

Ar	LDA	EXX	EXXc
Γ	-14.57	-14.48	-14.51
	0.00	0.00	0.00
	8.16	9.61	10.14
	15.51	16.01	16.37
	17.89	18.08	18.37
X	-14.28	-14.20	-14.25
	-1.27	-1.14	-1.06
	-0.45	-0.42	-0.39
	10.85	12.02	12.57
	12.34	13.24	13.70
L	14.89	16.31	16.67
	-14.35	-14.27	-14.32
	-1.40	-1.25	-1.16
	-0.15	-0.14	-0.14
	11.03	12.17	12.65
	13.29	14.80	15.24
	15.12	15.69	16.09

Table 6.6: Ar-solid Kohn-Sham eigenvalues in eV from the LDA, EXX and EXX plus LDA correlation (EXXc) schemes at high-symmetry points. The presented eigenvalues are from the upper lying valence states and lowest conduction states.

Kr	LDA	EXX	EXXc
Γ	-14.81	-13.74	-14.62
	-0.73	-0.65	-0.67
	0.00	0.00	0.00
	6.47	7.87	8.02
	13.18	13.43	13.80
X	-14.55	-13.45	-14.39
	-1.77	-1.65	-1.59
	-0.88	-0.82	-0.79
	-0.54	-0.52	-0.49
	8.76	9.65	10.05
	10.09	10.70	11.11
	13.28	14.49	14.78
16.94	17.63	17.96	
L	-14.62	-13.53	-14.45
	-1.88	-1.74	-1.66
	-0.59	-0.54	-0.54
	-0.18	-0.18	-0.17
	8.92	9.88	10.16
	11.79	13.07	13.41
	12.77	13.09	13.47

Table 6.7: Kr-solid Kohn-Sham eigenvalues in eV from the LDA, EXX and EXX plus LDA correlation (EXXc) schemes at high-symmetry points. Spin-orbit splittings are included. The presented eigenvalues are from the upper lying valence states and lowest conduction states.

Xe	LDA	EXX	EXXc
Γ	-13.01	-11.14	-12.71
	-1.44	-1.27	-1.34
	0.00	0.00	0.00
	5.26	6.69	6.51
	10.07	9.96	10.50
X	-12.70	-10.71	-12.41
	-2.43	-2.29	-2.24
	-1.20	-1.15	-1.09
	-0.67	-0.66	-0.61
	6.53	7.01	7.47
	7.43	7.64	8.17
	11.66	12.62	12.84
14.18	13.85	14.42	
L	-12.77	-10.81	-12.48
	-2.48	-2.34	-2.27
	-0.93	-0.86	-0.85
	-0.23	-0.23	-0.21
	6.85	7.53	7.78
	9.73	9.68	10.22
	9.78	9.73	10.28

Table 6.8: Xe-solid Kohn-Sham eigenvalues in eV from the LDA, EXX and EXX plus LDA correlation (EXXc) schemes at high-symmetry points. Spin-orbit splittings are included. The presented eigenvalues are from the upper lying valence states and lowest conduction states.

	E_g^{LDA}	E_g^{EXX}	E_g^{EXXc}	E_g^{Expt}	Δ^{Expt}
Ne	11.32	14.15	14.76	21.4	17.4
Ar	8.16	9.61	9.95	14.2	12.2
Kr	6.47	7.87	8.02	11.6	10.2
Xe	5.26	6.69	6.51	9.8	8.4

Table 6.9: Calculated and measured energy gaps in noble-gas solids in eV. E_g^{LDA} , E_g^{EXX} and E_g^{EXXc} are Kohn-Sham gaps from the LDA, pure EXX and EXX plus LDA correlation schemes respectively. E_g^{Expt} is the experimental fundamental gap. Δ is the experimental optical gap.

	LDA	EXX	$+\Delta_x$	HF	Exp.
Ne	11.3	14.4	25.9	25.1 ^a	21.1 ^b
Ar	8.2	9.6	18.7	18.5 ^a	14.2 ^c
Kr	6.7	8.1	15.8	16.5 ^a	11.6 ^d
Xe	5.7	7.1	14.1	13.5 ^a	9.8 ^e

Table 6.10: Addition of the exchange-only derivative discontinuity to the KS gaps at the Γ point. LDA is the local density approximation result. EXX means exact-exchange and no correlation. Δ_x is the exchange contribution to the derivative discontinuity. HF is the all-electron Hartree-Fock orbital gap. ^aRef.[201] ^bRef.[202] ^cRef.[203] ^dRef.[202] ^eRef.[202]

Appendix A

Codes Used in this Thesis

All codes will be available on pbe@dft.rutgers.edu in /home/pbe/rudys_thesis/.

A.1 Codes Specifically Written for this Thesis

- Deltium.f

Solves the Bethe-Ansatz equations for the ground-state energy density for Deltium, the one-dimensional uniform Fermi gas.

- Diracium.f

Calculates the ground-state energy or related quantities for Diracium, the one-dimensional delta-function-interacting analog of Helium, using a momentum space representation.

- LDAShoot.f

Uses the shooting method to solve the KS equations with exact-exchange or LDA in one dimension for a delta-functional external potential.

- Hooke1d.f

Uses the shooting method to solve the KS equations with exact-exchange or LDA in one dimension for a harmonic external potential.

- HookeExact.nb

Gives the exact ground-state energy for the one-dimensional analog of Hooke's atom. (Mathematica Notebook)

- PolyFit.f
Fits a set of data points on the interval $[0,1]$ to various order polynomials.
- GetW.f
Solves the SCE model for a two-electron density and returns the values for $U_{xc}(\infty)$ and $U'_{xc}(\infty)$.
- WcPoli.f
Performs a similar function to PolyFit.f but uses data points in the range $[0.5,1]$ and at 0.
- MakePade.f
Generates an approximate $U_{xc}(\lambda)$ for various inputs and interpolation formulae, most notably, the Interaction Strength Interpolation.
- GetUc.f
Converts the output of multi, $E_C[n_{1/\lambda}]$, to $U_{xc}(\lambda)$.
- Superadft.f
Finds the value of functionals evaluated on the spin-scaled densities of various atoms. (Doctored version of Adft.f)

A.2 Other Codes Used in this Thesis

- Adft.f

Calculates the ground-state energy and related quantities for various atoms in three dimensions using DFT with various E_{xc} functionals including exact-exchange.

- Multi.f

Finds the various DF components of the total energy for a given density. The density can be inputted or calculated for Hooke's atom.

- Exx.f

Solves for the band structure of various compounds using a plane-wave basis, pseudo-potentials, and exact-exchange.

- PWbulk.f

Solves for the band structure of various compounds using a plane-wave basis, pseudo-potential, and the local density approximation.

- fhi98md.f

Generates the exact exchange pseudo-potentials that are used in EXX.f.

Publicly available at: <http://www.fhi-berlin.mpg.de/th/fhimd/>

References

- [1] *Combined Electronic Structure and Evolutionary Search Approach to Materials Design* G. H. Jóhannesson, T. Bligaard, A. V. Ruban, H. L. Skriver, K. W. Jacobsen, & J. K. Nørskov, Phys. Rev. Lett. **88**, 255506 (2002).
- [2] *Catalyst design by interpolation in the periodic table: Bimetallic ammonia synthesis catalysts*, C.J.H. Jacobsen, S. Dahl, B.S. Clausen, S. Bahn, A. Logadottir, and J.K. Nørskov, J. Am. Chem. Soc. **123**, 8404 (2001).
- [3] *Molecular calculations on the conformation of HIV-1 reverse transcriptase inhibitor*, S. Hannongbua, V. Saen-oon, P. Pungpo, & P. Wolschann, Monatshefte für Chemie **132** 1157-1169 (2001).
- [4] *A hypothetical mechanism for HIV-1 integrase catalytic action: DFT modeling of a bio-mimetic environment*, F. Bernardi, A. Bottoni, M. De Vivo, M. Garavelli, M. Keseru, & G. Naray-Szabo, Chem. Phys. Lett. **362**, Iss. 1-2, 1-7 (2002).
- [5] *The density functional approximation, its applications and prospects*, R.O. Jones & O. Gunnarson, Rev. Mod. Phys. Vol **61**, 689 (1989).
- [6] *Density Functional Theory: An Introduction*, N. Argaman & G. Makov, Am. J. Phys. **68**, 69 (2000).
- [7] F. Jensen, *Introduction to Computational Chemistry*, (Wiley & Sons, New York ,1999).
- [8] *The wave mechanics of an atom with a non-coulomb central field*, D.R. Hartree, Proc. Camb. Phil. Soc., **24**, 89 (1927).
- [9] *Self-consistent field with exchange for Sodium*, V.A. Fock, Zeit. Phys. 1930, Bd. **62**, N 11, S. 795. Transactions GOI, 1931, Vol. **5**, iss. 51, s. 29.
- [10] *On a quantum exchange energy*, V.A. Fock, Zeit.Phys.,1933, Bd. **81**, N 3, S. 195. JHCEcTcF, 1934, Vol. **4**, iss. 1, s. 1. Transactions GOI, Vol. **10**, iss. 92, s. 1.
- [11] *Note on an Approximation Treatment for Many-Electron Systems*, C. Møller and M. S. Plesset, Phys. Rev. **46**, 618 (1934).
- [12] J.M. Thijssen, *Computational Physics*, (Cambridge University Press, New York, 1999).

- [13] *Quantum Monte Carlo simulations of solids*, W.M.C. Foulkes, L. Mitas, R.J. Needs, & G. Rajagopal, Rev. Mod. Phys. **73**, 34 (2001).
- [14] E.N. Economou, *Green's functions in quantum physics*, (Springer, New York, 1979).
- [15] *Electronic excitations, density functional versus many-body Green's functions approaches*, G. Onida, L. Reining, & A. Rubio, Rev. Mod. Phys. **74** 601 (2002).
- [16] *Quasi-particle Calculations on Solids*, W.G. Aulbur, L. Jönsson, & J.W. Wilkins, Solid State Phys. **54**, 1 (2000).
- [17] J. Cioslowski, *Many-Electron Densities and Reduced Density Matrices*, (Kulwer, New York, 2000).
- [18] Robert G. Parr and Weitao Yang, *Density-Functional Theory of Atoms and Molecules*, (Oxford University Press, New York, 1989).
- [19] *The Thomas approximation*, L.H. Thomas, Proc. Camb. Phil. Soc. **23**, 542 (1926).
- [20] *The Fermi approximation*, E. Fermi, Zeit. Phys. **48**, 73 (1928).
- [21] *The von Weizsäcker functional*, C. F. von Weizsäcker, Zeit. Phys. **96**, 431 (1935).
- [22] *A Simplification of the Hartree-Fock Method*, J. C. Slater, Phys. Rev. **81**, 385 (1951); **82**, 538 (1951); **91**, 52 (1953).
- [23] *Inhomogeneous electron gas*, P.Hohenberg & W. Kohn, Phys. Rev. B **136**, 864 (1964).
- [24] *Self-consistent equations including exchange and correlation effects*, W. Kohn & L.J. Sham, Phys. Rev. A **140**, 1133 (1965).
- [25] *On the interaction of electrons in metals*, E. Wigner, Phys. Rev. **46**, 1002 (1934) & E. Wigner, Trans. Faraday Soc. **34**, 678 (1938).
- [26] *Electron interaction in metals*, D. Pines, Solid State Physics **1**, 367 (1955).
- [27] *Correlation Energy of an Electron Gas at High Density*, M. Gell-Mann & K.A. Brueckner, Phys. Rev. **106**, 364.
- [28] *Ground state of the electron gas by a stochastic method*, D. M. Ceperley and B. J. Alder, Phys. Rev. Lett. **45**, 566 (1980).
- [29] *Applications of density functional theory to atoms, molecules and solids*, Ulf von Barth, Chemica Scripta **26**, 449 (1986).

- [30] *Local-density-functional calculations of the energy of atoms*, S. Kotochigova, Z.H. Levine, E.L. Shirley, M.D. Stiles, and C.W. Clark, Phys. Rev. A, **55**, 191 (1997). erratum Phys. Rev. A **56**, 5191 (1997).
- [31] *Accurate spin-dependent electron liquid correlation energies for local spin density calculations: a critical analysis*, S. H. Vosko, L. Wilkes, and M. Nusair, Can. J. Phys. **58**, 1200 (1980).
- [32] *Self-interaction correction to density-functional approximations for many-electron systems*, J. P. Perdew and A. Zunger, Phys. Rev. B **23**, 5048 (1981).
- [33] *Accurate and simple analytic representation of the electron-gas correlation energy*, J. P. Perdew and Y. Wang, Phys. Rev. B **45**, 13244 (1992).
- [34] *The exchange-correlation energy of a metallic surface*, D.C. Langreth and J.P. Perdew, Solid State Commun. **17**, 1425 (1975).
- [35] *Exchange and correlation in atoms, molecules, and solids by the spin-density-functional formalism*, O. Gunnarsson and B.I. Lundqvist, Phys. Rev. B **13**, 4274 (1976).
- [36] *Theory of nonuniform electronic systems. I. Analysis of the gradient approximation and a generalization that works*, D.C. Langreth and J.P. Perdew, Phys. Rev. B **21**, 5469 (1980).
- [37] *Beyond the local-density approximation in calculations of ground-state electronic properties*, D.C. Langreth and M.J. Mehl, Phys. Rev. B **28**, 1809 (1983).
- [38] *Density-functional exchange-energy approximation with correct asymptotic behavior*, A. D. Becke, Phys. Rev. A **38**, 3098 (1988).
- [39] *Development of the Colle-Salvetti correlation-energy formula into a functional of the electron density*, C. Lee, W. Yang, and R.G. Parr, Phys. Rev. B **37**, 785 (1988).
- [40] *Pair distribution function and its coupling-constant average for the spin-polarized electron gas*, J. P. Perdew and Y. Wang, Phys. Rev. B **46**, 12947 (1992); *ibid.* **56**, 7018 (1997) (E).
- [41] *Generalized gradient approximation made simple*, J.P.Perdew, K.Burke, & M.Ernzerhof, Phys. Rev. Lett. **77**, 3865 (1996); **78**, 1396 (1997) (E).
- [42] *Universal variational functionals of electron densities, first order density matrices, and natural spin-orbitals and solution of the v -representability problem* M. Levy, Proc. Natl. Acad. Sci. (U.S.A.) **76**, 6062 (1979).
- [43] *Electron densities in search of Hamiltonians*, M. Levy, Phys. Rev. A **26**, 1200 (1982).

- [44] Gaussian 92/DFT, M.J. Frisch, G.W. Trucks, M. Head-Gordon, P.M.W. Gill, M.M. Wong, J.B. Foresman, B.G. Johnson, H.B. Schlegel, M.A. Robb, E.S. Replogle, R. Gomperts, J.L. Andres, K. Raghavachari, J.S. Binkley, C. Gonzales, R.L. Martin, D.J. Fox, D.J. DeFrees, J. Baker, J.J.P. Stewart, and J.A. Pople (Gaussian Inc., Pittsburgh, PA, 1992).
- [45] Wolfram Koch & Max C. Holthausen, *A Chemist's Guide to Density Functional Theory*, (New York, Wiley-VCH, 2000).
- [46] *A new mixing of Hartree-Fock and local density-functional theories*, A.D. Becke, J. Chem. Phys. **98**, 1372 (1993).
- [47] *Inclusion of Hartree-Fock exchange in the density functional approach. Benchmark computations for diatomic molecules containing H, B, C, N, O, F atoms*, V. Barone, Chem. Phys. Lett. **226**, 392 (1994).
- [48] *Nobel Lecture: Electronic structure of matter - wave functions and density functionals*, W. Kohn, Rev. Mod. Phys. **71**, 1253 (1999).
- [49] *Density-functional theory for time-dependent systems*, E. Runge and E.K.U. Gross, Phys. Rev. Lett. **52**, 997 (1984).
- [50] *Density Functional Theory of Time-Dependent Phenomena*, E.K.U.Gross, J.F.Dobson, and M.Petersilka, Topics in Current Chemistry, **181**, 81 (1996).
- [51] *Optical Properties from Density-Functional Theory*, M.E. Casida, C. Jamorski, F. Bohr, J. Guan, and D.R. Salahub in *Theoretical and Computational Modeling of NLO and Electronic Materials* ed. S.P. Karna and A.T. Yeates (ACS Press: Washington, D.C. 1996).
- [52] *Pressure-induced phase transitions in solid Si, SiO₂, and Fe: Performance of local-spin-density and generalized-gradient-approximation density functionals*, A. Zupan, P. Blaha, K. Schwarz, and J.P. Perdew Phys. Rev. B **58**, 11266 (1998).
- [53] *Quantum-molecular-dynamics simulations of liquid-metals and highly degenerate plasmas*, J. Theilhaber, Phys. Fluids B, **4**, 2044 (1992).
- [54] *First-principles molecular dynamics studies of liquid tellurium*, R. Stadler and M.J. Gillan, J. Phys.Condens. Matt., **12**, 6053 (2000).
- [55] *Density functional theory calculations of the visible spectrum of chlorophyll a*, Dage Sundholm, Chem. Phys. Lett. **302**, 480 (1999)
- [56] *Unified Approach for Molecular Dynamics and Density-Functional Theory*, R. Car and M. Parinello, Phys. Rev. Lett. **55**, 2471 (1985).
- [57] *Density functional theory-based molecular dynamics of biological systems*, P. Carloni, Quantitative Structure-Activity Relationships **21** 166-172 (2002).

- [58] *A self-consistent charge density-functional based tight-binding method for predictive materials simulations in physics, chemistry and biology*, T. Frauenheim, G. Seifert, M. Elstner, Z. Hajnal, G. Jungnickel, D. Porezag, S. Suhai, and R. Scholz, Phys. Status. Solidi B Basic Re. **217**, 41 (2000).
- [59] *Effect of protein dynamics on biological electron transfer*, I. Daizadeh, E. S. Medvedev, and A. A. Stuchebrukhov, Proc. Natl. Acad. Sci. U. S. A. **94**, 3703 (1997).
- [60] *Intermolecular hydrogen bonding between carotenoid and bacteriochlorophyll in LH2*, Z. He, V. Sundstrom, and T. Pullerits, FEBS Lett. **496**, 36 (2001).
- [61] *Time-dependent density-functional theory for super-conductors*, O.J. Wacker, R. Kümmel, and E.K.U. Gross, Phys. Rev. Lett. **73**, 2915 (1994).
- [62] C.A. Ullrich, S. Erhard, and E.K.U. Gross, in *Super Intense Laser Atom Physics IV*, edited by H.G. Muller (Kluwer, Dordrecht, 1996).
- [63] *Performance of the 'parameter free' PBE0 functional for the modeling of molecular properties of heavy metals*, V. Vetere, C. Adamo, and P. Maldivi, Chem. Phys. Lett., **325**, 99 (2000).
- [64] *Magnetic coupling in ionic solids studied by density functional theory*, F. Illas, R. M. Martin, J. Chem. Phys., **108**, 2519 (1997).
- [65] B.L. Gyorffy, J.B. Staunton, and G.M. Stocks, in *Fluctuations in Density Functional Theory: Random metallic alloys and itinerant paramagnets*, eds. E.K.U. Gross and R.M. Dreizler, (Plenum, NY, 1995).
- [66] *Quantum Fluid Dynamics from Density Functional Theory*, S. Kümmel & M. Brach, Phys. Rev. A **64**, 022506 (2001).
- [67] *Unrestricted shapes of light nuclei in the local-density approximations: comparison with jellium clusters*, M. Koskinen, P.O. Lipas, and M. Manninen, Nuclear Phys. A, **591**, 421 (1995).
- [68] *Density functional approach to quantum hydrodynamics: local exchange potential for nuclear structure calculations*, R.N. Schmid, E. Engel, & R. M. Dreizler, Phys. Rev. C, **52**, 164 (1995).
- [69] *What is time-dependent density functional theory? Successes and Challenges*, N.T. Maitra, A. Wasserman, and K. Burke, in *Electron Correlations and Materials Properties 2*, ed. A. Gonis, N. Kioussis, M. Ciftan, (Kluwer/Plenum, 2003).
- [70] Abinit, <http://www.abinit.org/>, *First-principles computation of material properties: the ABINIT software project*, X. Gonze, J.-M. Beuken, R. Caracas, F. Detraux, M. Fuchs, G.-M. Rignanese, L. Sindic, M. Verstraete, G. Zerah, F. Jollet, M. Torrent, A. Roy, M. Mikami, Ph. Ghosez, J.-Y.

- Raty, D.C. Allan. *Computational Materials Science* **25**, 478 (2002). (URL <http://www.abinit.org>).
- [71] Octopus, <http://www.tddft.org/programs/octopus/>, Miguel A. L. Marques, Alberto Castro, Angel Rubio, Kazuhiro Yabana, George W. Bertsch (Spain, 2002).
- [72] Tuan, S (Editor), Sakurai, J.J, *Modern Quantum Mechanics (2nd Edition)*, (Addison-Wesley Pub Co. New York, 1994)
- [73] *Hohenberg-Kohn theorem for nonlocal external potentials*, G.L. Gilbert, Phys. Rev. B. **12** 2111 (1975).
- [74] *Orthonormal orbitals for the representation of an arbitrary density*, J.E. Harriman, Phys. Rev. A **24**, 680 (1981).
- [75] *N-representability of electron density and first-order density matrix*, N.H. March, Phys. Rev. A **26**,1845 (1982).
- [76] *New approach to the calculation of density functionals*, G. Zumbach and K. Machke, Phys. Rev. A **28**, 544 (1983).
- [77] *N-representability of the electron pair density*, E.R. Davidson, Chem. Phys. Lett. **246**, 209 (1995).
- [78] *Hohenberg-Kohn theorem and non-v-representable densities*, H. Englisch & R. Englisch, Physica **121A**, 253 (1983).
- [79] *Solution to the Kohn-Sham equations using reference densities from accurate, correlated wave functions for the neutral atoms helium through argon*, R. Morrison and Q. Zhao, Phys. Rev. A, **51**, 1980 (1995).
- [80] *Quantities $T_S[n]$ and $T_C[n]$ in density-functional theory*, Q. Zhao and R.G. Parr, Phys. Rev. A **46**, 2337 (1992).
- [81] *Local exchange-correlation functional: Numerical test for atoms and ions*, Q. Zhao and R. Parr, Phys. Rev. A, **46**, 5320 (1992).
- [82] *Multicomponent density-functional theory for electrons and nuclei*, T. Kreibich & E.K.U. Gross, Phys. Rev. Lett. **86**, 2984 (2001).
- [83] *Role of the Exchange-Correlation Energy: Nature's Glue*, S. Kurth, J. P. Perdew, International Journal of Quantum Chemistry, Vol. 77, 814 (2000).
- [84] *Jacob's Ladder of Density Functional Approximations for the Exact Exchange-Correlation Energy Functional*, John P. Perdew and Karla Schmidt, in *Density Functional Theory and Its Applications to Materials*, edited by V.E. Van Doren, K. Van Alseoy, and P. Geerlings (American Institute of Physics, 2001).

- [85] *Density functional theory, the exchange hole, and the molecular bond*, M. Ernzerhof, K. Burke, and J.P. Perdew, in *Recent developments and applications in density functional theory*, ed. J.M. Seminario (Elsevier, Amsterdam, 1996).
- [86] *Density functionals: where do they come from, why do they work?*, M. Ernzerhof, J.P. Perdew, and K. Burke, in *Density Functional Theory*, ed. R. Nalewajski, Springer-Verlag, Berlin, 1996.
- [87] *Accurate density functional for the energy: Real-space cutoff of the gradient expansion for the exchange hole*, J.P. Perdew, Phys. Rev. Lett. **55**, 1665 (1985); **55**, 2370 (1985) (E).
- [88] *Accurate density functional with correct formal properties: A step beyond the generalized gradient approximation*, J.P. Perdew, S. Kurth, A. Zupan, P. Blaha, Phys. Rev. Lett., **82**, 2544 (1999); **82**, 5179 (1999) (E).
- [89] *Climbing the Density Functional Ladder: Non-Empirical Meta-Generalized Gradient Approximation Designed for Molecules and Solids*, J. Tao, J.P. Perdew, V.N. Staroverov, & G.E. Scuseria, unpublished.
- [90] *Exchange functionals and potentials*, R. Neumann, R.H. Nobes, N.C. Handy, Mol. Phys. **87**, 1 (1996).
- [91] *Simple Iterative Construction of the Optimized Effective Potential for Orbital Functionals, Including Exact Exchange*, S. Kümmel & J.P. Perdew, PRL **90**, 043004-1 (2003).
- [92] *Orbital functional for exchange and correlation: Self-interaction correction to the local density approximation*, J. P. Perdew, Chem. Phys. Lett. **64**, 127 (1979).
- [93] *Density-functional thermo-chemistry. III. The role of exact exchange*, A.D. Becke, J. Chem. Phys. **98**, 5648 (1993).
- [94] *Effect of Fock exchange on the electronic structure and magnetic coupling in NiO*, I.P.R. Moreira, F. Illas, & R.L. Martin, Phys. Rev. B **65**, 155102 (2002).
- [95] *Rationale for mixing exact exchange with density functional approximations*, J.P. Perdew, M. Ernzerhof, & K. Burke, J. Chem. Phys. **105**, 9982 (1996).
- [96] *Construction of the adiabatic connection*, M. Ernzerhof, Chem. Phys. Lett. **263**, 499 (1996).
- [97] *An improved lower bound on the indirect coulomb energy*, E. H. Lieb and S. Oxford, Int. J. Quantum Chem. **19**, 427 (1981).
- [98] *Density-functional exchange-correlation through coordinate scaling in adiabatic connection and correlation hole*, M. Levy, Phys. Rev. A **43**, 4637 (1991).

- [99] *Fermi holes and Coulomb holes*, M.A. Buijse and E.J. Baerends, in *Density Functional Theory of Molecules, Clusters, and Solids*, ed. D.E. Ellis (Kluwer Academic Publishers, Amsterdam, 1995).
- [100] *Generalized gradient approximation for the exchange-correlation hole of a many-electron system*, J.P. Perdew, K. Burke, and Y. Wang, Phys. Rev. B **54**, 16533 (1996); **57**, 14999 (1998) (E).
- [101] *Hellmann-Feynman, virial, and scaling requisites for the exact universal density functionals. Shape of the correlation potential and diamagnetic susceptibility for atoms*, M. Levy & J.P. Perdew, Phys. Rev. A **32**, 2010 (1985).
- [102] M. Levy, in *Density Functional Theory*, eds. R. Dreizler and E. K. U. Gross, NATO ASI Series (Plenum, New York, 1995).
- [103] R. M. Dreizler and E. K. U. Gross, *Density-Functional Theory, An Approach to the Quantum Many-Body Problem* (Springer, Berlin Heidelberg, 1990).
- [104] *The adiabatic connection method: A non-empirical hybrid*, K. Burke, M. Ernzerhof, & J.P. Perdew, Chem. Phys. Lett. **265**, 115 (1997).
- [105] *Density-functional theory for the Hubbard model: numerical results for the Luttinger liquid and the Mott insulator*, Capelle, N.A. Lima, M.F. Silva, L.N. Oliveira, 'The fundamentals of density matrix and density functional theory in atoms, molecules, and solids', N.Gidopoulos and S.Wilson eds. (Kluwer Series 'Progress in Theoretical Physics and Chemistry', 2003)
- [106] *Density Functionals Not Based on the Electron Gas: Local-Density Approximation for a Luttinger Liquid*, N.A. Lima, M.F. Silva, L.N. Oliveira, & K. Capelle, PRL **90**, 146402-1 (2003).
- [107] *Low-density, one-dimensional quantum gases in a split trap*, Th. Busch & C. Huyel, J. Phys. B **36**, 2553 (2003).
- [108] *Measurement of the spin-excitation continuum in one-dimensional $KCuF_3$ using neutron scattering*, D. Alan Tennant, Roger A. Cowley Stephen E. Nagler & Alexei M. Tsvelik, Phys. Rev. B **52**, 13368 (1995).
- [109] *Direct Observation of Field-Induced Incommensurate Fluctuations in a One-Dimensional $S = 1/2$ Anti-ferromagnet*, D. C. Dender, P. R. Hammar, Daniel H. Reich, C. Broholm, & G. Aeppli, Phys. Rev. Lett. **79**, 1750 (1997).
- [110] *Impurity in a Luttinger liquid away from half-filling: A numerical study*, S. Qin, M. Fabrizio, L. Yu, M. Oshikawa, & I. Affleck, Phys. Rev. B **56**, 9766 (1997).
- [111] G.D. Mahan, *Many-Particle Physics*, 2nd ed. (Plenum Press, New York, 1990).

- [112] *Many-body effects in the one-dimensional electron gas with short-range interaction*, A. Gold, Phys. Rev. B **55**, 9470 (1997).
- [113] *One-dimensional fermions with δ -function repulsion in the Brueckner theory*, F.D. Buzatu, Phys. Rev. B **55**, 2114 (1997).
- [114] *Ground-state energy and density response of a one-dimensional fermion system with repulsive δ -function interaction*, S. Nagano & K.S. Singwi, Phys. Rev. B **27**, 6732 (1983).
- [115] *Un Systeme a Une Dimension de Fermions en Interaction*, M. Gaudin, Phys. Lett. **24A**, 55.
- [116] *Exact Analysis of an Interacting Bose Gas. I. The General Solution and the Ground State*, E.H. Lieb & W. Liniger, Phys. Rev. **130**, 1605 (1963).
- [117] *Delta-Function Gas with Two-Spin Deviates*, M. Flicker & E. H. Lieb, Phys. Rev. **161**, 179 (1967).
- [118] *Some Exact Results for the Many-Body Problem in One Dimension with Repulsive Delta-Function Interaction*, C.N. Yang, Phys. Rev. Lett. **19**, 23 1312 (1967).
- [119] *Solution of the Integral Equations for the Many-Body Problem in One-Dimension*, A.D. Jannussis, Phys. Rev. Lett. **21**, 523 (1968).
- [120] M. Takahashi, *Thermodynamics of One-Dimensional Solvable Models*, (Cambridge Univ. Press, New York, 1999).
- [121] *Dielectric response of a one-dimensional electron gas*, W.I. Friesen & B. Bergersen, J. Phys. C: Solid St. Phys. **13**, 6627 (1980).
- [122] *δ -function bosons in a one dimensional potential well*, You-Quan Li, Phys. Rev. A **52**, 65 (1995).
- [123] *Quantum critical phenomena and stability of atomic and molecular ions*, S. Kais & P. Serra, Int. Rev. Phys. Chem. **19**, No 1, 97 (2000).
- [124] *Electronic structure critical parameters from finite-size scaling*, J.P. Neirotti, P. Serra, & S. Kais, Phys. Rev. Lett. **79**, 3142 (1997).
- [125] *Critical phenomena for electronic structure at the large-dimension limit*, P. Serra, & S. Kais, Phys. Rev. Lett. **77**, 466 (1996).
- [126] *Phase transitions for N -electron atoms at the large-dimension limit*, P. Serra, & S. Kais, Phys. Rev. A **55**, 238 (1997).
- [127] *Solution of the Delta Function Model for Helium-like Ions*, C. Rosenthal, JCP. **55**, 2474 (1971).

- [128] *Heavy atoms in the strong magnetic field of a neutron star*, E. H. Lieb, J. P. Solovej, and J. Yngvason Phys. Rev. Lett. **69**, 749 (1992).
- [129] *Double excitations in time-dependent density functional theory linear response*, N.T. Maitra, F. Zhang, R.J. Cave and K. Burke, submitted to Phys. Rev. Lett. (2003).
- [130] *Applications of coordinate-scaling procedures to the exchange-correlation energy*, Q. Zhao, M. Levy, and R. Parr, Phys. Rev. A, **47**, 918 (1993).
- [131] *New exact relations for improving the exchange and correlation potentials*, M. Levy and A. Görling, Int. J. Quant. Chem. **56**, 385 (1995).
- [132] *Virial energy density in density functional theory*, F.G. Cruz, K.C. Lam, and K. Burke, J. Phys. Chem. A. **102**, 4911 (1998).
- [133] *A local exchange-correlation potential for the spin polarized case*, U. von Barth and L. Hedin, J. Phys. C **5**, 1629 (1972).
- [134] *Inhomogeneous Electron Gas*, Rajagopal, A.K, Calloway, J. Phys. Rev. B **7**, 1912 (1973)
- [135] *Nonuniqueness of the Potentials of Spin-Density-Functional Theory*, K. Capelle and G. Vignale, Phys. Rev. Lett. **86**, 5546 (2001).
- [136] *The Performance of a Family of Density Functionals*, B.G. Johnson, P.M.W.Gill, J.A.Pople, J. Chem. Phys. **98**, 5612 (1993).
- [137] *Band magnetism in ATSn - A= Ce, U ; T= Ni, Pd from local spin density functional calculations*, Samir Matar, Alexander Mavromaras. J. Solid State Chem. **149**, 449 (2000).
- [138] *Scaling the spin densities separately in density functional theory*, R.J. Magyar, T.K. Whittingham, and K. Burke, Phys Rev A **66**, 022105 (2002).
- [139] *Coordinate scaling and adiabatic connection formulation in density-functional theory*, Y.A. Wang, Phys. Rev. A, **56**, 1646 (1997).
- [140] *Digging into the exchange-correlation energy: The exchange-correlation hole*, K. Burke in *Electronic Density Functional Theory: Recent Progress and New Directions*, eds. J.F. Dobson, G. Vignale, & M.P. Das (Plenum, NY, 1997), page 19.
- [141] *Density functionals for non-relativistic Coulomb systems*, J.P. Perdew and S. Kurth, in *Density functionals: Theory and applications*, ed. D. Joubert (Springer, Berlin, 1998).
- [142] *Accurate exchange-correlation potentials and total-energy components for the helium isoelectronic series*, C.J. Umrigar & X. Gonze, Pys. Rev. A, **50**, 3827 (1994).

- [143] *Physics of transformation from Schrödinger theory to Kohn-Sham density-functional theory: Application to an exactly solvable model*, Z. Qian & V. Sahni, Phys. Rev. A **57**, 2527 (1998).
- [144] *Adiabatic connection from accurate wave-function calculations*, D. Frydel, W. Terilla, and K. Burke, J. Chem. Phys. **112**, 5292 (2000).
- [145] *Ground-state correlation energies for two- to ten-electron atomic ions*, E. Davidson, S. Hagstrom, S. Chakravorty, V. Umar, & F. Fischer, Pys. Rev. A, **44**, 7071 (1991).
- [146] *Mixing exact exchange with GGA: When to say when*, K. Burke, J.P. Perdew, and M. Ernzerhof, in *Electronic Density Functional Theory: Recent Progress and New Directions*, eds. J.F. Dobson, G. Vignale, and M.P. Das (Plenum, NY, 1997), page 57.
- [147] *Exact Kohn-Sham scheme based on perturbation theory*, A. Görling and M. Levy, Phys. Rev. A **50**, 196 (1994).
- [148] *Kinetic contribution to the correlation energy density: benchmark to $T_c[n]$ energy functionals*, P. Süle, Chem. Phys. Lett. **259**, 69 (1996).
- [149] *Unambiguous exchange - correlation energy density*, K. Burke, F.G. Cruz, and K.C. Lam, J. Chem. Phys. **109**, 8161 (1998).
- [150] *Requirements for Correlation Energy Density Functionals from Coordinate Transformations*, A. Görling and M. Levy, Phys. Rev. A **45**, 1509 (1992).
- [151] *Nonlocal density functionals for exchange and correlation: Theory and applications*, K. Burke, J. P. Perdew, and M. Levy, in *Modern Density Functional Theory: A Tool for Chemistry*, edited by J. M. Seminario and P. Politzer (Elsevier, Amsterdam, 1995).
- [152] *Toward reliable density functional methods without adjustable parameters: The PBE0 model*, C. Adamo & V. Barone, J. Chem. Phys. **110**, 6158 (1999).
- [153] *Strictly correlated electrons in density functional theory*, M.Seidl, J. Perdew, & M. Levy, Phys. Rev. A **59**, 51 (1999).
- [154] *Simulation of All-Order Density-Functional Perturbation Theory, Using the Second Order and the Strong-Correlation Limit*, M.Seidl, J. Perdew, & S. Kurth, Phys. Rev. Lett. **84**, 5070 (2000).
- [155] *Density functionals for the strong interaction limit*, M.Seidl, J. Perdew, & S. Kurth, Phys. Rev. A **62**, 012502 (2000).
- [156] *Improving energies by using exact electron densities*, K. Burke, J.P. Perdew, and M. Levy, Phys. Rev. A **53**, R2915 (1996).

- [157] *Adiabatic connection from accurate wave-function calculations*, D. Frydel, W. Terilla, & K. Burke, J. Chem. Phys. **112**, 5292 (2000).
- [158] *Accurate adiabatic connection curve beyond the physical interaction strength*, R.J. Magyar, W. Terilla, and K. Burke, J. Chem. Phys. **119**, 696 (2003).
- [159] *Density functionals and dimensional re-normalization for an exactly solvable model*, S. Kais, D.R. Herschbach, N.C. Handy, C.W. Murray, and G.J. Laming, J. Chem. Phys. **99**, 417 (1993).
- [160] *Energy spectra of two electrons in a harmonic quantum dot*, U. Merkt, J. Huser, & M. Wagner, Phys. Rev. B **43**, 7320 (1991).
- [161] *Correlation energies for two interacting electrons in a harmonic dot*, R. M. G. Garca-Casteln, W. S. Choe, & Y. C. Lee Phys. Rev. B **57**, 9792 (1998)
- [162] *Two electrons in an external oscillator potential: Particular analytic solutions of a Coulomb correlation problem*, M. Taut, Phys. Rev. A **48**, 3561 (1993).
- [163] *Correlation-energy functional and its high-density limit obtained from a coupling-constant perturbation expansion*, A. Görling and M. Levy, Phys. Rev. B **47**, 13105 (1993).
- [164] *DFT ionization formulas and a DFT perturbation theory for exchange and correlation, through adiabatic connection*, A. Görling and M. Levy, Int. J. Quant. Chem. **29**, 93 (1995).
- [165] *Strong-interaction limit of density-functional theory*, M. Seidl, Phys. Rev. A **60**, 4387 (1999).
- [166] *The ground state of harmonium*, J. Cioslowski, K. Pernal, J. Chem. Phys. **113**, 8434 (2000).
- [167] *Exploring the Adiabatic Connection Between Weak and Strong Interaction Limits in Density Functional Theory*, J. Perdew, S. Kurth, & M. Seidl, International Journal of Modern Physics B, Vol. **15**, 1672 (2001).
- [168] *Why semi-local functionals work: Accuracy of the on-top pair density and importance of system averaging*, K. Burke, J. Perdew, & M. Ernzerhof, J. Chem. Phys. **109**, 3760 (1998).
- [169] *Density-functional theory of Wigner crystallization*, H.B. Shore, E. Zaremba, J.H. Rose, and L. Sanders, Phys. Rev. B **18**, 6506 (1978).
- [170] *Physical Content of the Exact Kohn-Sham Orbital Energies: Band Gaps and Derivative Discontinuities*, J. P. Perdew and M. Levy, Phys. Rev. Lett. **51**, 1884 (1983).

- [171] *Density Functional Theory of the Energy Gap*, L. J. Sham and M. Schlüter, Phys. Rev. Lett. **51**, 1888 (1983).
- [172] *Density-functional theory for fractional particle number: Derivative discontinuities of the energy*, J.P. Perdew, R.G. Parr, M. Levy, and J.L. Balduz, Jr., Phys. Rev. Lett. **49**, 1691 (1982).
- [173] *Exact Kohn-Sham exchange potentials in semiconductors*, M. Städele, J.A. Majewski, P. Vogl, and A. Görling, Phys. Rev. Lett., **79**, 2089 (1997).
- [174] *Hardness of molecules and the band gap of solids within the Kohn-Sham formalism: A perturbation-scaling approach*, A. Görling & M. Levy, Phys. Rev. A **52**, 4493 (1995).
- [175] *Optimized effective atomic central potential*, J.D. Talman and W.F. Shadwick, Phys. Rev. A **14**, 36 (1976).
- [176] *Orbital functionals in density functional theory: the optimized effective potential method*, T. Grabo, T. Kreibich, S. Kurth, and E.K.U. Gross, in *Strong Coulomb correlations in electronic structure: Beyond the local density approximation*, ed. V.I. Anisimov (Gordon and Breach, Tokyo, 1998).
- [177] *Exact exchange-potential band-structure calculations by the LMTO-ASA method: MgO and CaO* T. Kotani, Phys. Rev. B **50**, 14816 (1994).
- [178] *Exact exchange potential band-structure calculations by the linear muffin-tin orbital-atomic-sphere approximation method for Si, Ge, C, and MnO*, T. Kotani, Phys. Rev. Lett. **74**, 2989 (1995).
- [179] *KKR-ASA method in exact exchange-potential band-structure calculations*, T. Kotani & H. Akai, Phys. Rev. B **54**, 16502 (1996).
- [180] *Exact-exchange-based quasi-particle calculations*, W.G. Aulbur, M. Städele, and A. Görling, Phys. Rev. B **62**, 7121 (2000).
- [181] *Exact treatment of exchange in Kohn-Sham band-structure schemes*, A. Görling, Phys. Rev. B **53**, 7024 (1996); **59**, 10370(E) (1999).
- [182] *Exact Exchange Kohn-Sham Formalism Applied to Semiconductors*, M. Städele, M. Moukara, J.A. Majewski, P. Vogl, and A. Göling, Phys. Rev. B **59**, 10031 (1999).
- [183] *LDA, GW, and exact-exchange Kohn-Sham scheme calculations of the electronic structure of sp semiconductors*, A. Fleszar, Phys. Rev. B **64**, 245204 (2001).
- [184] *Exchange-correlation potentials at semiconductor interfaces*, R.W. Godby and L.J. Sham, Phys.Rev. B **49**, 1849 (1994).

- [185] *Positron and electron energy levels in rare-gas solids*, M.J. Piska & R.M. Nieminen, Phys. Rev. B **46**, 1278 (1992).
- [186] *Relationship of Kohn-Sham eigenvalues to excitation energies* A. Savin, C. J. Umrigar, X. Gonze, Chem. Phys. Lett. **288**, 391 (1998).
- [187] *Evidence of physical reality in the Kohn-Sham potential: The case of atomic Ne*, A. I. Al-Sharif, R. Resta, C. J. Umrigar, Phys. Rev. A **57**, 2466 (1998).
- [188] *Excitations in time-dependent density-functional theory*, H. Appel, E.K.U. Gross, and K. Burke, Phys. Rev. Lett. **90**, 043005 (2003).
- [189] *Ab initio simulations of II-VI semiconductors: bulk properties, surfaces, and implications for crystal growth*, Stefan Gundel, Diplomarbeit, Würzburg, Germany, 2001.
- [190] *Bloch's theorem*, F. Bloch, Zeit. Phys. **81**, 363 (1933).
- [191] *Special points for Brillouin-zone integration*, H. J. Monkhorst and J. D. Pack, Phys. Rev. B **13**, 5188 (1976).
- [192] *Iterative minimization techniques for ab initio total-energy calculations: molecular dynamics and conjugate gradients*, M.C. Payne, M.P. Teter, D.C. Allen, T.A. Arias, & J.D. Joannopoulos, Rev. Mod. Phys. **64**, 1045 (1992).
- [193] *Generalized Kohn-Sham schemes and the band-gap problem*, M. Seidl, A. Görling, P. Vogl, J.A. Majewski, & M. Levy Phys. Rev. B **53** 3764 (1996).
- [194] *Efficacious Form for Model Pseudopotentials*, L. Kleinman & D.M. Bylander, Phys. Rev. Lett. **48** 1425 (1982).
- [195] *Norm-conserving pseudopotentials in the exact-exchange Kohn-Sham formalism*, M. Moukara, M. Städele, J.A. Majewski, P. Vogl, and A. Göling, J. Phys. Condens. Matter **12**, 6783 (2000).
- [196] *Pseudopotentials that work: From H to Pu*, G.B. Bachlet, D.R. Hamann, and M. Schlüter, Phys. Rev. B **26**, 8 (1982).
- [197] *Efficient pseudopotentials for plane-wave calculations*, N. Troullier & J.L. Martins, Phys. Rev. B **43**, 1993 (1991).
- [198] C. J. Umrigar and X. Gonze, in *High Performance Computing and its Application to the Physical Sciences*, edited by D. A. Browne *et al.*, Proceedings of the Mardi Gras '93 Conference (World Scientific, Singapore, 1993).
- [199] *From electron densities to Kohn-Sham kinetic energies, orbital energies, exchange-correlation potentials, and exchange-correlation energies*, Q. Zhao, R. C. Morrison, and R. G. Parr, Phys. Rev. A **50**, 2138 (1994).

- [200] The fhi98md code of the Fritz-Haber-Institut, Berlin (URL <http://www.fhi-berlin.mpg.de/th/fhimd/>).
- [201] *Study of the Electronic Structure and the Optical Properties of the Solid Rare Gases*, A. B. Kunz & D. J. Mickish, Phys. Rev. B **8**, 779 (1973).
- [202] U. Rosserler, in *Rare Gas Solids*, edited by M.L. Klein and J. A. Venables (academic, New York, 1975), pp. 504 and 545.
- [203] *Reflection spectrum of solid argon in the vacuum ultraviolet*, R. Haensel, G. Keitel, E.E. Koch, M. Skibowski, & P. Schreiber, Phys. Rev. Lett. **23**, 1160 (1969).

Curriculum Vitae

Rudolph John Magyar

EDUCATION

- 1998-2003 Ph. D. Rutgers University, New Brunswick, NJ
- 1994-1998 B.A. Amherst College, Amherst, MA (May 1998)
 Magna Cum Laude in Physics and Classics,
 Departmental Honors in Physics
 Study Abroad - The American University in Cairo, Egypt

POSITIONS HELD WHILE A GRADUATE STUDENT

- 1999-2000 GAANN Fellow, Rutgers University Department of Physics
 1999 Summer Research Assistant,
 Fermi National Accelerator Laboratory, Batavia, IL
- 1999-2001 Graduate Student Organization President,
 Rutgers University Department of Physics
- 2000-2001 Teaching Assistant, Rutgers University Department of Physics
- 2001-2002 DAAD (German Academic Exchange Service) Fellow,
 Freie Universität and Würzburg
 Departments of Physics, Berlin and Würzburg, Germany
 Adviser: E.K.U. Gross
- 2002-2003 Graduate Assistant, Rutgers University Department of Physics

PUBLICATIONS LIST

Scaling the spin densities separately in density functional theory,
 R.J. Magyar, T.K. Whittingham, and K. Burke, Phys Rev A 66, 022105 (2002).

Accurate adiabatic connection beyond the physical interaction strength,
 R.J. Magyar and K. Burke, J. Chem. Phys. 119, 696 (2003).

Exact-exchange DFT calculations on noble solids,
 R.J. Magyar, E.K.U. Gross, and A. Fleszar,
 (2003, submitted to Phys. Rev. B, arxiv.org/abs/cond-mat/0307751).